UNIVERSITY OF L'AQUILA

Department of Industrial engineering and Information & Economics

PhD in Industrial engineering and Information & Economics

Curriculum Chemical engineering

XXXIII Cycle

Thesis title

Design of semi-industrial plant from biogas upgrading to biomethane by adsorption on spent material for energy purposes integrated with enzymatic conversion of CO_2 into precursors of bioplastic materials

SSD ING-IND/27 Industrial and technical chemistry

PhD student

Zaheer Ahmad

Course Coordinator

Prof. Giuseppe Ferri

Tutor

Prof. Katia Gallucci

A.A. 2019/2020

Summary

Increasing in population also increases the basic needs of the humanity and everyone is in search and need to find alternative sources and this research work is designed to keep in mind theses needs which is also less toxic to the environment. Biofuel is environment friendly and less effects to climate change.

This PhD research work, in the framework of Innovative Doctorates funded by National Operational Program for Research and Innovation (PON RI 2014-2020), is basically designed to utilize biowaste (fruits and vegetables waste) to make biogas that can be achieved from the fermentation process and to design a plant that will produce electricity and bioplastic from this biogas which will be used as a biofuel. It consists of three parts related to three different fields and, therefore, it is divided into three sections.

First part of the thesis was completed in the laboratory of applied thermodynamics and chemical reactors (University of L'Aquila, Italy) and is related to biogas upgrading to biomethane (environment friendly biofuel) by CO_2 capture using hydro-char as an adsorbent material to produce electricity, to use as a sustainable biofuel for the transportation vehicles and for cooking purposes.

Second part was accomplished in the department of organic chemistry (university of Graz, Austria) and is related to enzymatic conversion of captured CO_2 in biogas upgrading, into precursors of bioplastic sheets for food coverage.

Third and final part of the PhD was achieved in the company (APS S.p.A, Rome, Italy) and is related to design of semi-industrial plant that will produce electricity from upgraded biogas (biomethane) and bioplastic material from CO_2.

TABLE OF CONTENTS

LIST OF FIGURES

LIST OF TABLES

LIST OF ABBREVIATIONS

IPCC – Intergovernmental panel on climate change

CO_2 – Carbon dioxide

OFG - Oxygenated functional groups

HTC – Hydrothermal carbonization

HC – Hydro-char

BECCS - Bioenergy with carbon capture and storage

PSD - Particle Size Distribution

IUPAC - International Union of Pure and Applied Chemistry

CHP - Combined heat and power

PSA – Pressure swing adsorption

TSA – Temperature swing adsorption

ESA – Electric swing adsorption

BFD – Block flow diagram

GHG – Greenhouse gas

UNIVERSITY OF L'AQUILA
Department of Industrial engineering and Information & Economics

SECTION 1

Biogas upgrading to biomethane by CO_2 capture using hydro-char as an adsorbent material

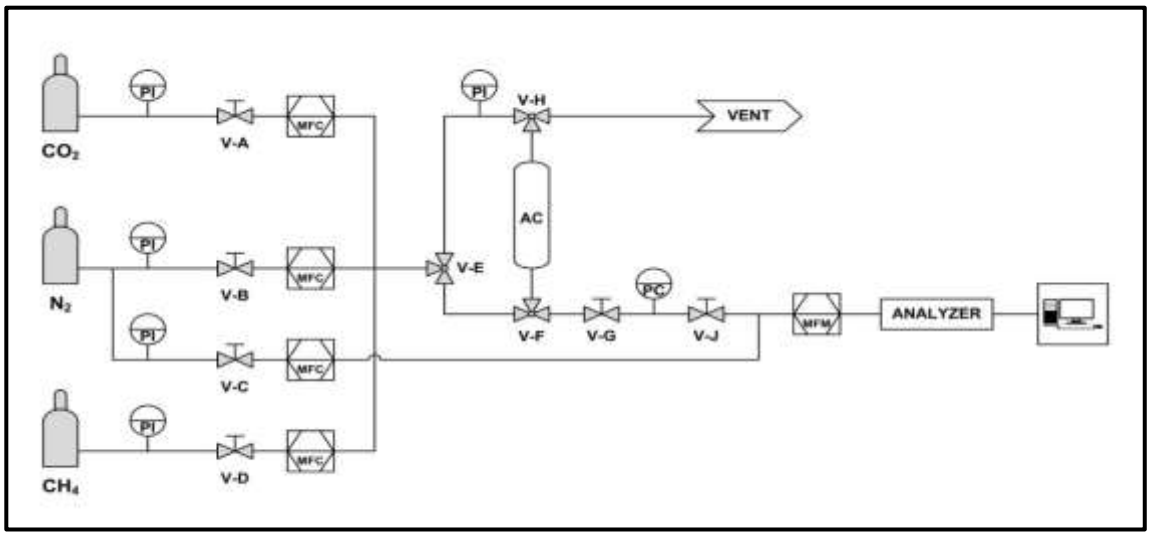

ABSTRACT

Biogas upgrading to biomethane is an alternative and renewable energy resource and a lot of research and industrial work has been done on it [1]. This work is related to adsorption in spent material and pressure swing adsorption (PSA) technique is used. Hydro-char, which was obtained from residual lignocellulose biomass through hydrothermal carbonization process, has been used here as an adsorbent material to capture carbon dioxide from biogas. Biomass obtained from silver fir saw dust (carbon rich material) was hydrothermally treated at 200 °C and with a persistent water biomass proportion 7:1, and residence time 0 and 120 min, then the hydro-char was activated according to a well-known method: potassium hydroxide impregnation and subsequent thermal treatment at 600 °C for 1 hour. Hydro-char was then characterized from a physico-chemical point of view, using CHNS, BET & BJH analyses. Experimental adsorption tests were conducted to evaluate the possibility of using hydro-char in CO_2 capture and range of pressure was selected from 2-5 bar. Finally, a selectivity test was carried out by processing a mixture consisting of CO_2 and CH_4, similar to typical biogas composition, to mimic the upgrading to biomethane product.

The dynamic lab-scale tests allowed the evaluation of sorption capacity (4.96 mmol / g of CO_2), selectivity (65%), purity (95.4%) and low recovery (68%) of CH_4. The results were analyzed and compared with literature data.

Keywords

Lignocellulosic biomass; thermochemical processes; hydrothermal carbonization; hydro-char activation; CO_2 capture

1. INTRODUCTION

1.1 Research Background

Greenhouse gases, especially CO_2 emissions is a critical issue given the important role in the climate change around the worldwide [2], since carbon dioxide generated by the use of any fossil fuel is now discharged into the environment, contributing to the increment of the gas concentration in atmosphere, resulting in the rise of global temperature. With the depletion of fossil and the natural resources, the focus of the world is now towards renewable and bioenergyBiogas is also an alternative renewable energy resource, but there is a huge percentage of CO_2 is present in it, which needs to be removed before supplying to the energy sector for better efficiency and high heating value.

In the past few years, multiple researchers have been done for the development of capturing and storage capacity techniques of carbon dioxide in order to improve the energy efficiency and generation from other non-fossil sources.

1.2 Research Motivation

To decrease the effect of CO_2 into the environment and to accommodate climate change it is better to use biofuel and renewable energy resources which are environment friendly. It is also important to use the CO_2 that is emitted from the industries and also to capture CO_2 from the biogas in order to make some bio base products.

A promising technology for carbon capture and separation is the use of porous solids including vacuum adsorption systems, pressure, or temperature. Among the many porous solids tested are zeolites, porous coals, organic-inorganic hybrid adsorbents and carbon-based porous solids have huge potential for carbon capture. These materials have countless cost advantages, as they can be obtained by a large range of waste residues, have defined porous structure, high specific surface area, low energy, and high availability requirements of regeneration.

Hydro-char is a porous carbon rich adsorbent that is being used in the system to capture CO_2 from the biogas in order to upgrade to biomethane that will be used for energy related

purposes or conveyed via the existing methane network, more or less widespread in the various countries.

1.3 Aim and objectives

Aim:

The main aim of the research work is the biogas upgrading to biomethane by using hydro-char as an adsorbent material, in compliance with the principles of Green Chemistry.

Objectives:

The main objectives of the current research work are as follows:

1. To produce hydro-char from silver fir raw wood, activation, and characterization of hydro-char.
2. To design bed, column, and scheme of setup for test capture to perform experimentation under different operating conditions.
3. To analyze the data and calculate the purity and recovery methane, before sending to the energy sector.
4. Compare results with the literature.

1.4 Research Methodology

The Figure 1.1 represents in detail about the research methodology of the thesis work performed.

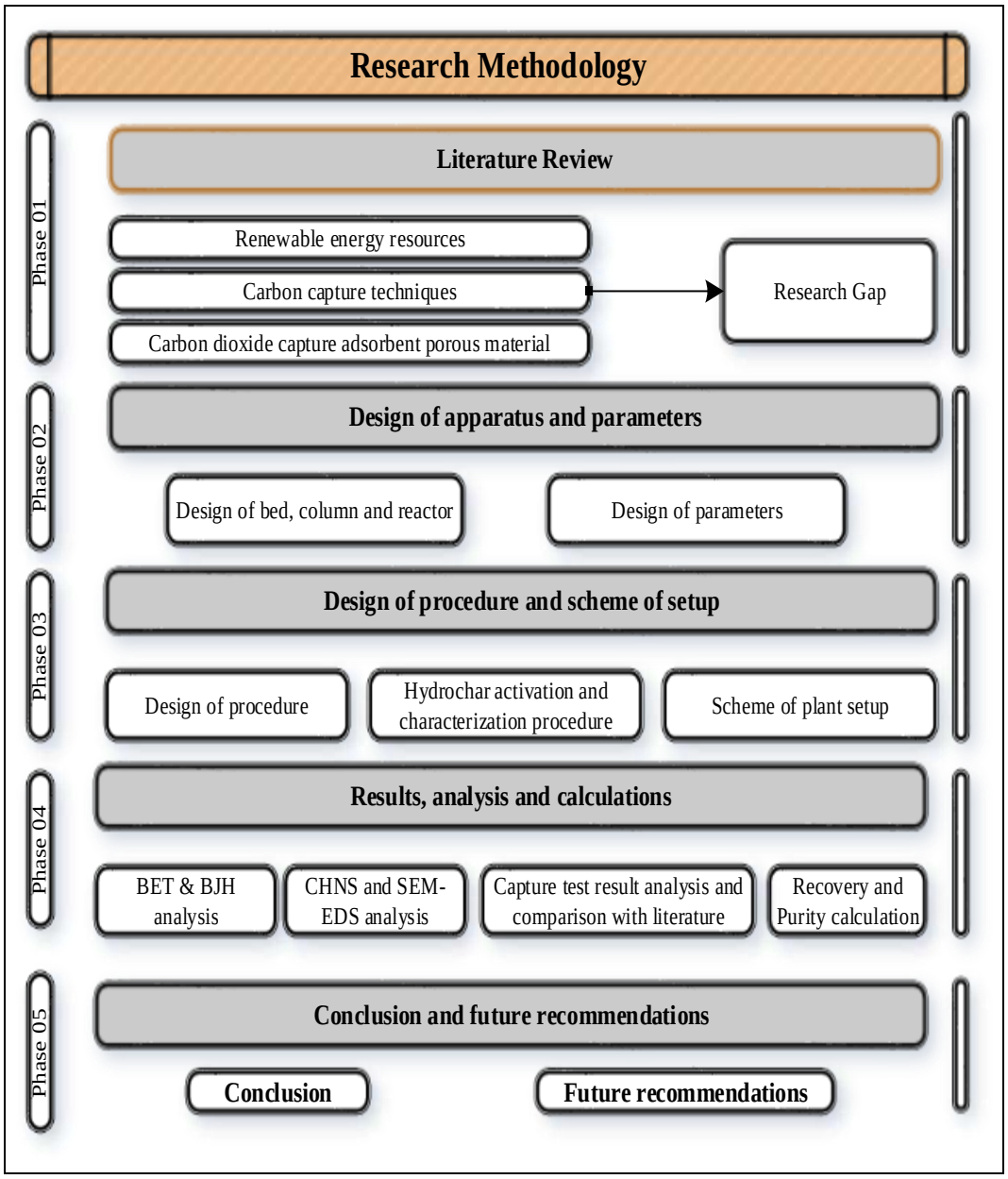

Figure 1.1: Research methodology

1.5 Scope of Research

Hydro-char is investigated by measuring pore size diameter and surface area in order to analyze the carbon capture capability.

Following were the parameters that were analyzed:

I. During conversion from biochar to hydro-char by using hydrothermal carbonization the factors temperature, residence time and processing conditions were analyzed.

II. During experimentation, the effect of adsorption pressure was analyzed by calculating adsorbent capacity of hydro-char and results were compared with the literature.

III. Selectivity on the basis of CO_2 and purity of biomethane was calculated, analyzed, and compared with the literature.

1.6 Thesis Structure (Part 1)

- Introduction: The research background, research motivation, aim and objectives, research methodology and scope of research are briefly explained in this chapter.
- Literature Review: Literature review of all the related articles is described in this chapter.
- Materials and Methods: Experimental design and setup of the research study are explained in this chapter.
- Results, Analysis and Discussions: This chapter covers the results, analysis, and discussion session.
- Conclusions and Recommendations: In this chapter, conclusions and future recommendations are described.

2. LITERATURE REVIEW

2.1 Introduction

Increase in the population and high utilization of fusil fuels are the reasons of the increase in the greenhouse emission and deletion of ozone layer in the faster rate which eventually increasing the global warming. Carbon dioxide highly affects the global warming and increasing earth's temperature. To minimize the effects of carbon dioxide a large number of researches have already been carried out on its reduction and its capturing techniques [3]. The challenge nowadays is to reduce the emission of carbon dioxide to the moderate level of the regional and global climate change [4].

Regarding weather temperature of global records from 1880 and over the last five years (2014–2018) which comprises the hot weather during the month of Septembers of these four years. It has been recorded that the September of 2015 year is observed to be the warmest month with the temperature of +0.93°C (+1.67°F). Whereas, in 2018, the September was marked the 42^{nd} consecutive month of September and 405^{th} month in which temperature was recorded that much in the 20^{th} century on average [5].

Intergovernmental panel on climate change (IPCC) was reported that there is an increase of 1.5 °C temperature in the form of global warming and because of the increasing global warming the increase in the rate of greenhouse gases is also included in the conference of climate change held in United Nations and decision was made to follow the Paris agreement (to limit global warming to well below 2 °C, preferably to 1.5 degrees Celsius, compared to pre-industrial levels) over minimizing effects of climate change [6, 7].

Also, because of increasing usability and reducing resources of fossil fuels usages it is important to find an alternative resource of energies to accommodate daily needs, because rise in population and decrease in natural sources is the key point that requires consideration. Bioenergy is the renewable energy that have taken cluster stage in replacing the conventional fossil-based energy sources.

Due to constant decrease in fossil and natural energies the focus of the world is now towards renewable and bioenergy and due to this reason it has been forecasted in 2017 by

the international energy agency to supply about 10% basic supply of energy can be fulfilled with the bioenergy over the year of 2035 [8].

The report shows the consumption of renewable energy sources in the year of 2017 in which renewable energy was utilized for the electricity production except biomass which if 5.6 % whereas the thermal energy was observed to be 4.2 % and utilization of biofuels was recorded to be 1 % utilization as shown in Figure 2.1.

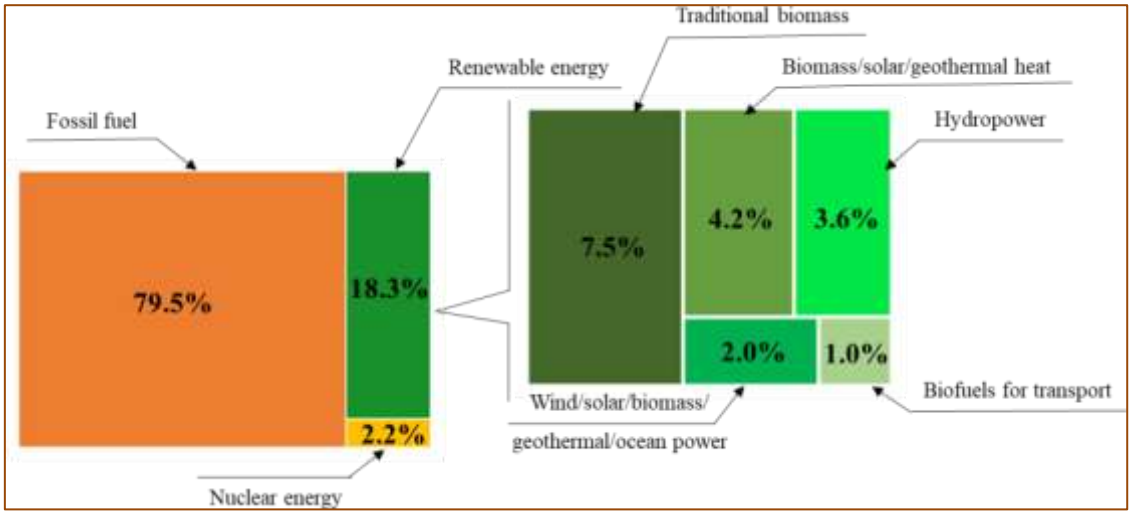

Figure 2.1: Reported renewable energy of total energy consumption, 2017 [9]

Various research has been carried out in recent years for the development of different kinds of efficient chemical and biological techniques to convert biomass into biobased chemical and fuels. For example, fermentation of corn and sugar cane in order to produce bioethanol [10, 11], and treatment of vegetable/cooking oil by using trans-esterification method to obtain biodiesel [12].

A new report on capture/ removal of carbon dioxide suggests four simple ways planting trees, take better care of existing forests, rebuilding of soil used to grow crops that emits a lot of carbon and biomass energy with carbon capture and storage which involves burning of some kinds of plant matter to produce electricity, fuel or heat. The report said that BECCS could remove the largest amount of carbon dioxide from the air but it is costly too [13]. CO_2 separation techniques are the most common field of research world in order to capture the carbon dioxide in a closed environment and utilize it for the power production with the aim to minimize the emission of greenhouse gasses to the environment [14].

Biogas is basically a renewable energy source. It is a mixture of different types of gases like Carbon dioxide (CO_2), Hydrogen sulphide (H_2S), Methane (CH_4), and some moisture. Biogas can be used as a fuel for cooking and transportation purposes after compression because the gases in biogas can be oxidized or combusted with oxygen as a fuel or used for power and heat generation in CHP plants.

Biogas is produced from the remains of bacteria such as plants and animals and their waste products in the environment. Biogas can also be produced by anaerobic fermentation of biodegradable materials [15]. Biogas composition produced from anaerobic digestion is shown in the Figure 2.2 below.

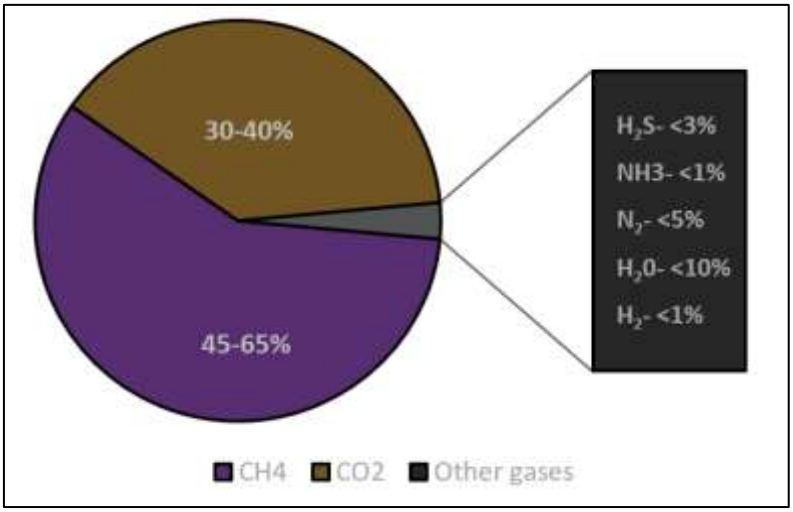

Figure 2.2: Biogas composition produced from anaerobic digestion [15]

Biogas production plant are the plants in which biogas is produced through the process of fermentation containing substrates are used as input for the production of methane or biogas. Many researchers utilized different types of biogas plants for different type of applications. For example, Raven et al. installed 35 farm scale plants and 20 centralised plants for the working on the digestion of waste material and manure in Denmark. He reviewed the whole setup of biogas plants in the Denmark while keeping the certain effecting factors on record [16]. Tom et al. worked on the development of domestic level biogas plants for the restoration of kitchen wastes in the form of separation of methane from the biogas wastes. This restored gas was further treated to be used for the production of power [17]. Walla et al. used biogas plant in its study to produce electricity from the maize silage. Author conducted a survey to find out the best suitable plant size to achieve

the maximum amount of efficiency [18]. Similarly, Lukehurst et al. did research work on the anaerobic digestion (AD) process in order to obtain two important products from the organic matter which are biogas and digestate. This process is carried out in the absence of air [19].

Number of authors worked on different type of the biogas plants which are differ in it shape and size i.e., Lou et al. worked on floating drum type of biogas plant in which biogas was stored in the floating drum type of biogas plant and was entered in the semi-continues way of process [20], whereas, Kaur et al. worked on the fixed-dome shape of biogas power plant. He designed the dome type of fixed biogas plant for the digestion of paddy straw [21] and Kanwar et al. performed enhancement assessment on the balloon type of biogas plant in a hilly environmental conditions [22]. Figure 2.3 shows different types of drum plants.

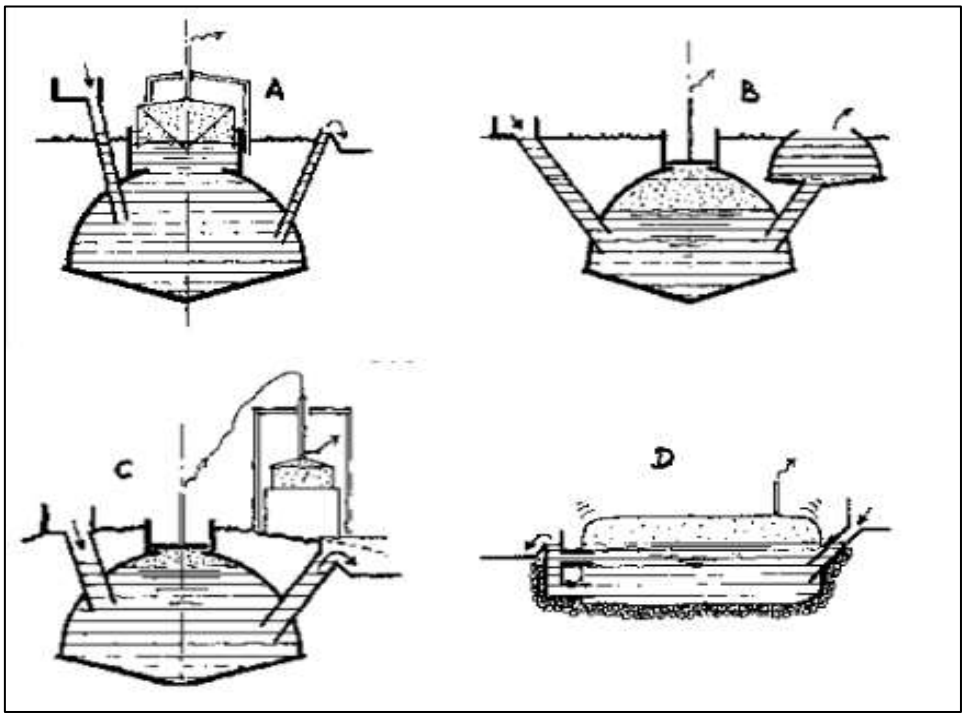

Figure 2.3: Biogas plants; (A) Floating-drum plant, (B) Fixed-dome plant, (C) Fixed-dome plant with separate gas holder, (D) Balloon plant.

In this scenario, it is most important to invent new kinds of materials and technologies to develop the alternative of fossil fuels that is environment friendly, cost effective and easily obtainable from natural and renewable resources like zeolites being effective

adsorbent in order to remove hydrogen sulphide (H_2S) from biogas holding good capacity to contain Sulphur, good re-generality, stable structure and selectivity [23].

Carbon based material like pyrogenic carbon (biomass-derived) materials have a very good regeneration and can be produced at a very low cost that makes it very suitable for use in industrial applications. In the absence activation phenomenon, the pyrogenic carbon was able to absorb the significant carbon dioxide. Actually in the pyrolysis, it provides the required surface area for the absorption of carbon dioxide [24].

Biomass is the energy form which is oldest and commonly using for the production of energy traditionally. It is used as energy material and present in the form of plant or animal. It can also be achieved from waste from animal slurry and food crops and forest or wood residues. It is utilized in processes in industries, and it is used as a raw material in these industrial processes. Second generation of biomass energy is made from the wood wastes (64%), agricultural waste (5%), landfill gases (5%) and MSW (24%) [25].

Carbon based materials have versatile properties and have wide range of use like improvement of soil quality, purifies air and an excellent method for managing wastewater, helps in carbon sequestration, due to less treatment time it can produce high amount of biofuel. high surface area and high sorption capacity is achieved thanks to the development of micropores structure [26, 27].

However, cultivation of biomass into biobased chemicals and fuels depends on available food resources, land and high feedstock cost and this deficiency can be removed by using different thermochemical routes like pyrolysis, gasification, hydrogenation, and combustion which have the advantages of high processing efficiency and broad range of biomass feedstock [28].

Pyrolysis is a process that has been used in the earlier period to produce charcoal, which is used to convert biomass to biobased fuels and from biobased fuels from solids which derived from biomass, the products of liquid and gaseous have temperature range of 400-650 °C without the presence of oxygen [29].

Charcoal is an amorphous carbon in the form of highly porous microcrystalline graphite. It is basically produced from wood at relatively low temperatures [30, 31].

2.2 Carbon Capture techniques

The flow diagram of all the carbon capture technique including traditional and emerging are given in the Figure 2.4.

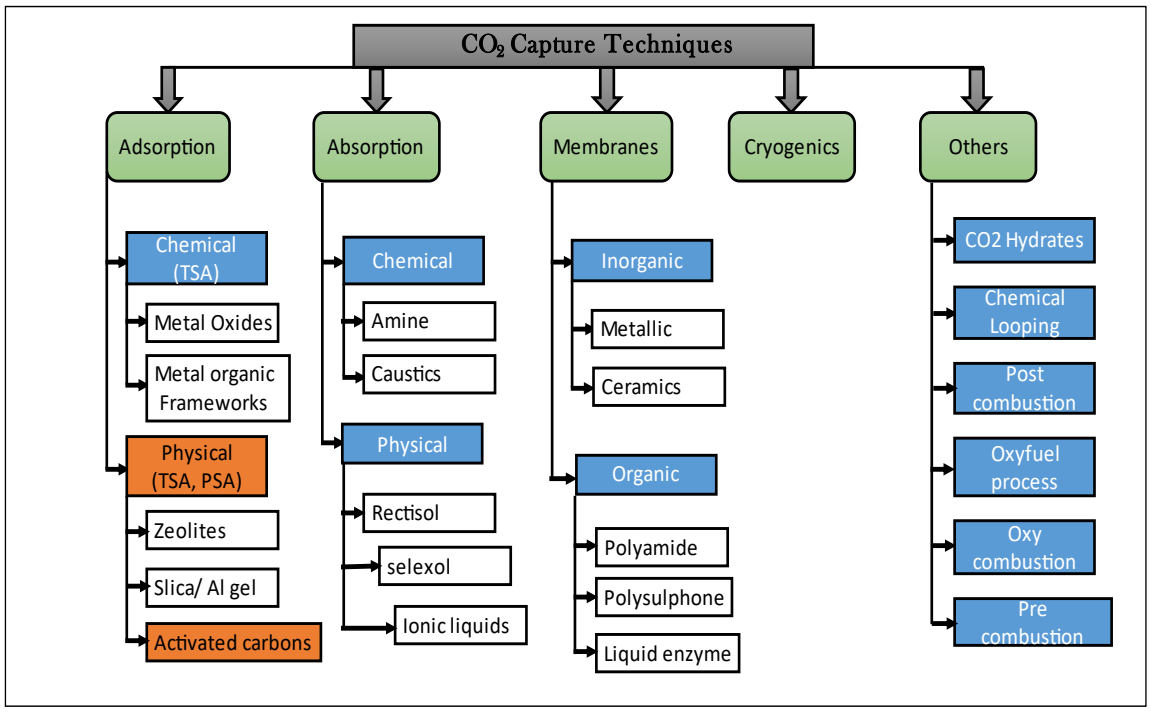

Figure 2.4: Types of CO_2 capture techniques

2.2.1 Traditional technologies

A lot of work has been done in the past for biogas upgrading and several techniques were established that are now available in commercial use, laboratory scale and industrially worldwide. It consists of typically like adsorption, absorption, membrane, cryogenic and hydrate based separation etc. [32]. Most of the capturing techniques of carbon dioxide like adsorption and absorption growing rapidly rather than other like membrane, enzymatic and thermodynamics and is mostly used industrial capture technique worldwide, having more patent applications and published articles [33].

2.2.1.1 Adsorption

A process that consists of physical interaction of gas or liquid on solid surface is called adsorption. Adsorbents that can be used for the capturing of carbon dioxide are composed of activated carbon like biochar, zeolites, metallic oxides, and alumina. The adsorbent

regeneration is carried out by heat application (TSA, temperature swing adsorption) or pressure reduction (PSA, pressure swing adsorption) [34]. For the regeneration process it is necessary to lower the energy, solid adsorbents with a lower heat capacity having greater advantage and potential as compared to the traditional solutions of aqueous amine solutions [35].

The most important and valuable adsorbent method is that in which pressure swing adsorption is utilized for the sorption and adsorbent regeneration (reduction of pressure) and typical adsorbent materials used are composed of resins, zeolites, activated carbon, coconut shell, alumina, and silica gel [36].

When a gas or liquid is brought in contact with a solid surface, particles from the gas or liquid start to accumulate on the surface area of the solid. This trend of a gathering of gas or liquid particles on the surface of the solid is known as adsorption. A substance which adds on the solid surface is known as adsorbate and the solid surface on which it occurs is known as an adsorbent. Figure 2.5 shows the methane adsorbed at different pressures on Metal-organic frameworks.

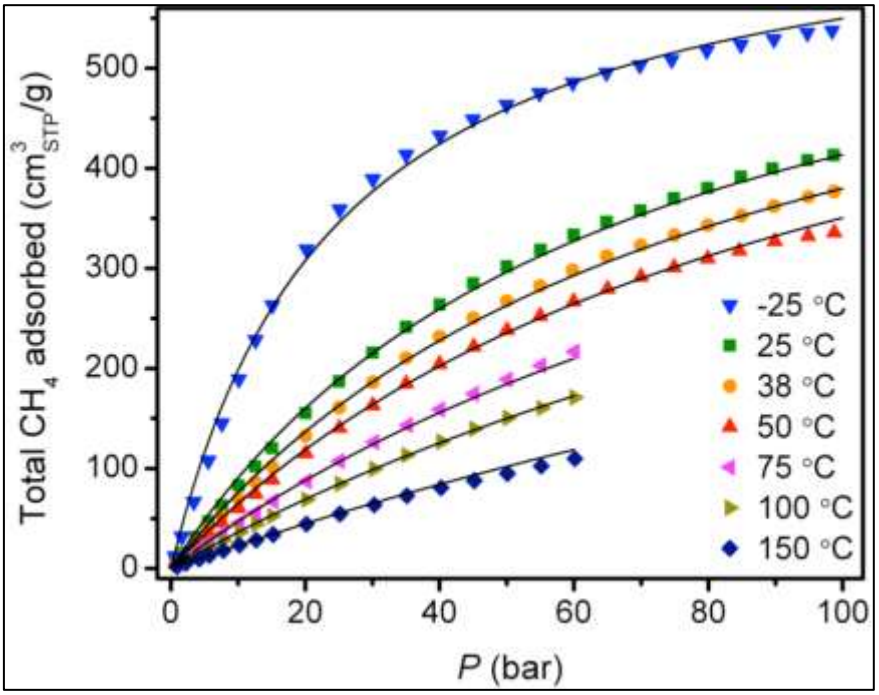

Figure 2.5: Total CH_4 adsorption isotherms [37]

Anthropogenic control of CO_2 emissions plays a very important role in order to control the gasses in climate change. As described in first the most common method of catching CO_2 is absorption by alkaline solutions. There are some disadvantages of the process which includes the toxicity, higher energy consumption, equipment corrosion and solvent regeneration of the solvents used [38]. Promising technologies, alternatives to absorption in the liquid phase, are those that exploit porous solids. Over the years, number of porous solids are studied including metal-organic structures (MOF), porous coals and zeolites. Porous coals have important advantages which includes the availability, cost factor, easy to design pore structure, low energy requirements, sample surface area and hydrophobicity. Sevilla M. et al. in a research study worked on the adsorption and wanted to relate the porous characteristics of hydro-char activated with potassium hydro oxide and their gas-phase adsorbing capacity [39].

2.2.1.1.1 Pressure Swing Adsorption

The method in which mixture of gases passes through the fixed beds at set pressure and relatively low temperature, or without considering temperature until the CO_2 adsorption is reached to stable condition at the exit of the bed, is known as pressure swing adsorption. After the pressurizing step, the feed mixture flow will stop, and regeneration of bed will happen when pressure reduces, and the separation of the element is done from a gas which have relatively low absorptivity. Hence the cycle continues as adsorption cycle over a four fixed bed columns, each of working alternatively in one of four stages [40]. There are two different modes of an adsorption process: specifically, temperature swing adsorption (TSA) and Pressure Swing Adsorption (PSA). Adsorbent particles are present on both of the processes in the columns in which one adsorb and the second desorb so that the column work mutually on a concurrent way. The adsorption principle is followed by the pressure swing adsorption which means that it operates at constant temperature and low pressure at desorption scenario and at high pressure when adsorption took place at column. Special adsorptive materials (e.g., zeolites and active carbon) are used as a molecular sieve, preferentially adsorbing the target gas species at high pressure [41, 42] as shown in the Figure 2.6.

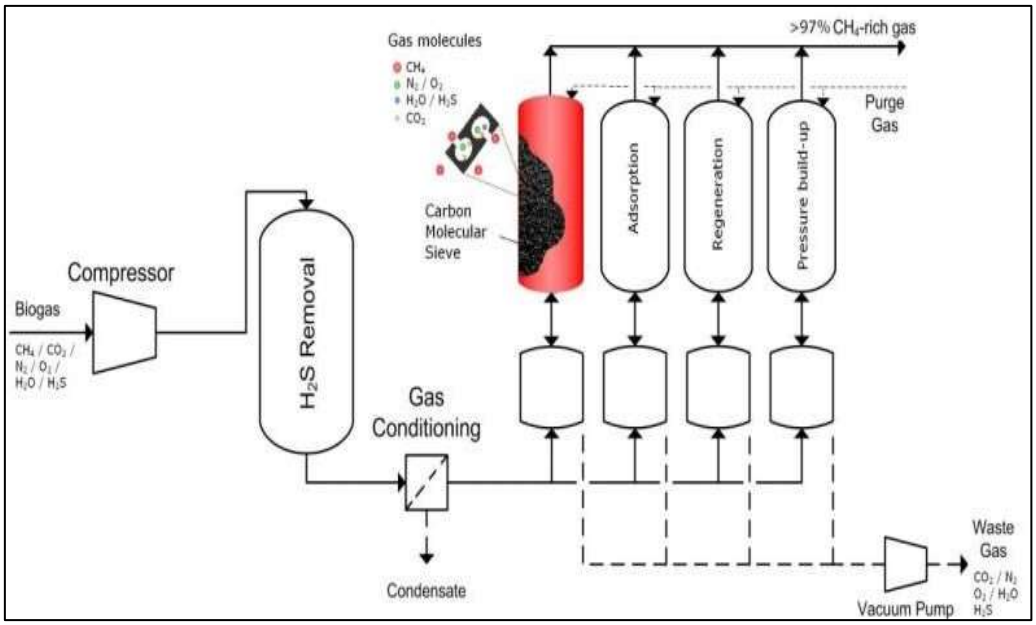

Figure 2.6: Pressure swing adsorption schematic diagram [42]

The important factors which affecting the adsorption capacity of carbon dioxide are relied on the type of functionalization, surface area and the pore structure. Some other factors which may further influence on the adsorption capacity of carbon dioxide are the humidity, temperature and partial pressure of carbon dioxide [43]. For the gas treatment in the power plant on the larger scale, the adsorption system working are not be enough or suitable to work with, so this type of issues produce a challenging environment for the available adsorbents [44]. The present adsorbents exhibit low selectivity in general and the fuel gas is processed in a high level of carbon dioxide concentration. On contrary, zeolites present high strength water vapour and strong affinity [45].

2.2.1.1.2 Temperature Swing Adsorption

Temperature Swing Adsorption (TSA) has an alternative regeneration procedure. Selective adsorption takes places on the adsorbent until to reach equilibrium. Desorption is done by providing extra heat so that higher temperature is maintained. So that requirement of extra heat make TSA costlier as compared to the PSA [40].

2.2.1.1.3 Electric swing adsorption

Electric swing adsorption (ESA) can have ability to lessen the CO_2 capturing cost which is associated to the other technologies of adsorption traditionally [46].

Electric swing adsorption is understood to be a lot more economical as compared to other carbon dioxide capturing techniques of PSA and TSA [47]. The electric current flow from the adsorbent in the electric swing adsorption [32].

2.2.1.2 Absorption

2.2.1.2.1 Physical absorption

Another class of solvents used for CO_2 separation are so-called physical absorption . It is based on the solubility of gases with solvents and low interaction between the acidic compounds in the feeding and liquid sorbent. Physical solvents substitute the chemical solvents when the acid impurities concentration in the flue gas is very high. Also, the physical solvents are non-corrosive in nature as compared to the chemical solvents. In general, the cost-effectiveness in the recovery of CO_2 depends on its gas partial pressure. Therefore, at low pressure, to compress the gas for the physical absorption is not practical as the process is too much expensive to proceed. So, Physical solvent is used for the purpose to execute the process at high pressure. Because of this solvent, regeneration is usually carried out by series of flash stages up to atmospheric pressure (and even vacuum) or by a stripping section with an inert gas [48].

The advantage of physical absorption is that the regeneration heat is low as compared to the amount required for the usage in amine-based solutions, as the desorbing heat is far lower than that of reaction. The ideal physical solvent should have a very low vapour pressure to limit leaks, high selectivity towards acid compounds over methane, hydrogen, and carbon monoxide. It is also desirable that it has low viscosity, high heat stability and a poor tendency to corrosion metals and an affordable cost. The most common physical solvents used in industry include: N-Methyl-2-Pirrolidone (NMP), MeOH (MeOH) Dimethyl Ether of Polyethylene Glycol (DEPG) and Propylene Carbonate (PC) [49].

2.2.1.2.2 Chemical absorption

Chemical adsorption took place when the carbon dioxide reacts with the chemical solvent to produce a compound which is weakly bonded and can be regenerated to produce the carbon dioxide and chemical solvent back to its original form [50]. The adoption of the chemical absorptivity technique is higher than other carbon dioxide capturing techniques as pure carbon dioxide is again regenerated at the end of the reaction or process [51].

2.2.1.3 Cryogenic separation

Cryogenic method is used for the separation of carbon dioxide commercially having high concentration of carbon dioxide so that it contains more than 50 % of concentration typically. To dilute carbon dioxide this technique is not used as flue gasses from the coal or natural gas boilers because a lot of energy is required for the refrigeration which is highly uneconomical [52].

Different stages of cryogenic separation involve cooling and compression processes from gas mixtures in order to sustain the phase changes of carbon dioxide and other components of gasses present in flue gasses or mixture. It is highly dependent upon the operating conditions of solid or liquid form of carbon dioxide or the components from which it gets distilled. Carbon dioxide present in the water vapours when mixed with the mixture it forms the solid carbon dioxide in the form of ice which lead to make major problems [40]. Advantage of the using this cryogenic separation technique there is no need requirement of chemical absorbent as it is operated in atmospheric pressure. Additionally, it produces carbon dioxide in liquid form which is a big advantage for the movement or transportation of carbon dioxide in an economical way [52].

To remove carbon dioxide from the high pressurized gasses is the most important application of this cryogenic carbon separation technique. The processes in which carbon dioxide present in great concentration like oxyfuel combustion and pre-combustion carbon capturing processes, this technique is very suitable [52].Disadvantages of using the cryogenic separation technique involves the liquid form of carbon contents in the cooling units may plug the system because of the formation of ice so the water content in the system is a high risk to the operation of the system and to prevent the water content running the system, the procedure is costly in terms of removal of water content from the gases. Another disadvantage of using the cryogenic technique is that the solid carbon dioxide in the system forms a layer which affect the heat transfer affects and seriously effect he overall efficiency of the system [53].

2.2.1.4 Membrane separation

Membrane separation is the novel capturing concept of carbon dioxide in which membrane is used for the separation of certain gasses from the substance, like in the case

in which carbon dioxide got separated from flue gasses (post-combustion system), separation of carbon dioxide from natural gas (natural gas processing), and separation of hydrogen and carbon dioxide (pre-combustion systems), separation of nitrogen and oxygen (oxyfuel combustion system). Different mechanism is used in the membrane separation technique as this technique is composed of semi-permeable barriers. Some of which are ionic transport, adsorption, molecular sieve, diffusion, and solution diffusion. Different types of materials are used as a membrane which involves organic polymeric and non-organic compounds like metallic, zeolites, carbon or ceramics or it could be porous or non-porous material [54]. In gas adsorption, the membranes behaved as contacting medium in between liquid solvent and gas and it does not provide the selectivity addition most commonly. There is some common advantage of the membrane separation techniques which involves its compactness in size, as the membranes are in the form of packed columns and minimize the risk of entrainment, flooding and foaming or channelling. It is required that the gas and liquid pressure should be kept constant or equal when carbon dioxide is transported across the membrane. The partial pressure of carbon dioxide highly influence on the efficiency of the separation technique [55]. Membranes are appropriate applications when the concentration of carbon dioxide is above 20%vol like IGCC and oxyfuel gas stream processes [50]. In the membrane separation technique, the membranes could also provide the selectivity by themselves and consist of the different mixtures including polymeric films and other components present in different composition and spread on the body throughout. The size of the components and the membrane material diffusion coefficient highly influence on the rate of separation between different components of the mixture. The partial pressure on the sides of the membrane is the driving force for the permeation. Due to the low selectivity of the membrane separation process, the fraction of the carbon dioxide capture also gets low and hence the purity of the captured carbon dioxide [56].

There are different types of materials that are used as membrane in the membrane separation technique, some of which are inorganic, cross-inked polymers, carbon-based and metallic-based [57].

2.2.2 Emerging technologies

There are many emerging techniques in the field of carbon capture and major are given in the Figure 2.7 in detail.

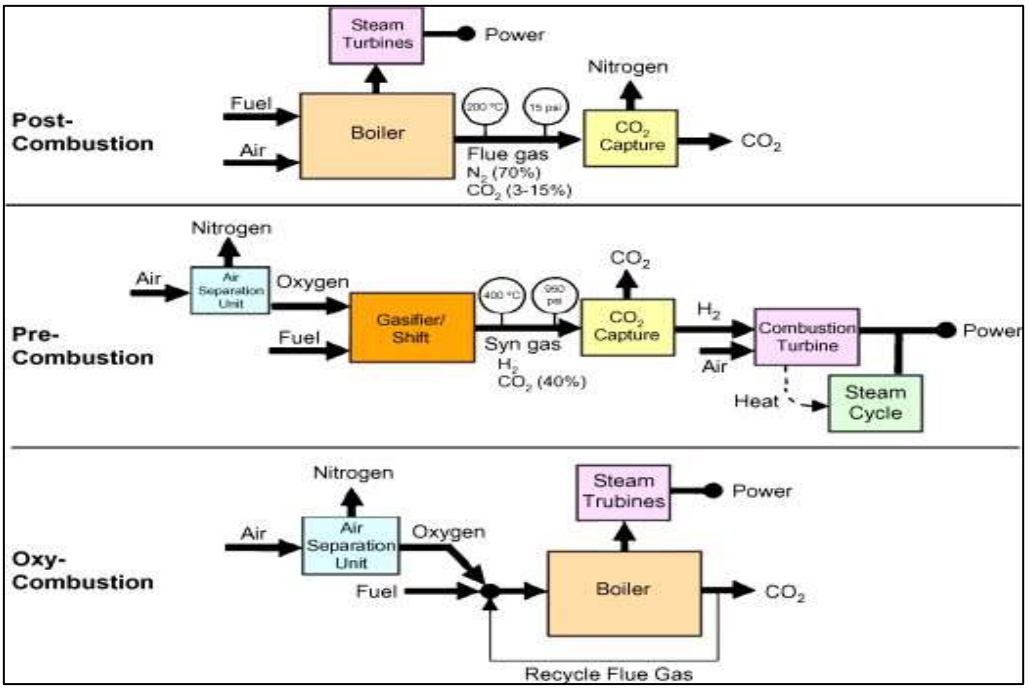

Figure 2.7: Emerging CO_2 capture techniques [58]

2.2.2.1 Pre-combustion

It is relatively an emerging technology and process for carbon separation normally used as physical solvent at low cost in the process i.e., selexol and rectisol presence in separation process. When pressure is high, carbon dioxide is inducing, and it is released when pressure gets lowered. No external source of heat is needed for the regeneration of carbon dioxide and atmospheric pressure is enough for the release of carbon dioxide from the system. In pre-combustion technique of carbon separation, the required energy consumption is half of the actual energy requirement for combustion processes [59]. The pre-combustion syngas is mainly composed of hydrogen and carbon monoxide [60]. Oxygen is also included in the process because of the reason that the carbon dioxide is not present before the combustion process as it is present in the form of coal not in the form of precursor. Fossil fuels of all types are classified as reformed or partially combusted and with the amount of oxygen in the sub-stoichiometric amount at the

specific pressure within the range of 30-70 atmospheric pressure to form the hydrogen and carbon monoxide i.e. the syngas. Steam is then added with the syngas to pass through the catalytic bed on which the water gas shift (WSG) reaction takes place for the conversion of carbon monoxide to carbon dioxide. The decrease in the temperature and increase in the steam composition during the WSG reaction amplifies the conversion from carbon monoxide to carbon dioxide and also increases the hydrogen yield [59]. The use of the physical solvent for the regeneration of carbon dioxide is the great advantage of using this separation technique as it not only best in economical ground but also consume less energy [60] and the disadvantage of using this process is its space consuming factor, as this technique of carbon separation required a whole power plant near to the turbine. Other than that, the complex chemical processes involved in the pre-combustion technique of carbon separation causes shut-downs in the plant which eventually effect the efficiency of the whole power plant [61].

2.2.2.2 Post combustion capture

Post combustion technique for the capturing of carbon include the removal of carbon dioxide from the flue gasses. The CO_2 in the flue gasses obtained from the combustion chamber of the thermal power plant is captured [60]. The advantage of using the technique of post combustion capture technology is the high rate of production of electricity than the other Integrated Gasifier Combined Cycle (IGCC) pre-combustion capturing technology and hence yield high thermal efficiency and lower the cost of electricity [59, 62]. The challenge of using this technique is to handle the very high temperatures and the protective use of high powered chemicals to capture carbon dioxide, for the purpose of eco-friendly regeneration of chemical solvent for the release of carbon [54].

2.2.2.3 Oxy-fuel combustion

The modification of the combustion process is called the oxyfuel combustion technique of the carbon capturing technology. The fuel gas is mixed with the pure oxygen during the combustion of fuel. As soon as the combustion starts, the fuel proportion gets lowered and the concentration of carbon dioxide increases and hence the cost of the process is less than other technologies for the separation of carbon dioxide; however, the cost consumed for the recirculation of fuel gasses and air separation may lower the cost benefit, but it is still the most economic carbon separation technique [61].

2.2.2.4 Hydrate-based separation

Hydrate-based separation is the very promising technique used for the separation of carbon capturing mechanism and has steal many attentions. In this process, the gasses containing carbon dioxide are exposed to water to form hydrates, as hydrates are formed the carbon dioxide gets separated as the hydrates of gas are in crystalline form under specific conditions of temperature and pressure. So when the hydrates of gas are formed, the concentration of gas components present are more than the gas phase quantity , it is because the hydrates has more tendency to store gas as compared to the components in gaseous state [63].

2.2.2.5 Chemical looping combustion

Chemical looping combustion technique is famous for the carbon dioxide separation from flue gasses. In this process, the direct contact of exhaust gasses and fuel gasses are prevented in order to avoid the mixing of air and carbon dioxide [64]. So, the oxygen is added in the process via oxygen-carriers solid material having the oxidant capacity by reducing themselves. So, after reaction the products would be the carbon dioxide and water vapours. Hence, the water vapours formed can easily be separated from carbon dioxide by the condensation processes and in this way the carbon dioxide gets captured separately [32, 61, 62, 65].

2.3 Biochar

In order to remove the carbon dioxide from environment, it is necessary to convert the biomass which is in the form of bio-graded coal into the form of carbon like charcoal which could be used in many applications in industry and domestically and which minimizes the effects of carbon dioxide emission. So, biochar is formed as a product after the treatment of coal. From many years this cyclic usage of carbon dioxide has caught sight of many researchers' industrialists. However, analysing the process there are two drawbacks. First, biomass pyrolysis produces many dangerous gasses like CO, C_2-hydrocarbons, polycyclic aromatic hydrocarbons (PAH) and CH_4 [66]. These types of harmful gases must not be sent to atmosphere and capture for utilization in the production of energy i.e., bioenergy. In order to control and adopt the capturing techniques the devices and instrumentation are too much costly and the procedure to adopt is much

complex to adopt for a traditional environment. Second drawback of the biochar is the risk of self-depletion as the biochar is stored in batteries and when it is exposed to air it oxidizes and undergo oxidation reaction and depletion could occur [67].

2.4 Hydrothermal Carbonization

In 1911, hydrothermal charcoal (HTC) was first discovered by a German, namely Friedrich Bergius, as a result of the study or production of H_2 from coal partial oxidation and the reaction of "Water Gas Shift" [26]. He was able to produce H_2 and CO at below 600 °C temperatures in presence of transitional metal (Ni & Pd) as a catalyst. It was observed during the experimentation and research analysis that a great quantity of CO were produced as peat was utilized as carbon during a chemical reaction and carbon remains present in the reactor also bear a resemblance to natural coal [68]. Studies conducted in the following years showed that biomass, treated in the presence of water at temperatures in the order of 180-250 °C and in high-pressure vessels, did not decompose into gas but mainly in solid products. For his studies in the research and development of high-pressure techniques, Bergius won the Noble Prize for Chemistry in 1931. After being somehow forgotten, hydrothermal charcoal was found again at the start of 21st century [26].

2.4.1 HTC to convert biochar into hydro-char

Hydrothermal carbonization biomass involves the treatment of material and then mix it with water with autoclave having a temperature of 250 °C (pressure - 4 MPa) in the time spam of about 2-6 hours [26]. During the process of HTC, the raw material goes through a very large network of different simultaneous reactions. The products are enhanced solid carbon residue and high level of OFG (oxygenated functional groups), small quantity of carbon in an aqueous form which is not harmful for the environment [69].

The final product has got different physical or chemical properties as compared to the original reactants or raw material. Actually, during the chemical reaction of HTC, different processes undergo to form the final product. Different processes involve flavoring, dehydration, decarbonation, re-condensation and hydrolysis. Hydrolysis used to decompose the biomass into by splitting foreign and ether bonds of bio-

macromolecules, mainly lignin and cellulose. Because of this process, the fragment and saccharides are formed which then transfer to the liquid state. Lignin can convert the hydrolyze into the phenol, whereas the saccharides cause further reactions and secondary chemicals. Hydrolysis is also, among the reactions listed above, the one that requires the least activation energy and always represents the first step of the HTC. Dehydration is the process in which the biomass matrix is formed with the removal of water causing elimination of oxidic sets. In decarbonization, CO_2 is removed from biomass and simultaneous removal of carboxylic groups. Because of decarbonization and dehydration aromatization occurs, and some replacements also occurs like C-C and C-O in a single binding functional oxidizing groups in biomass matrix. Hydrolysis is done when these mechanism proceeds and generate the furfural compounds which then break into aldehydes, acids, phenols etc. Inorganic elements are released because of the presence of these acids which act as catalyst in biomass matrix. If the compounds formed during the reactions are highly reactive in nature, then they must pass through a re-condensation process. Due to the flavor of cellulose degradation, the polymers of lignin are very reactive in nature and easily condense. Hence after the condensation process and the degradation of HTC, hydro-char is formed. Compared to the starting biomass, hydro-char has a high carbon content (an aromatic form due to decarboxylation reactions) and a low oxygen content. This is due to decarboxylation reactions and dehydration reactions that the removal of oxygen and hydrogen takes place in the solid state like CO_2 and H_2O. However, hydro-char generally contains a low ash content compared to the starting biomass, this is because after release from biomass degradation, the inorganic elements gets dissolved in liquid phase [70].

The presence of oxygenated functional groups (OFG) makes HC obtained a hydrophilic substance and therefore suitable to be used as a material for absorption, as a precursor of the activated hydro-char for synthesis processes or in catalysis reactions.

2.4.2 Hydrothermal carbonization parameters

In the process, parameters that affect the presence of OFGs are shown in the Figure 2.8:

- Temperature
- Residence time
- Reactant’s concentration

- Catalyst and processing conditions

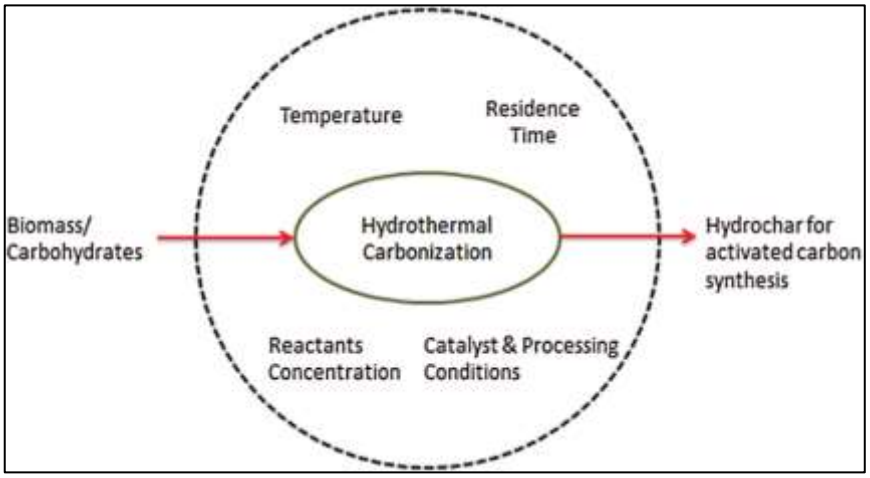

Figure 2.8: Parameters of Hydrothermal Carbonization [71]

2.4.2.1 Temperature

The temperature of treatment plays a very important role in the assessment of the progress about the degradation reaction stage, involving radicals and/or ions, and it is a very complex stage subject of the process'or kinetic studies. At low temperature the ionic reactions took place whereas, at higher temperatures ruptures occur in the homolytic bond. Higher yield and wide variety of products are formed at the higher achievable temperature ranges [71].

Higher temperatures lead to higher degradation rate and higher degree of condensation for the hydro char. Sevilla et al. worked on the ratios of atomic H/C ratios and O/C ratios, and stated that the ratios gets decreased as the process temperature increased [72]. In fact, many studies confirm that the carbon content in the final HC increases as the temperature increases as a result of biomass dehydration, which leads to the rupture of weak bonds of hydrogen and oxygen. This also leads to decrease in the hydrogen and oxygen content at the final product, this is because probably the fractions in which they are contained are more soluble and more easily volatile at high temperatures and pressures [73].

Moreover, temperature factor plays an important role in the processes in terms of final product and structure with the presence of oxygenated groups (OFGs) in the final structure of the hydro-char, the presence of which has the fundamental value in the porosity during the next activation phase [74]. In the study conducted by A. Jain et al.

[25], the value of carbonation hydrothermal temperature (200, 275, 315 and 350 °C) was studied in the OFGs content with the HC obtained from coconut shells. The rise in the attributes was partially polysaccharide (structural and energy storage) because of the presence of lignin in the shell. The temperature achieved at the maximum OFGs was 275 °C, and then they have a progressive decrease passing for 315 and 350 °C due to decomposition OFGs themselves in gaseous phases at higher temperatures. The treatment temperature also affects the size of hydro-char microspheres, which in turn is an important indicator of OFGs content. Using cellulose as a biomass, it has been possible to verify that for temperatures below 210 °C, these microbeads are not significantly developed; at more than 210 °C and with progressive increases in treatment temperature of up to 250 °C, a rise in the shape and size of the microbeads were noted.

The temperature also affects the final yield of the hydro char, understood as the ratio of the amount of HC produced to the amount of biomass at the start. In particular, some studies have shown that as the temperature rises, yields decrease. For example, a lignocellulosic biomass consisting of pine and fir wood has been observed to reduce HC yield by increasing the treatment temperature from 210 °C to 255 °C[75]. Yang G et al. worked in a study in which Canfor leaves were used for the production of HC: yield decreased from 64% to 62% from an initial temperature of 210 °C to 240 °C, and then decreased even more sharply to 56% to 270 °C [76].

2.4.2.2 Residence time

The time of residence of the treatment of hydrothermal carbonization is of fundamental importance to understand the progress of the distribution and reactions of the different products, the obtained species and quality. It has been observed that as the time of residence increases from 4 to 12 hours, there is a fall in the OFGs content (-OH and -COOH) of the HC surface. The excellent point was recorded after 6 hours of treatment, happened due to the decrement of either extra charring or dehydration process and the development of the stable groups of oxygenated from OFGs, or the decomposition of gaseous products at high time of residence [77].

With shorter residency times you will get products with lower condensation (high atomic ratios O/C and H/C) due to a lower degree of hydrolysis and curing. High residency times can process to form condensed products because of excessive degree of curing, which can

result in a reduction of OF groups on the surface of the HC due to intermolecular dehydration or aldolic condensation phenomena that convert the OFGs into stable oxygenated groups. This also affects the grain distribution of particles. In the presence of these stable oxygenated groups leads to an increase in the size of particles [78].

Finally, as the time of residence increases, a reduction in yield was observed, expressed as grams of solid residue (HC) on grams of starting biomass. This is mainly due to the curing of fragments dissolved at the liquid state which led to the formation of insoluble solids.

2.4.2.3 Reagent concentration

One of the main effecting factors, other than temperature, is the concentration of reagent (biomass) during the reaction environment. In particularly, low reagent concentrations minimise the possibility of cross-reactions of the species involved, and this produces a clearer final product spectrum. It is also true that a higher reagent-water ratio results in a greater degree of curing at relatively shorter stay duration whereas, most of non-hydrolysed reagent leaves at same time duration. At high concentrations of substrate, products which are less condensed (higher atomic H/C ratios and o/C ratios) produced precisely because of incomplete hydrolysis. This results in a higher content of OF groups on the HC surface even at high treatment temperatures [79].

Lignin, a component of lignocellulosic biomass, which has significant impact on the chemical and physical properties of HC. In particular, its presence in the raw material has been shown to hinder or in some cases prevents the process of charring, due to the development of a protective shield on the biomass surface. Type of raw material has an influence on final energy and HC yield content, nevertheless they have no significant impact on the final content of carbon statistically [80].

The type of substrate influences the final characteristics of the hydro-char produced and this is widely demonstrated in the literature. It has been shown that, for example, the exorcism of the sugar, glucose and fructose to name a few, degrade during hydrothermal treatment in hydroxy methyl furfural (HMF) and condense into carbon solid materials with similar chemical and structural composition [81].

2.4.2.4 Catalyst and processing conditions

Catalysts are used during HTC to fasten the reaction. Carbon-based materials and in particular porous type of state are in demand for the large amount of versatility in their properties and due to their large range in applications such as air or water purification, gas separation, water purification, double layer electrodes, fuel cells, chromatography, catalyst supports, drug delivery, electrochemical capacitors and sensors [26]. Some of these included Ni, CeO_2, Al_2O_3 In the production of electrodes for lithium-ion batteries, supercapacitors, catalysts are used for the reaction of oxygen reduction in combustible cells [66, 82].

2.5 Hydro-char

Hydro-char generally consists of a partial charred type of product having brown in color. When it is exposed to microscopic techniques for the inspection purposes, it exhibits interesting changes in its material properties obtained after hydrothermal treatment compared to the starting biomass [83].

Some of the limitations that hinders the direct exploitation and effectiveness of products obtained by HTC for usage in different applications (e.g., separation techniques, catalysis, energy storage and production), are the based porosity and surface area [84].

Figure 2.9: Hydro-char prepared at laboratory of "Principles of chemical engineering and applied thermodynamics" at University of L'Aquila

2.5.1 Hydro-char properties

From the analysis of the literature, it was possible to compare the most common data regarding the hydrothermal treatment of different forms of biomass.

For example, the surface area of the HC at 250 °C (2-6 h) obtained from eucalyptus sawdust, barley straw and corn stover are 4.4 m^2/g, 4 m^2/g and 8.3 m^2/g respectively [19]. In a research study it was mentioned that, using pine wood as biomass gives surface area of about 21 m^2/g and which was achieved by HTC on 300 °C for 20 minutes [83]. Falco et al. worked on this type of biomass at the start and substantial difference is found within the same biomass at different treatment temperatures: the maximum surface area is at a temperature of 200°C. The resulting HC pores are varying in size, but in any case, not exceed 50 nm (macropores) [85].

In the case of HCs obtained or by monosaccharides, the problem relating to the low surface area and porosity was overcome by the use of strategies related with hard-templating or it could be done by adding structuring agents. Such synthetic pathways are effective due to the homogeneity of the reaction mixture. While, in case of general lignocellulosic biomass and cellulose biomass the approaches which were used previously was not applicable because of the insolubility of the substrate of cellulose in the presence of water, therefore, for introducing the porosity into the HTC coals obtained from lignocellulosic biomass, post-synthesis methods, such as chemical activation, are needed [85].

3. MATERIALS AND METHODS

3.1 Introduction

The literature shows that with the passage of time different kinds of techniques have been applied to capture carbon. Modern techniques now a days using different kinds of adsorbents for carbon capture like, zeolite, charcoal, membrane, and biochar etc. and each one has their own pros and cons. Similarly, hydro-char has been used in some cases and based on the literature review results of previous chapter indicates that hydro-char is also a good adsorbent and a good precursor for carbon capture, environmentally friendly

The following chapter will briefly explain about the method to achieve hydro-char from residua lignocellulosic biomass, activation of hydro-char and the description of experimental set-up. Finally, different kinds of tests have been performed to check the capability of hydro-char for carbon dioxide capture.

3.2 Materials

Silver fir raw wood has been used in this research work to obtain hydro-char. Raw wood was first cracked into small pieces of sawdust (also called biomass) with the help of a reaper. Since this sawdust might have water contents inside and to obtain dry biomass for proper weighing it was placed in an oven at 55 °C for 24 hours. The conversion of raw wood into reaped sawdust is shown in the Figure 3.1.

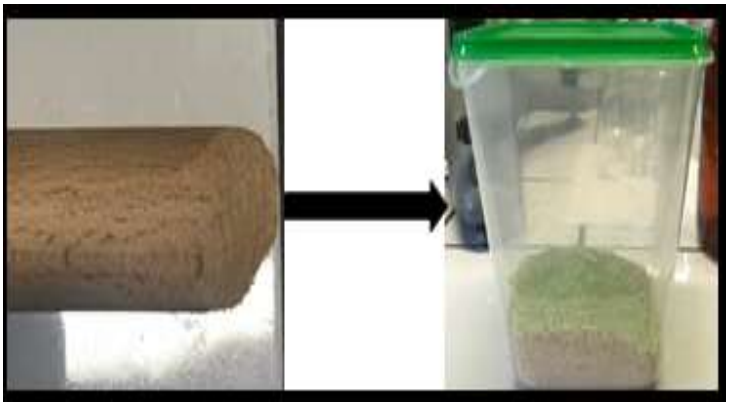

Figure 3.1: Silver fir wood to Reaped sawdust.

The dry biomass was further processed. Water that was used to prepare hydro-char from sawdust during all the hydrothermal carbonization experiments was demineralized having $\sigma = 0.005$ mS/cm.

For the activation of hydro-char, Hydrogen chloride (HCl) (Sigma-Aldrich grade 24.5%-26.0%) and Potassium hydroxide (KOH) (Sigma-Aldrich Corporation US, grade ACS reagent, Reg. Ph. Eur.) were used.

Gases used during the dynamic adsorption tests belongs to Rivoira S.p.A. company with following grade: methane grade 4.5, carbon dioxide grade 4.0 and nitrogen grade 5.5. Glass beads were used during the packing of the column (density = 2500kg/m^3 and particle diameter =106-355 µm), blocked in the reactor and separated from the hydro-char with quartz wool layers.

3.3 Experimental procedure for hydro-char

Water and biomass in the ratio of 7:1 respectively as decided through literature [86, 87] before experimentation were added into the reactor in which vacuum is created before with the help of a vacuum-pump. The parameters for the preparation of hydro-char have been set according to the Table 3.1 given below.

Table 3.1: Operating parameters for hydro-char preparation

Biomass	Water	Temperature	Residence time
9.5 g	66.5 g	200 °C	0, 30 & 120 min

The reactor, after proper sealing, was placed inside the oven and the residency time was recorded when the desired temperature of the oven is reached. After the test, the reactor is first taken off from the oven and cooled by compressed air to the temperature of 150 °C and then with the help of running normal water under the tap up to the room temperature.

3.3.1 Mass balance (200°C_0M and 200°C_120M)

Mass balance of the tests (200°C_0M and 200°C_120M) are shown in the Table 3.2 and the liquid analysis in this case was not possible.

Table 3.2: Mass balance of the tests

Temperature [°C]	**Residence time** [Min]	**Biomass** [g]	**Water** [g]	**Hydrochar Yield** [%]	**Hydrochar** [g]	**Process water recovered [**g]	**Gas** [g]
200	0	9.51	66.54	0.824	7.830	48.579	-
200	120	9.50	66.53	0.714	6.785	50.328	0.009

The final product consists of a mixture of liquid and solid phases in which hydro-char is in the color of dark brown as shown in the Figure 3.2.

Figure 3.2: Final product before filtration

The solid product (hydro-char) is separated from the liquid phase by filtering on filter paper from 0.45 µm with the help of a vacuum pump attached as shown in the Figure 3.3.

Figure 3.3: Filtration of hydro-char by using vacuum pump

After filtration, both the solid phase and the wet filter are first weighed and then placed in the muffle furnace at 100-120 °C for 24 hours. Both the dry phases are added together and then shifted to the Endecott's sieves with size of 355 µm and 106 µm.

The fraction collected in the 106 µm sieve was used for the next activation phase. Figure 3.4 shows the Endicott's sieves including bottom sieve.

Figure 3.4: Endecott's sieves of size 355 and 106 µm

3.3.2 Hydro-char activation

The procedure for hydro-char activation like selection of pressure, temperature, and weight ratio (KOH, HCl and hydro-char) was adopted by considering in depth literature review.

Formation of porous structure of hydro-char improved by chemically activating with KOH [88]. KOH activated carbons are better as compared to commercial activated carbons [89]. Activation of carbon by using $ZnCl_2$ shown the increase in surface area as compared to normally produced biomass by up to 80% [77]. The authors have concluded in the previous research that highest adsorption capacity of hydro-char (activated) obtained at a temperature of 600 °C and with KOH/HCl ratio of 2:1 at same temperature and pressure conditions [90]. Potassium hydroxide with KOH/hydro-char ratio of 2:1 was combined with all the three types of hydro-char samples, respectively. The mixture is then placed in a muffle under nitrogen flow and heated up to the temperature of 600 °C at the heating rate of 3 °C/min, as shown in the Figure 3.5. After reaching the desired temperature, the crucible stayed inside for one hour. The sample was then cooled down at the rate of 5 °C/min to about 100 °C and then placed in the dehumidifier until room temperature reached.

Figure 3.5: Mixture placed in the muffle for activation purpose.

Meanwhile, 10% by weight solution of hydrochloric acid was prepared. The use of molar solution of HCl was actually used to neutralize the KOH moles present inside the solution and through washing to ensure complete removal of inorganic salts that was formed during activation process, that can affect the adsorption capacity.

The color of the hydrochar after activation was changed to black from dark brown as shown in the Figure 3.6.

Figure 3.6: Colour change after activation

HCl suspension were mixed with activated hydro-char in an autoclave bottle and passed through slow agitation process throughout the night as shown in the Figure 3.7. Finally, the filtration process was carried out by using funnel and conical flask. The wet solid residue was then washed with distilled water in a beaker and left in the agitation for 20 minutes after that it was filtered again, and pH was measured because required pH is between 5-7 which was achieved after 5 to 6 successful washes.

Figure 3.7: HC suspension activated with 10% HCl solution.

The wet solid part was weighed and then placed in an oven for dry process at 105 to 200 °C. Summary of each individual test is shown in the Table 3.3.

Table 3.3: Summary of Activated Hydro-char samples

Sample	HCl (g)	KOH (g)	Washes	Yield (g)
HCA_200^{0}C_0M	10.012	20.026	5 washes of 800 mL each	1.324
HCA_200^{0}C_30M	10.015	20.0887	4 washes of 800 mL each	1.5
HCA_200^{0}C_120M	10.07	20.167	4 washes of 750 mL each	1.97

3.3.3 Hydro-char characterization

Hydro-char characterization methods used to relate morphological, textural, and chemical composition to the operating parameters, such as temperature, pressure, rate of heating and atmospheric reaction with the hydro-char properties are the following techniques.

- Surface area measurement (BET theory) [91]
- Pore size distribution determination method (BJH) [93]
- Elemental analysis (CHNS)
- Scanning electron microscopy (SEM) equipped with Energy Dispersive Spectrometer (EDS)

3.3.3.1 Porosimetric BET-BJH analysis

BET (Brunauer–Emmett–Teller) theory is a useful analysis technique that describes the physical adsorption of gas molecules on asolid surface for the measurement of the specific surface area of the materials [91]. It is a non-destructive physical adsorption technique generally made at low temperatures (77 K) and tends to assess the amount of a gas, usually nitrogen (or helium), adsorbed on the surface of the solid at different pressures after being properly degassed. With gas systems, the field of analyzed pores ranges from micropores to macropores, i.e. from pores of about 2 degrees to pores about 0.4 μm in diameter [92]. Using the experimental measurement of the physical isotherm as of $N_{2,}$ at boiling temperature of nitrogen (77 K), it is possible to determine when a "statistical" monolayer has been reached, that is, when in the isothermal the amount of gas absorbed is equivalent to the complete absorption of a single layer knowing then the number of gas molecules needed to cover the surface of the solid with a monolayer and notice the area occupied by a single molecule.

The instrument used for the measurement is NOVA 1200e Alfatest of Quart chrome, shown in Figure 3.8.

Figure 3.8: NOVA Porosimeter for BET & BJH analysis

Barrett, Joyner, Halenda (BJH) theory is a pore size distribution determination method. It is a mathematical numerical integration process, through which the distribution curve of the diameter of the pores is derived from the Kelvin equation, which relates the r^i_k radius to the relative pressure (P/P_0), at which the condensation of nitrogen within the pores occurs [93, 94]. The absorption of a gas on the surfaces of dusts and solids is also used to determine the distribution of the size of the pores. The diameter of the pores and the specific volume, in fact, can be determined by the data of adsorption or desorption of isotherms through iterative calculation methods.

3.3.3.2 Elemental CHNS

It is both qualitative (which one) and quantitative (how many) technique and is beneficial in organic matrices and other types of materials for quick determination of carbon, nitrogen, hydrogen, and sulfur.

In the combustion process at about 1000 °C, carbon was converted into carbon dioxide, hydrogen into water, nitrogen into nitrogen dioxides and sulfur into sulfur dioxide. The combustion products are sent out of the combustion chamber by an inert transport gas such as helium and passed through heated copper (about 600 °C) in high purity. Copper can be located at the base of the chamber to remove unconsumed oxygen in the initial combustion and convert any nitrogen oxides into nitrogen dioxides. The gases are then passed through the absorbent cones to leave only carbon dioxide, water, nitrogen, and sulphur dioxide. Gas recognition can be carried out in a number of ways, including (i) a separation in Gas Chromatography (GC) followed by quantification by detection of thermal conductivity (ii) a partial separation by GC ("frontal chromatography") followed by the detection of thermal conductivity (CHN but not S) (iii) a series of separate infrared and thermal conductivity cells for the detection of individual compounds. Quantifying the present elements requires a first phase of calibration using compounds called "micro-analytical standards" of high purity such as acetanilide and benzoic acid [95]. The tool used for analysis is the PERKINELMER-2400 SERIES II analyzer as shown in the Figure 3.9.

Figure 3.9: PerkinElmer 2400 Series II CHNS/O Elemental Analyzer

3.3.3.3 SEM-EDS Analysis

Scanning electron microscopy (SEM) and energy dispersive X-ray spectroscopy (EDS) are used for the analysis of the morphology and elemental composition of surface of the sample . These methods are broadly used for material surface analysis, examination of product malfunctions, reverse engineering, and contaminant identification.

When a focused electron beam is used to scan the material or sample surface the SEM produces a lot of different kinds of signals to detect the behaviour of sample surface. The three most common modes of operation in SEM analysis are backscattered electron imaging (BSE), secondary electron imaging (SEI), and EDS [96].
The physical process behind SEM is comparatively easy and same of a cathode ray tube. The electrons are generated at the cathode by passing current through a metallic filament. The produced electrons are then moved to the direction of anode using high voltage. At the anode, the electron beam is collimated via a series of magnificent orifices and produced electromagnetic fields that covers the column. The electron beam eventually exits the column directed in the direction of the sample surface. When the contiguous beam strikes the sample, several physical phenomena appear in which one of them is the microscopic structural image. The EDS detector is the device for calculating the energy of the released photons in the X-ray electromagnetic spectrum. The detector is a crystal that is cooled to superconducting temperature for high quantum efficiency. The detected X-rays are segregated into energy channels based on their interaction with the detector and form a spectrum of detected energies.

With the spectrum, we can identify the peak energies and determine what electron transition occurred and thus what element it corresponds to. We can also couple this data to the SEM imaging technique to form X-ray "maps" of data to overlay or present areas of high individual elemental concentrations [97]. The instrument used is a Philips XL30 CP Scanning Electron Microscope (SEM) equipped with an Energy Dispersive Spectrometer (EDS), shown in the Figure 3.10.

Figure 3.10: Philips XL30 CP Scanning Electron Microscope (SEM) equipped with an Energy Dispersive Spectrometer (EDS)

3.4 Experimental apparatus

All the experimental apparatuses used for the preparation of hydro-char and capture tests performed were either prepared or available at the laboratory of "Principles of chemical engineering and applied thermodynamics" and "Fluid-dynamics and chemical reactors" of the University of L'Aquila.

3.4.1 Bed design

The fixed bed (43 cm height) for CO_2 capture tests is made of stainless steel having different sections used for quartz wool, rough glass beads and the adsorbent as shown in the Figure 3.11.

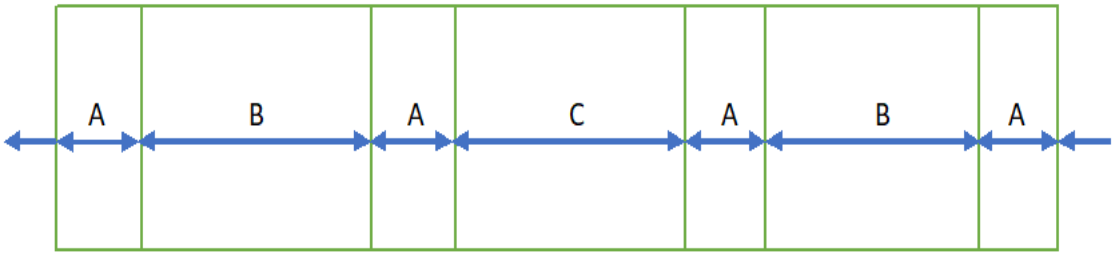

Figure 3.11: Fixed bed layout: A quart wood; B glass beads; C hydro-char

The mass of the materials used in the bed and the space of the bed used by these materials are shown the Table 3.4.

Table 3.4: Materials used in fixed bed reactor

Layer	Material	Mass	Height
A	Quartz wool	7.8 g	1.5 cm
B	Rough glass beads	33.5 g	31.5 cm
C	Hydro-char	0.5-2 g	10 cm

Quartz wool as a flow distributor was used to close the reactor at both ends and to separate the rough glass bead materials from the hydro-char. The polished glass beads made of glass having diameter less than 250-355 µm were used as a filling material.

Total weight of the glass beads were 33.5 g and the corresponding height of 31.5 cm of the bed was used. Remaining height of 10 cm was used for the different amounts of hydro-char that depends on the density of all the prepared samples as shown in the Table 3.5.

Table 3.5: Hydro-char mass loaded in each 3 tests

Hydro-char	Mass (g)
Hydro char (not activated) at 200 °C and 120 Minute	1.835
Hydro char (activated) at 200 °C and 120 Minute	1.135
Hydro char (activated) at 200 °C and 0 Minute	0.695

Pressure drops in the column were calculated by using Ergun equation [98] and minimized by using spherical glass beads.

$$\frac{\Delta P}{\Delta z} = \frac{v}{D_p} \cdot \frac{1-\varepsilon}{\varepsilon^3} \cdot \left(\frac{150\ (1-\varepsilon)\mu}{D_p} + 1{,}75\ \rho v \right) \qquad \text{(Equation 3.1)}$$

where $\Delta P/\Delta z$ is the pressure drop per unit length of the column, v is the space velocity, D_p is the mean diameter of the glass particles, ε the void fraction, μ and ρ the viscosity and density of the gas, respectively.

3.4.2 Reactor

The first equipment used was a batch reactor (R1) in AISI 316 stainless steel with an inner volume of around 200 ml. The control instruments the design of the piping are shown in the Figure 3.12. Stainless steel rod having internal diameter of 1mm has been used for the connections among different devices (pressure and temperature gauges etc.). R1 reactor is equipped with a three-way valve. Before each test vacuum was created with the help of a pump P1 through valve V1 inside the reactor for 15 minutes. During HTC's treatment there was a valve V2 connected to valve V1 for the gases that were produced during the reaction. The R1 reactor is also equipped with the temperature and pressure gauges connected through thermocouples. All thermocouples through transmitter send the information to the controller, which keeps the temperature on the desired set point [69, 87, 99].

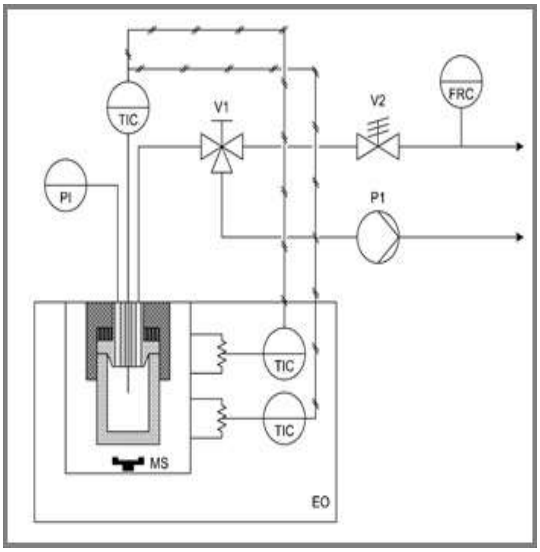

Figure 3.12: Layout design of the reactor [69]

3.4.3 Plant design

The layout design of the scheme used to measure the adsorption capacity of the hydro-char is shown in the Figure 3.13. The supply of the gases (CO_2, N_2 & CH_4) was sent through the cylinders by the piping having diameter of 6 mm made of stainless steel (AISI 316L).

The scheme also includes mass flow meters/controllers (Bronkhorst high-tech), pressure gauges to control pressure, three-way valves (A, B, C & D), filters and the on-line ABB analyzers (Individual gas components are quantitatively analyzed in a binary or quasi-binary mixture based on their thermal conductivity.) which are connected to the computer. After the column there is a pressure regolator (Bronkhorst) to keep the pressure at the desired level.

After every two seconds the data of the samples are captured by the analyzer and stored in the computer for the analysis.

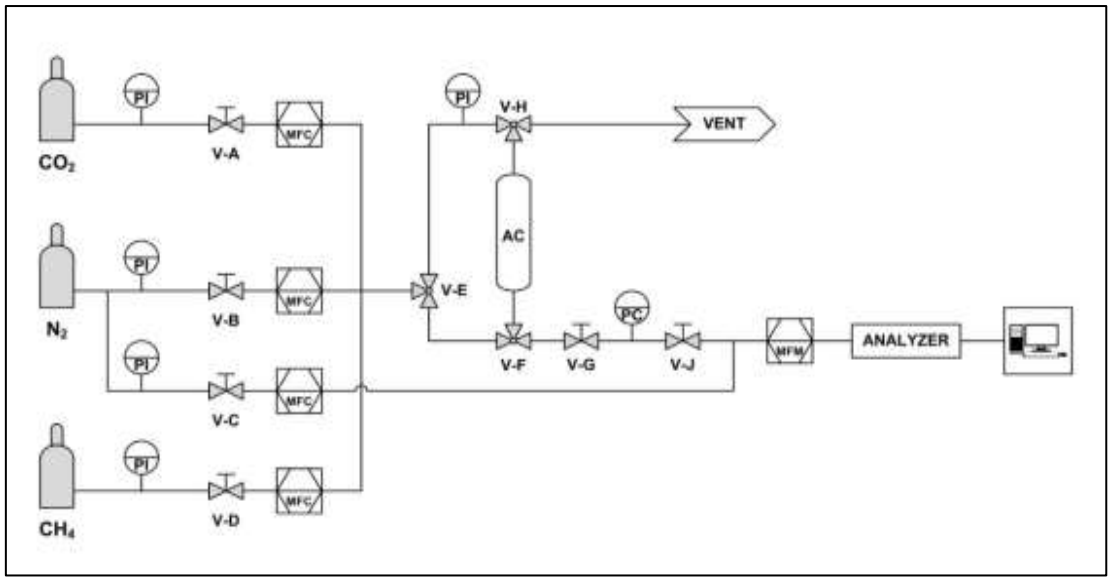

Figure 3.13: Plant description flow sheet

The gases carbon dioxide (CO_2) and nitrogen (N_2) go inside the column through the respective mass flow meters (MFM) on which scale was set at 100 Nml/min for both. Nitrogen is used in the scheme for reaching the optimal flow rate for ABB system and finally for washing of bed. Supply of the gases through different line is shown in the Figure 3.14. The MFM-BB valve sends N_2 line to the system and has a bottom scale of

100 NmL/min, the MFM-D with a full scale of 10NL/min sends N_2 dilution to the analyzers, while the MFM-C, with a full-scale of 5 Nl/min, sends a counter-current stripping nitrogen into the reactor.

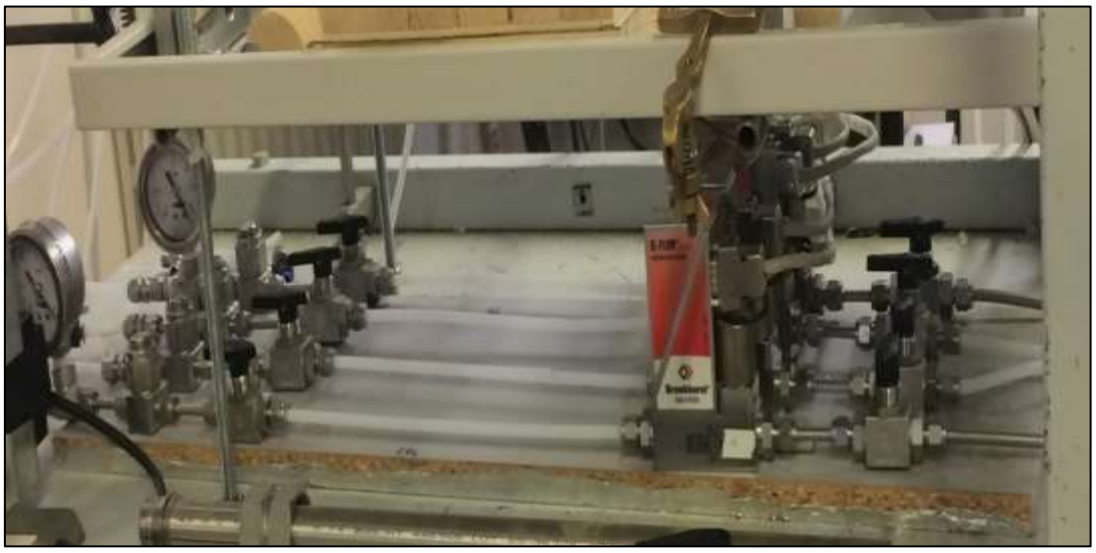

Figure 3.14: Gases supply lines

Before mixing sent to the reactor via a 3-way V-E valve, V-F needed to ensure the ability to by-pass the bed at the beginning of each test to calculate the actual composition of the inlet gas and total flow rate. At the head of the reactor there is a second 3-way V-H valve used during the bed regeneration phase (PSA). The flow enters the fixed-bed reactor, consisting in an AISI 316L stainless steel tube with an inner diameter of 0.96 cm and a length of 80 cm. The gas is kept at the chosen pressure by the pressure regulator. dilution N_2, after the pressure reducer, passes first through the MFM, which measures the flow rate, and then to the ABB analyzers, which communicates the concentration data to the *WDA* software, made by *Digi power Ltd.*

3.4.4 Column design

The setup picture of the column design was made at the laboratory of Fluid-dynamics and chemical reactors is shown in the Figure 3.15. The vertical column shown with white and orange tapes on it is the actual column for the test in which hydro-char has been added to capture CO_2. Dial gauge was used to monitor and control the pressure inside the column and different valves were used to release and control the gases inside the column.

Figure 3.15: Column design

3.5 Operating procedure

The following was the operational procedure executed in the capture tests.

V-A (CO_2)

V-B (N_2 Stripping/ Process)

V-D (N_2 Technical Dilution)

V-C (N_2 Addition)

- ❖ Set pressure at PC and start WDA software to operate the MFM/Cs.

1. Open V-B (N_2 Stripping/ Process) and V-D (N_2 Technical Dilution).
2. Washing bed with V-A (N_2 Stripping/ Process) and record outlet, % CO_2 & Pressure (Until pressure set at PC is constant).
3. Close bed and open bypass by valves V-E and V-F until stable pressure is reached.
4. Open V-A sending CO_2 and note % outlet, % CO_2 & Pressure.
5. Close V-A and wash bypass with N_2 until CO_2=0 and outlet constant.
6. Close Bypass and open bed until setting pressure is achieved at PC.
7. Open V-A and start chronometer and PC recorder. Write down dead time read from the chronometer (it is not a compulsory step, but it is for safeguarding the

result). Wait until the same point 3 values are reached. Note that those values should be almost the same of the same point for blank test in order not to wrongly estimate the amount of CO_2 adsorbed.

8. PSA regeneration:

a) Close V-A (stop CO_2) and V-B (Stop N_2 Stripping/ Process)
b) Set P=0 bar on computer
c) Close V-G
d) Open V-H valve to vent until P=0 bar is reached in the bed (few seconds)
e) Close V-H valve
f) Open V-G
g) Open N_2 Stripping/ Process until % CO_2 step 5 is reached and take note of % outlet, % CO_2 & Pressure.
h) Save data recorded from software and press stop.

9. Preparing bed for the next test:

a) Set new pressure on PC and start WDA.
b) Open N_2 Stripping/ Process until desired pressure is reached.
c) Go back to step 6.

Once we reach point seven, we move on to the regeneration stage of the bed. At this stage, the CO_2 adsorbed on the hydro-char according to PSA technology is removed. During this phase, the bed is depressurized favoring the removal of the gas trapped in the porous structure of the material. The bed regeneration procedure can be considered finished when the value of the volumetric percentage of CO_2 recorded in point 7 reaches 0.00 vol%. The advantage of this technique over other technologies such as the TSA or ESA, is that the time required for the desorption phase is considerably shorter, in the order of minutes or seconds since the bed can be put under pressure and depressurized very quickly.

After this phase, the bed is returned to the desired pressure in order to start a new test. Before each test, a test was performed to seal the plant with pressure nitrogen to detect any gas leaks.

The analyzed samples of the activated hydro-char obtained at a temperature of 200 °C and with a reaction time of 0, 30 & 120 minutes, were tested at 2, 3, 4 & 5 bar pressure

and an inert material that was used during packing of column as "Polished Glass Beads" with a diameter less than 250-355 µm and density equal to 2580 kg/m^3.

Cyclical tests were carried out to assess the stability of the material related to the adsorption capacity. The summary of the tests carried out are shown in the Table 3.6.

Table 3.6: Summary of tests based on pressure range

Sample	Pressure (bar)			
	2	3	4	5
Blank	✓	✓	✓	✓
HCA_200C_0M	✓	✓	✓	✓
HCA_200C_120M	✓	✓	✓	✓

3.6 Operating conditions

The assessment of the adsorption capacity of the samples analyzed was carried out by processing a mixture of gas consisting of CO_2 and N_2 in volumetric ratio 60% - 40%. The capacity of gases passes through the system has a range of 180 NmL/min, of which 100 NmL/min of CO_2 and 80 NmL/min of N_2. The technical nitrogen has a range of 750 NmL/min at a pressure of 1.5 bar is not sent to the column, but joins the mixture downstream of the reactor with the sole purpose of allowing the reading to the ABB analyzer, for which the optimal range value is 1NL/min. The operating temperature is 25 °C.

Table 3.7: Operating conditions

Gas	Valve Opening	Flowrate	Pressure
CO_2 line	MFC-A =100%	100 mL/min	6 bar
N_2 line	MFC-B = 80%	80 mL/min	6 bar
N_2 technical(dilution)	MFC-D = 7.5%	750 mL/min	1.5 bar
N_2 (addition)	MFC-C = 4%	200 mL/min	6 bar

The flow rates were chosen according to the maximum range permissible by the Bronkhorst pressure reducer of 50 NmL/min.

3.7 Adsorption capacity calculation

The data analysis method for capturing CO_2 is the model that describes the dynamics of the process by comparing a blank test, carried out with the adsorbent material. The main use of the blank test is to allow the calculation of the holdup of the gas phase, hold up the system when there is no adsorption. The model correlates the instantaneous concentration of CO_2 in the gas current coming out of the reactor with the amount of CO_2 adsorbed [100]. The mathematical model used in this work to determine the amount of adsorbed CO2 is a first order model with dead time flow distribution and it was proposed by Di Felice et al. [100].

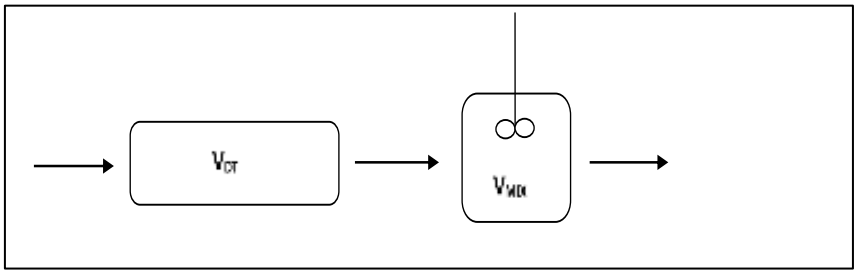

Figure 3.16: First order descriptive dead-time model for gas mixing in the entire system

The volumetric flow of CO_2 was calculated with the following formula:

$$Q\ \left[\frac{L}{min}\right] = \frac{\%Outlet}{100} \cdot \frac{\%\ CO_2}{100} \cdot C_{corr} \cdot 5000\ NmL/min \qquad \text{(Equation 3.2)}$$

where 5000 Nml/min is the bottom scale of the MFM Bronkhorst. This coefficient is calculated using the following formula, provided by the Bronkhorst manual:

$$\frac{1}{C_{corr}} = \frac{\frac{\%CO_2}{100}}{C_{CO_2}} + \frac{\frac{\%N_2}{100}}{C_{N_2}} \qquad \text{(Equation 3.3)}$$

where $C_{CO_2}\ and\ C_{N_2}$ they are corrective factors and are worth 0.74 and 1, respectively.

Finally, by dividing the volumetric flow by the molar volume occupied by a mole of gas at the pressure of an atmosphere and at the °C (normal condition), 22.414 NL/mol, you get the molar flow:

$$\left[\frac{mol}{min}\right] = \frac{Q}{22.414} \qquad \text{(Equation 3.4)}$$

This figure was then normalized by dividing the molar flow recorded at all times by the average molar flow data, calculated from the average of the last twenty points recorded in the adsorption test.

Figure 3.17 shows the blank test response curve at the pressure of 2 bar. As can be seen from the response curve, 100 seconds pass before the analyzer starts recording the presence of carbon dioxide. This time frame is called dead time which is associated to the plug flow behavior of the system and depends on the pressure applied to the gas.

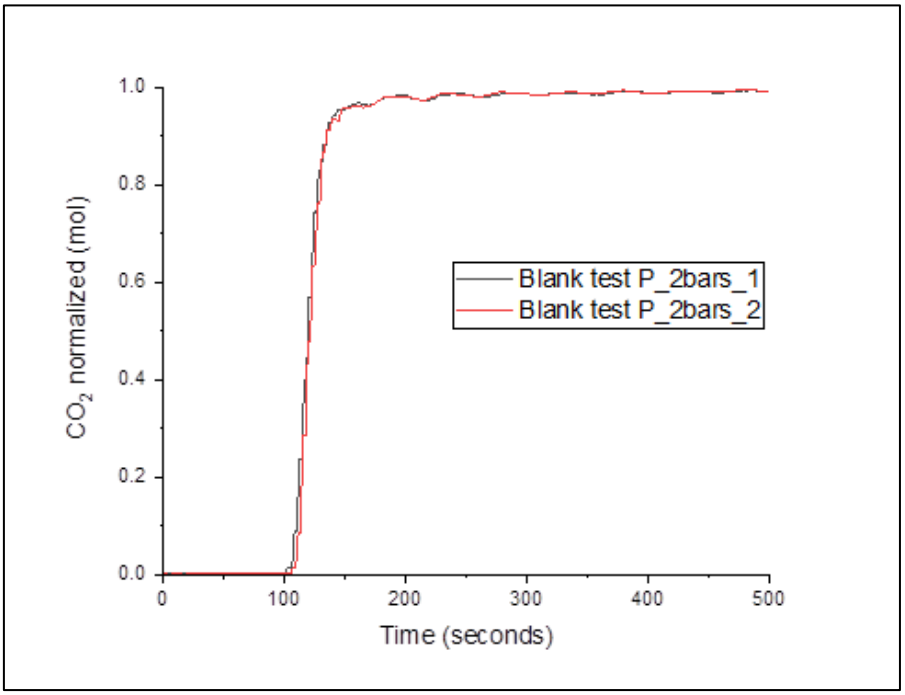

Figure 3.17: Response curves, first and second cycle, at the pressure of 2 bar

If there is an adsorbent in the reactor, there is a more delay in the curve due to the adsorption of CO_2. This is correct only if inside the reactor the physical arrangement of the material is the same as that of the blank test (same volume and length of each section, i.e., quartz wool, glass beads and sample). By keeping the pressure, flow rate and all other operational parameters constant, we expect the adsorption curves obtained for the analyzed samples to move along the horizontal axis relative to the blank test curve.

The accumulation of CO_2 in the solid phase of the fixed bed is the difference among the gas hold-up and the total amount of CO_2 calculated in the blank test present in the whole

system. Unlike a gas that flowed through the bed filled with the sample and with blank, it was possible to assess the ability to absorb at a given pressure[101]. For this reason, the calculation of the area below the blank and sample response curve was calculated by integration, choosing as the integration range for ordinate axis 0-500 seconds as shown in the Figure 3.18.

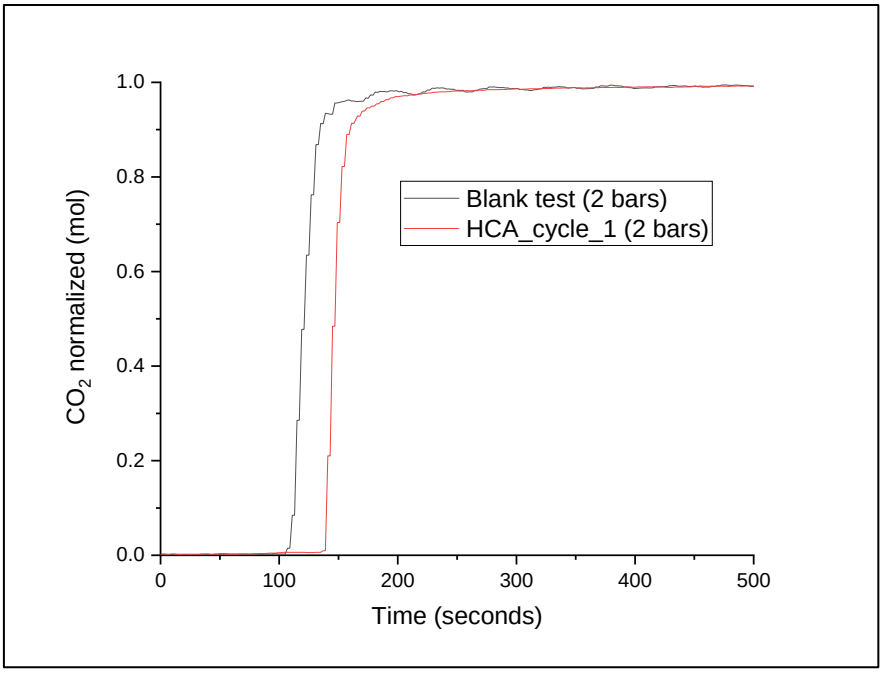

Figure 3.18: Comparison of CO_2 blank response curve with a hydro-char adsorption cycle activated (HCA) at the pressure of 2 bar

Multiplying the difference of the areas by the average molar flow rate of plateau obtained as an average of the last twenty points recorded, and dividing this result by the amount of adsorbent present in the column, you get the adsorbent capacity of the sample expressed in mmol/g

$$\int_0^{600} Blank \cdot dt - \int_0^{600} sample \cdot dt = \Delta A\ [s] \qquad \text{(Equation 3.5)}$$

$$\downarrow$$

$$\Delta A \cdot Q_{CO_{2,plateau}} \cdot \frac{1}{60} = [mmol] \qquad \text{(Equation 3.6)}$$

$$\downarrow$$

$$C_{ads} = \frac{mmol}{weight\ of\ HC} = [\frac{mmol}{g}] \qquad \text{(Equation 3.7)}$$

3.8 Selectivity test

For the assessment of the selectivity, recovery, and purity the test was carried out in the following experimental conditions as shown in the Table 3.8:

Table 3.8: CO_2 & CH_4 operating conditions

Gas	% Valve Opening	Flowrate	Pressure
CO_2	MFC-A = 76 %	76 mL/min	6 bar
CH_4	MFC-B = 100 %	76 mL/min	6 bar
N_2 stripping	MFC-C = 4 %	200 mL/min	6 bar
N_2 technical (dilution)	MFC-D = 7.5%	750 mL/min	1.5 bar

The tests were conducted at two different pressures: 2 and 5 bar. The MFC-B valve is 100% open, but the flow rate is 76.5 mL/min. The reason for this is that the MFM is calibrated on nitrogen flow rates, so sending methane applies a corrective factor C_{CH_4} that is 0.76, as per the Bronkhorst manual.

As far as the operational procedure is concerned, this is similar to the previous one, only variation is that the methane-related valve, MFC-B, is opened and closed at the same time as the CO_2 valve. In addition, during regeneration with N_2 stripping the concentration of methane, in addition to that of carbon dioxide, also must reach 0.00%. The blank test was also repeated by sending a mixture of CO_2 / CH_4. Since the activated hydro-char sample processed at 200 °C and zero minutes has the highest adsorption capacity, the selectivity test was performed only on this sample as shown in the Table 3.9.

Table 3.9: Sample analyzed for selectivity tests

Sample	Pressure (bar)			
	2	3	4	5
Blank samples	✓	✗	✗	✓
HCA_200C_ 0M samples	✓	✗	✗	✓

Selectivity is used to calculate the tendency of the sample to preferably capture CO_2 over CH_4 and is calculated using the following formula:

$$Selectivity = \frac{mol_{CO_2}/kg_{adsorbent}}{mol_{CH_4}/kg_{adsorbent}} \quad \text{(Equation 3.8)}$$

The calculation of adsorbent capacities was done identically as before, by calculating the areas underlying the methane and carbon dioxide response curves of the sample and the blank test, choosing as the integration range for the axis.

In addition to the calculation of selectivity, the purity and recovery of methane were calculated. These calculations were made by referring to the following formulas proposed by Kacem M. [102].

$$Purity(i) = \left(\int_0^t (y_i\ q)_{OUT}\ dt\right) / \left(\int_0^t q_{OUT}\ dt\right) \quad \text{(Equation 3.9)}$$

$$Recovery(i) = \left(\int_0^t (y_i\ q)_{OUT}\ dt\right) / \left(\int_0^t (y_i\ q)_{BLANK}\ dt\right) \quad \text{(Equation 3.10)}$$

Purity is well-defined by the amount of i-th outgoing gas during the saturation phase of the material divided by the entire amount of gas coming out in the same period.

The recovery of the i-th gas is defined by the ratio of the amount of i-th gas recovered at the output related to the amount introduced.

The integration range was chosen by analyzing the methane response curves, so that a gas with a certain degree of purity could be had, especially 95% and 70%. These are the purity levels required for entry into the national grid or as fuel for self-traction as a result of biogas purification process and bio-methane upgrading [103].

4. RESULTS, ANALYSIS AND DISCUSSION

4.1 Characterization analysis

Three characterization analysis were performed to check surface area and pore size (BET-BJH analysis), amount of carbon, hydrogen, nitrogen, and sulphur (CHNS-analysis), and morphological structure (SEM-EDS analysis) and are given below in detail.

4.1.1 BET & BJH Analysis

BET and BJH analysis were conducted because they provide information regarding the area of the surface and the size of the pore that are very important parameters for assessing material adsorption capacity.

The isothermal curve of (HCNA_200 ^{0}C_0M) sample in the Figure 4.1 presents a trend meaningful of that of type III isothermal of the IUPAC classification, almost convex to the axis of the axes and which does not appear to show the formation of the molecular monolayer as in previous cases. According to IUPAC, this type of isotherms represents situations where the link between adsorbent and de-sorbate is weak. There is also hysteresis whose trend is similar to the H3 type of the IUPAC classification, which is often traced back to the presence of interstitial pores due to particle aggregates [104].

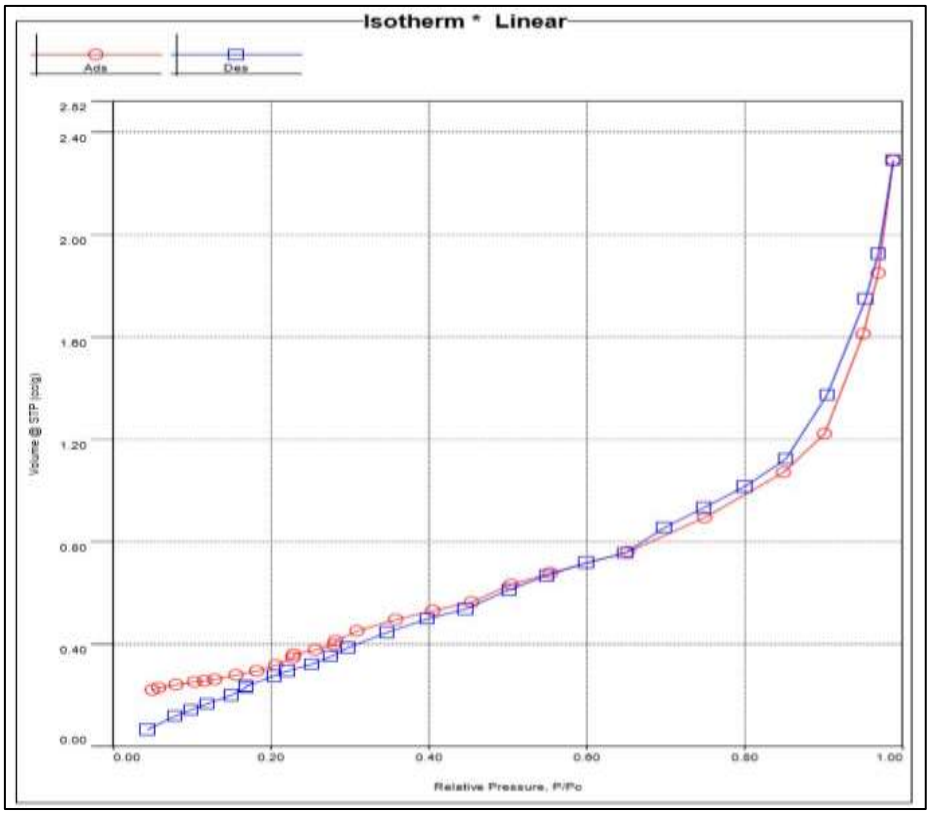

Figure 4.1: Sample isotherm curve HCNA_200 ^{0}C_0M

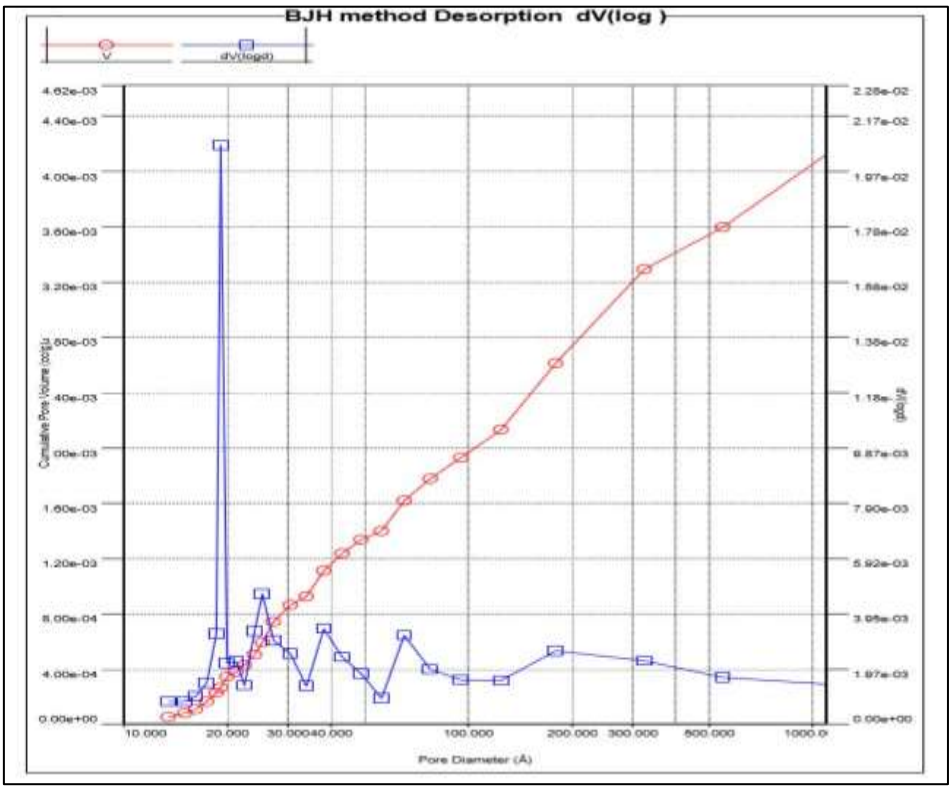

(a) BJH method desorption

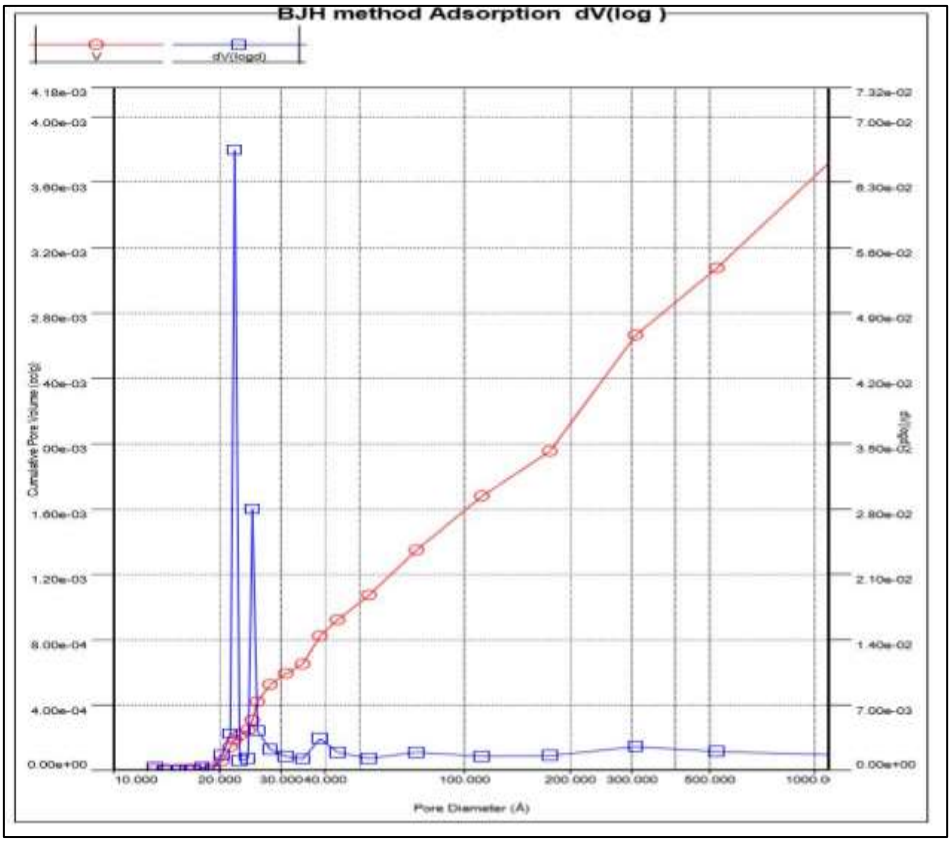

(b) BJH method adsorption

Figure 4.2: PSD of desorbent (a) and adsorbent (b) sample HCNA_200 ^{0}C_0M

The BET survey confirms these assumptions by showing a very low, or rather negligible, surface area equal to **1.127 m²/g**. This result is in line with what are the results of literature of surface areas on unactive hydro-char [105].

The cumulative Particle Size Distribution (PSD) curves show an almost total absence of micropores in the structure, marked presence of mesopore, the two largest peaks are at values greater than 20, and finally macropores, especially by analyzing the PSD curve of desorption. The total volume of pores is in any case very low in the order of **0.004 cm^3/g.** The average diameter pores calculated with *4V/A* relationship is approximately 14 nm [106].

Similarly, analysis was done for the other remaining samples and the final summary of BET & BJH surveys of analyzed samples are shown in the Table 4.1 below.

Table 4.1: BET & BJH analysis results

Sample Parameters	BET [m^2/g]	Volume of the pores desorption (BJH) [cm^3/g]	Average diameter of the pores (4V/A) [Å]
HC-200 °C-0M	1.127	0.004	142.0
HC-200 °C -0M-Activated	880.7	0.241	10.9
HC-200 °C -120M	1.326	0.008	241.3
HC-200 °C -120M-Activated	283.7	0.109	15.4

4.1.2 CHNS analysis

The results of the carbon, hydrogen, nitrogen, and sulfur (CHNS) analysis of the analyzed samples are shown in the Table 4.2.

Table 4.2: Elemental composition of analyzed samples in standard deviation values

Samples	C	H	N	S	O
HCA_200_0	0.503	0.06	0.00	0.0080	0.427
HCA_200_30	0.521	0.059	0.001	0.0078	0.411
HCA_200_120	0.555	0.0579	0.00	0.0075	0.377

Analyzing the results, it is clear that as the time of residence increases, the carbon percentage increases as an effect of a higher value of biomass dehydration, resulting in the removal of hydroxyl groups.

If after thirty minutes of treatment the increase in carbon content is almost 3.5%, after 120 minutes the increase is more than 10%. Literature surveys and data confirm that carbon after HTC's treatment has another degree of aromatization in the biomass matrix in which dual-bond such as C-O and C-C convert into single-binding hydroxyl and carboxyl groups.

In the final product, there is also a decrease in oxygen and some hydrogen content because of H_2O and CO_2 removal from the solid during dehydration and decarboxylation

reactions. It is also likely that longer residence times cause the fractions in which they are contained to solubilize more or volatilize much more easily. There are also little significant variations in nitrogen content. With shorter residency times, products with less degree of condensation (high atomic ratios O/C and H/C) will be obtained due to a lower degree of hydrolysis and polymerization.

4.1.3 SEM-EDS analysis

The characterization of materials was also performed by means of SEM-EDS analysis. The Figure 4.3 shows the proof of difference in the porosity of the hydro-char not activated, where the original wood structure is well visible and the active one with a porous sponge-structure.

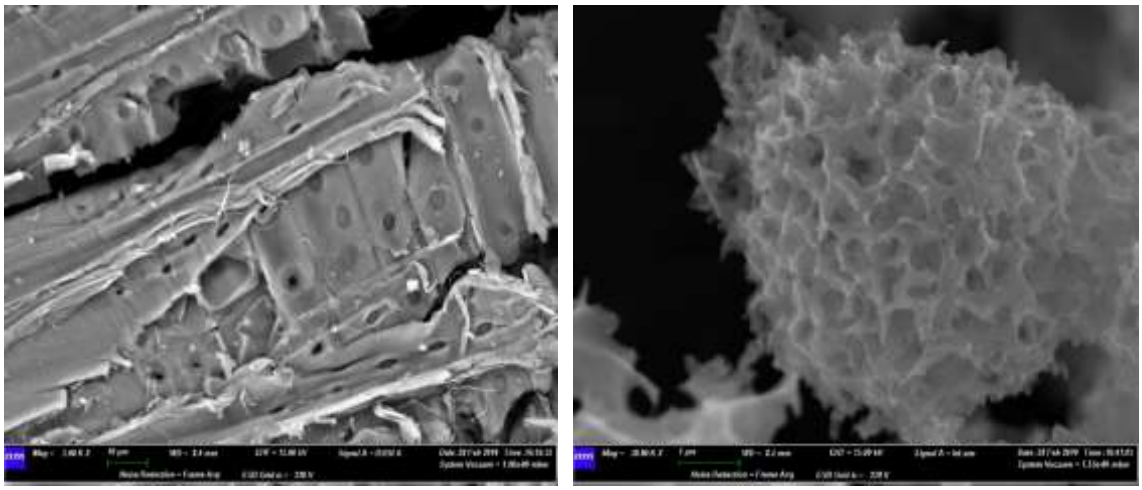

(a) Not activated (b) Activated

Figure 4.3: SEM-EDS analysis of not-activated (a) and activated (b) hydro-char

4.2 Capture test results analysis

Each sample will show the comparison between the test conducted with the CO_2-N_2 combine and the blank test. These comparisons are necessary to assess the adsorption capacity of the sample expressed in mmol/g (CO_2 adsorbate/g of adsorbent material).

4.2.1 Blank test

Figure 4.4 shows the response curves of the blank test for each exercise pressure (2, 3, 4 & 5 bar). Blank test is needed to compare before and quantify after, the ability to absorb the analyzed material.

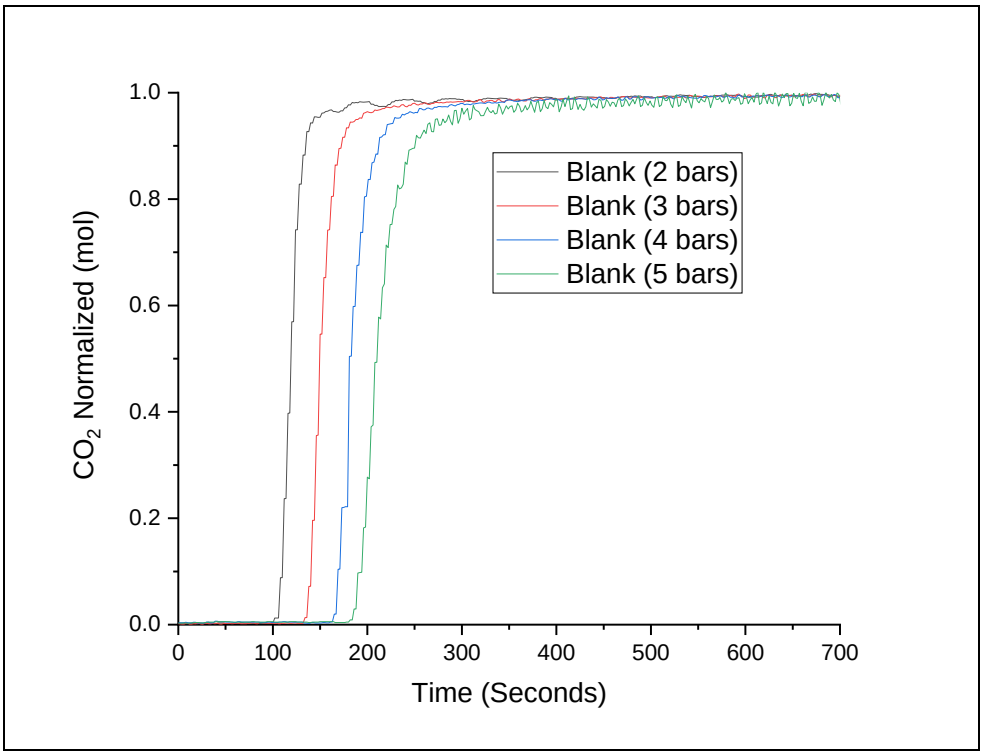

Figure 4.4: Response curves of blank test at 2, 3, 4 and 5 bar

It is clear that as the pressure applied increases, the delay time increases, causing the response curve to move further and further to the right. This effect is due to the increased amount of gas needed to completely fill the system.

4.2.2 Hydro-char HCA_200 ^{0}C_120M

In this section, the results of the hydro-char's adsorption capacity processed at 200 °Cand 120 minutes and activated will be described.

4.2.2.1 HCA_200 °C_120M (P_2_bar)

In this subsection, comparison of response curves of the sample was performed subjected to various adsorption-desorption cycles with that of blank at the pressure of 2 bar. It is clear that response curves are all shifted to the right of the corresponding blank curve

which there is, in any case, a higher adsorption capacity of the activated sample as shown in the Figure 4.5.

This is extremely important because it clearly certifies that the activation phase is absolutely necessary for the sample test adsorbent capabilities, thanks to a good specific surface and adequate porosity, highlighted by the presence of micropores.

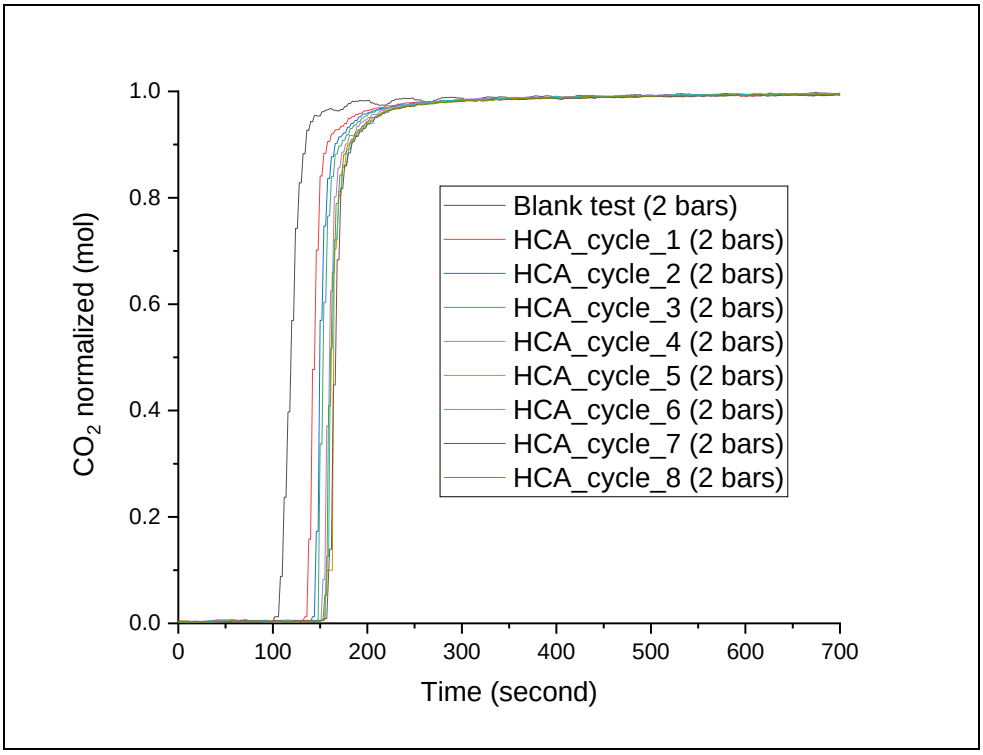

Figure 4.5: HCA adsorbed curves at 2 bar

With the exception of the value relative to the first cycle, all others are quite close together. As the cycles increase there is no decrease in adsorbent capacity, as is commonly the case with other adsorbent materials, but rather oscillates around the average value, a symptom that repeated cycles of adsorption do not alter the nature of the material.

The average adsorbent capacity calculated in the case of 2 bar pressure was **2.57 mmol/g** which is certainly a good result, given that the range of commercial active coal absorption capacity is 2.3-2.5 mmol/g at the atmospheric pressure [107, 108].

4.2.2.2 HCA_200 °C_120M (P_3_bar)

This segment contains the results for the adsorption capacity of the test material at a pressure of 3 bar. Again, it is clear, as you might expect, that the curves of responses are quite distinct from that of blank test as shown in the Figure 4.6 given below.

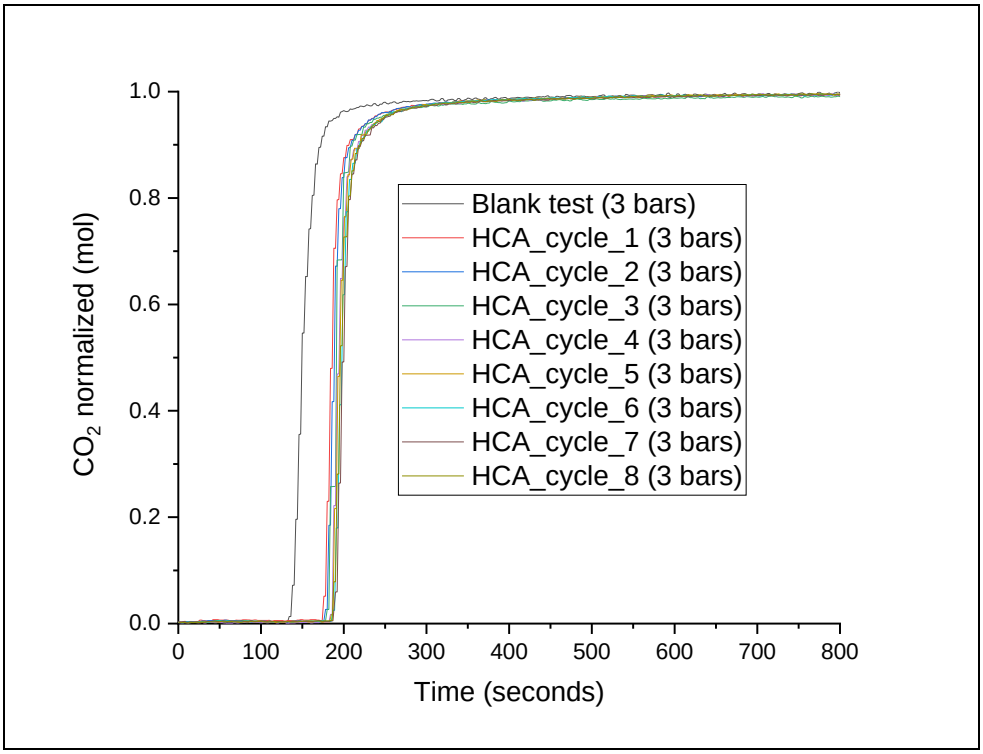

Figure 4.6: HCA adsorbed curves at 3 bar

The results show that the increase in pressure from 2 bar to 3 bar simultaneously produced increased adsorbent capacity from **2.57** to **3.30 mmol/g**. This result is not surprising because it is physical adsorption and as a result, we expect that, as we increase the exercise pressure, the capacity for adsorption will also increase at the same time.

4.2.2.3 HCA_200 °C_120M (P_4_bar)

In this section, analysis of the behavior of the activated hydro-char sample at a pressure of 4 bar was tested as shown in the Figure 4.7 given below.

As the pressure increases from 3 to 4 bar produce an increase in adsorbent capacity from **3.30** to **3.41 mmol/g**. This result confirms the trends highlighted in the previous graphs.

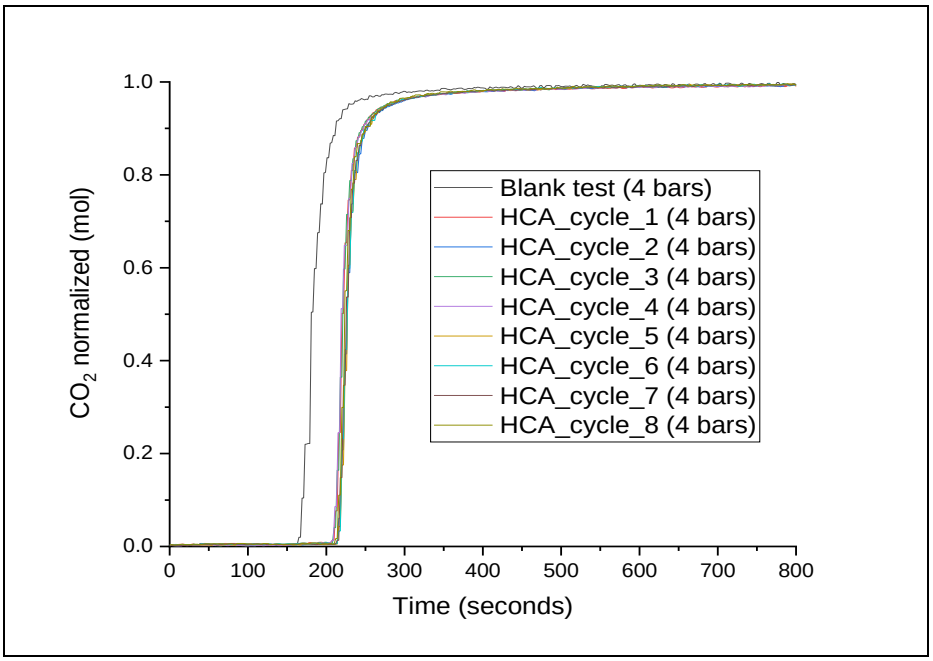

Figure 4.7: HCA adsorbed curves at 4 bar

4.2.2.4 HCA_200 ^{0}C_120M (P_5_bar)

In this last paragraph, the results of the sample analyzed at the highest exercise pressure of 5 bar. The curves confirm the trend already highlighted as compared to the previous case as shown in the Figure 4.8. The adsorption capacity calculated increased from **3.41** to **3.66 mmol/g**.

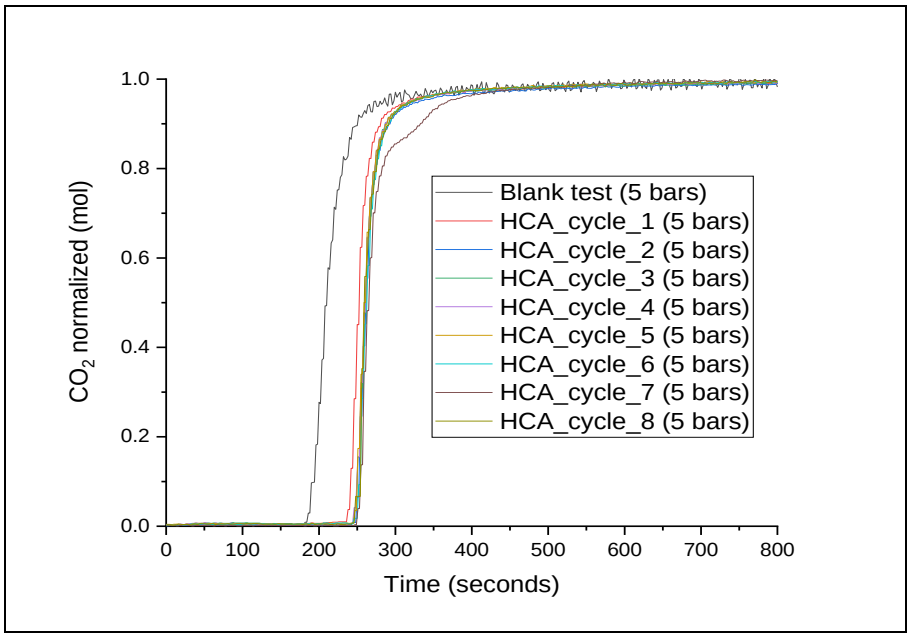

Figure 4.8: HCA adsorbed curves at 5 bar

4.2.2.5 Final results (200 °C_120M_Activated)

The average adsorbent capacity results carried out at a pressure of 2, 3, 4 & 5 bar with corresponding standard deviation values are represented in the Table 4.3.

Table 4.3: Final average results at 200 ^{0}C_120M

Parameters	Pressure [bar]	Area Blank test	Area Test	C Plateau	Weight HC [g]	Avg. Adsorbent Capacity [mmol/g]	Standard Deviation [mmol/g]
Activated-(200 °C-120M)	2	473.67	436.92	0.0050	1.135	2.57	0.35
	3	440.81	397.97	0.0051	1.135	3.30	0.34
	4	410.14	364.71	0.0050	1.135	3.41	0.37
	5	377.52	325.26	0.0050	1.135	3.66	0.44

From the final results, it is clear that adsorbent capacity increases only 8 % when pressure goes from 3 to 5 bar, while it is 37% compared to the 2-bar figure. The data at 3, 4 and 5 bar are not too far apart, and this could justify the choice not to operate under high pressures, but to seek an acceptable compromise.

By comparing the final outcomes with the characterization analysis results, it is clear that activated sample shows a good adsorption capacity, and the figure obtained at 2 bar is in line with that of active coals present in the literature.

4.2.3 Hydro-char HC_200 °C_0M activated

This section comprises the results of the activated hydro-char adsorption capacity processed at 200 degrees Celsius, zero minutes.

4.2.3.1 HCA_200 ^{0}C_0M (P_2_bar)

The first results are those obtained at the pressure of 2 bar. By integrating the curves as shown in the Figure 4.9 for blank test and each adsorption cycle, the average adsorbent capacity value of **4.94 mmol/g** was achieved, comparable to the literature data highlighted by the article equal to **4.8 mmol/g** [90].

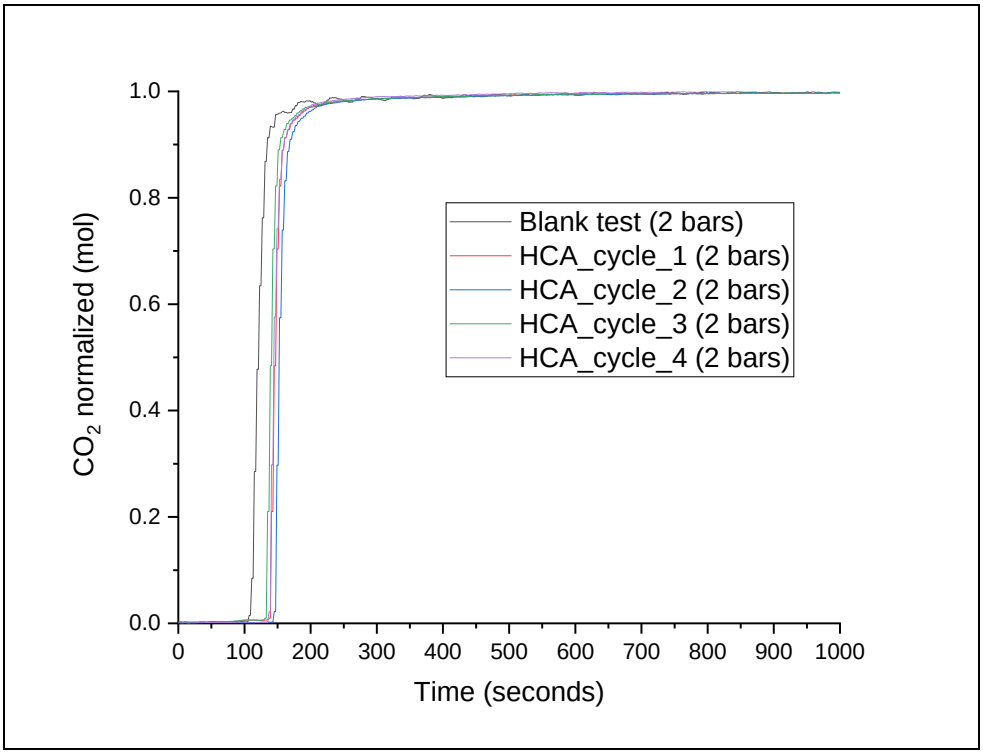

Figure 4.9: HCA adsorbed curves at a pressure of 2 bar

This value is justified by the results obtained from the characterization analysis, in which the sample showed a high area of the surface, about 881 m^2/g and a good porosity with the presence mainly of micropores and partly of mesopore. It is also evident from the standard deviation data, come that there is a heightened dispersion of data around the average value.

4.2.3.2 HCA_200 ^{0}C_0M (P_3_bar)

In this sub paragraph, we will look at the results of 3 bar curves as presented in the Figure 4.10. Related to the figure calculated at 2 bar, the capacity figure increased from **4.94** to **5.72 mmol/g** as was lawful and desirable to expect, with an increase of 14%. The data also shows a low dispersion value of 0.07 as highlighted by the standard deviation.

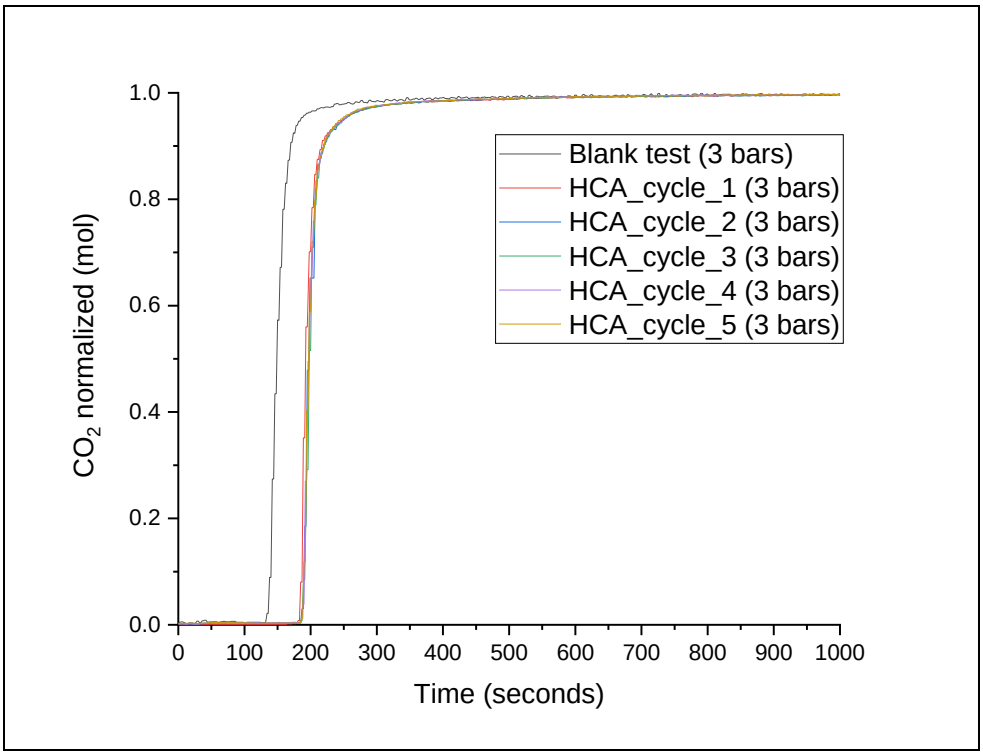

Figure 4.10: HCA adsorbed curves at a pressure of 3 bar

4.2.3.3 HCA_200 ° C_0M (P_4_bar)

This sub paragraph shows the results obtained at the pressure of 4 bar. The average value of the adsorbent capacity is greater than that of the 3-bar sample, which is **6.12 mmol/g**. The adsorption curves of each adsorption cycle are almost completely overlapping with each other, unlike for example the sample analyzed at the pressure of 2 bar and in a less marked way with that analyzed in 3 bar.

Note that the test areas are very similar to each other, making the adsorbent capacity values similar as demonstrated by the very low variation in the value of the standard deviation. The average value of adsorbent capacity enlarged by 9.5% compared to the 3 bar figure, confirming the growth trend as operating pressure increased.

The curves of blank test and hydro-char activated are shown in the Figure 4.11.

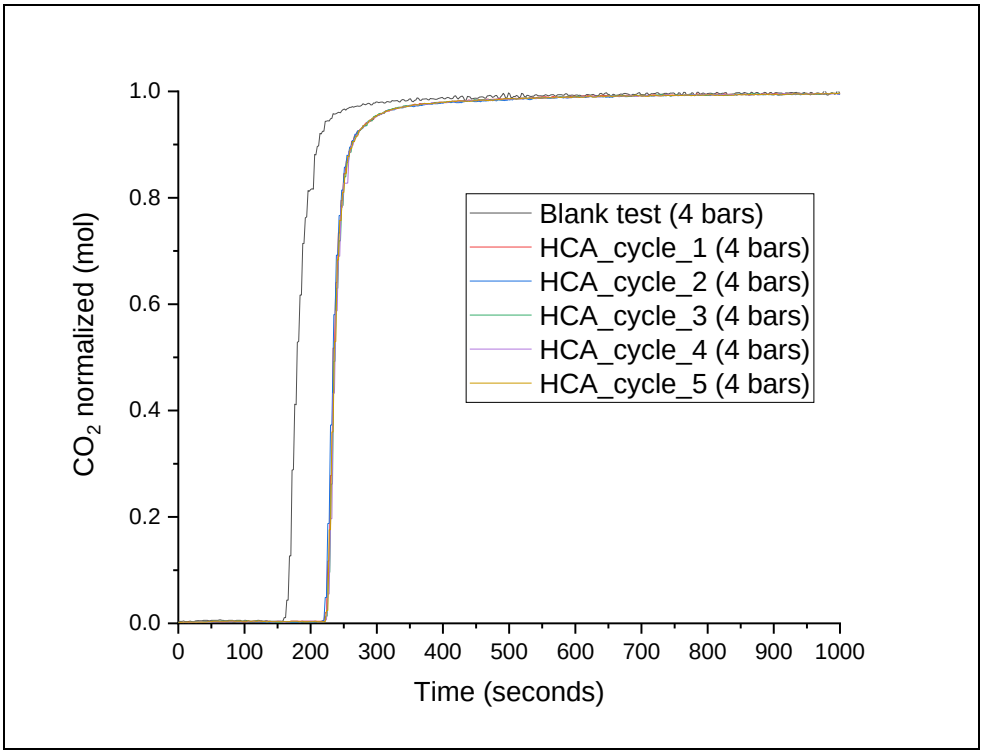

Figure 4.11: HCA adsorbed curves at a pressure of 4 bar

4.2.3.4 HCA_200 °C_0M (P_5_bar)

In the final subsection, the results for tests carried out at the maximum operating pressure, i.e., 5 bar, are reported with calculated adsorbent capacity of **6.60 mmol/g**. Note that only the curve of the first adsorption cycle is easily distinguishable from other curves that appear to overlap and therefore not identifiable.

By viewing on the adsorption capacity values, with the exception of the first value, all the others do not clearly deviate from the average value, the maximum differential is about 4%, and this is also evident from the value of the standard deviation.

The first figure, on the other hand, is about 10% lower than the average value evident by the trend of the response curves in the Figure 4.12 and the causes of which have already been discussed.

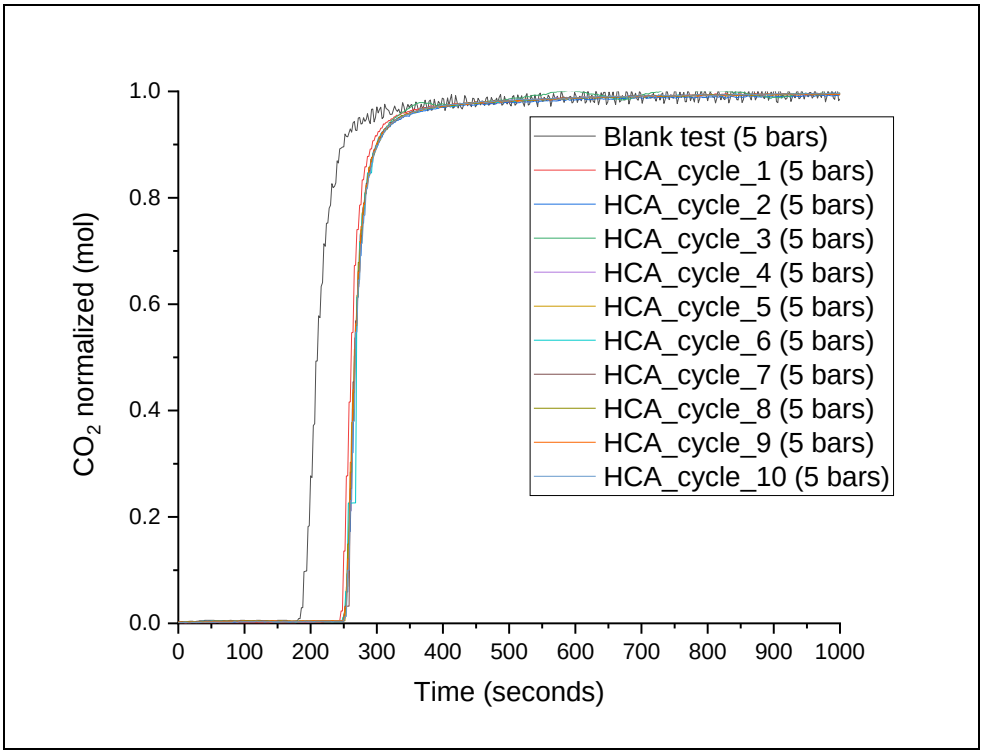

Figure 4.12: HCA adsorbed curves at a pressure of 5 bar

4.2.3.5 Final results (200 ˚C_0M_Activated)

The average adsorbent capacity results carried out at a pressure of 2, 3, 4 & 5 bar with corresponding standard deviation values are shown in the Table 4.4.

Table 4.4: Final average results at 200 °C_0M

Parameters	Pressure [bar]	Area Blank test	Area Test	C Plateau	Weight HC [g]	Avg. Adsorbent Capacity [mmol/g]	Standard Deviation [mmol/g]
Activated-(200 ^{0}C-0M)	2	473.67	432.74	0.00517	0.695	4.94	0.952
	3	440.80	397.58	0.0052	0.695	5.72	0.070
	4	410.14	360.15	0.00515	0.695	6.12	0.080
	5	377.50	322.58	0.00513	0.695	6.60	0.120

The graph clearly shows the trend in capacity that increases progressively as the operating pressure increases. Moving from the pressure of 2 bar to the maximum pressure of 5 bar,

there is an increase in the capacity of adsorbing by more than 32%. It is clear in this case that working at medium pressures is more advantageous than working at low pressure.

Average CO_2 sorbent capacity for the two samples of activated hydrochar as a function of the corresponding partial pressure in the gas phase is shown in the Figure 4.13. Data fit well to the Langmuir equation [109].

.

$$CO_{2_{\text{Sorbent capacity}}} = \left(C_{\text{Max}} \cdot p_{CO_2}\right)/\left(K + p_{CO_2}\right) \tag{4.1}$$

Regressions are reported as solid lines in the explored range and as dotted lines in the extrapolated ones. A wider partial pressure range should be explored to ascertain the correct equilibrium law as shown in the Figure 4.13.

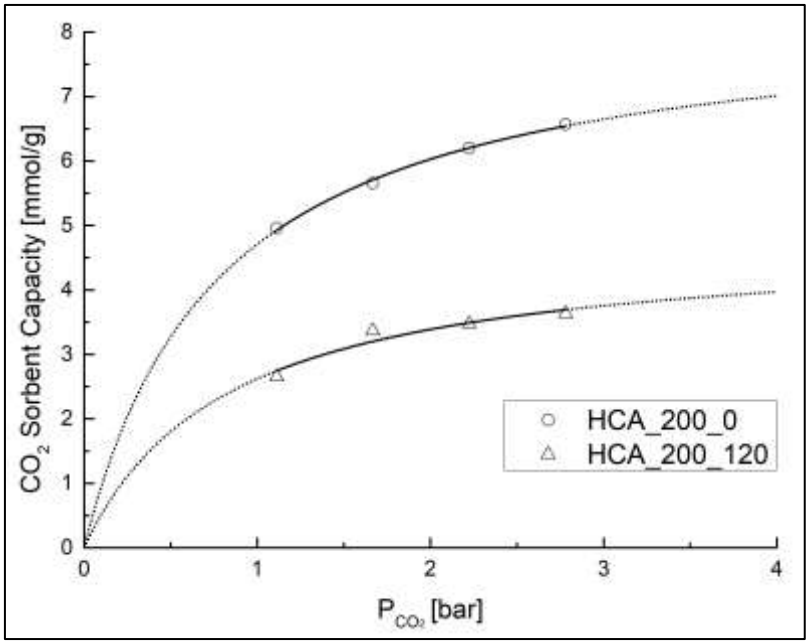

Figure 4.13: CO_2 sorbent capacity vs P_{CO2}.

The regression parameters are reported in the Table 4.5.

Table 4.5: Synopsis of regression parameters for Langmuir equation

Samples	C_{MAX}	K	R^2
HCA_200_0	8.38 ± 0.15	0.77 ± 0.05	0.99
HCA_200_120	4.79 ± 0.45	0.83 ± 0.26	0.90

4.3 Comparison with literature data

The results of the test samples and those from the literature analysis will be compared in this paragraph. Figure 4.14 shows the comparison of the results between the tested samples.

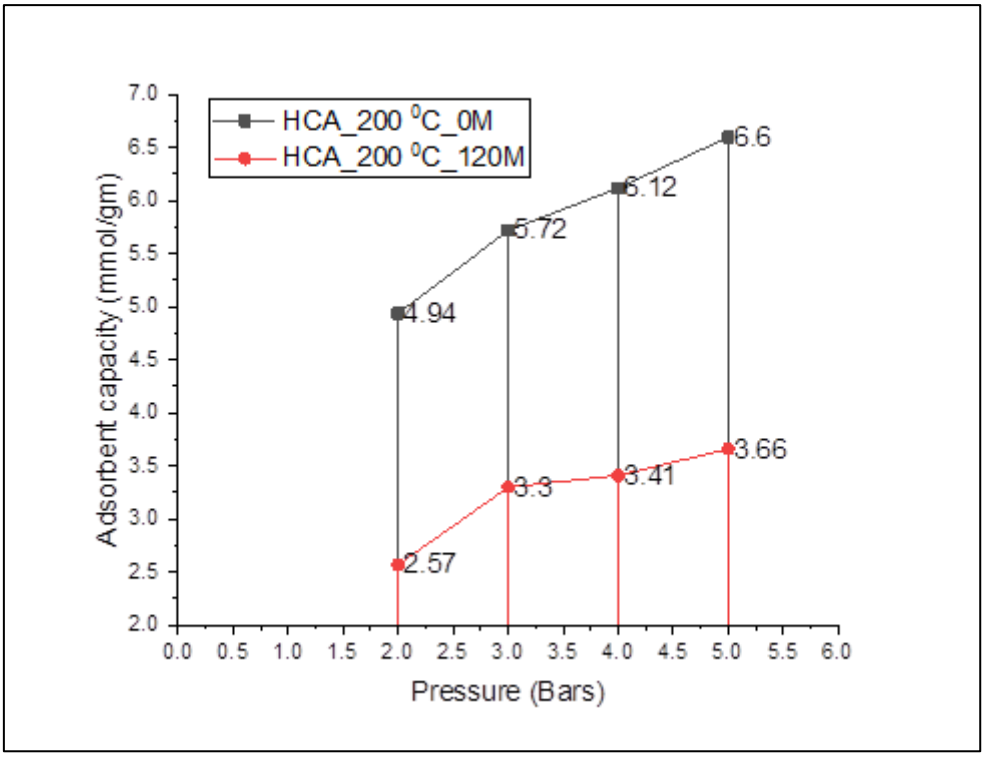

Figure 4.14: Comparison of tested samples

Note that at 2 bar adsorbent capacity of the HCA_200 ^{0}C_0M sample is about 87% larger than that of the HCA_200 $^{\circ}$C_120M sample.

The figure is not surprising considering that the sample processed at zero minutes develops, as per characterization analysis, a larger specific area of the surface, 881 m^2/g against the 284 m^2/g of the sample processed at 120 minutes, but also pores with a smaller average diameter, 10.9 Å versus 15.4 Å. It is due to the fact that during the treatment of 120 minute the formation of micropores may collapse causing the material in the next phase of activation to develop a specific low surface and a low porosity.

A comparison was made with data on the adsorption capacity of various commercial active coals found in the literature are displayed in the Table 4.6.

Table 4.6: Comparison with the literature

Adsorbent material	Reference	Adsorbent capacity [mmol/g]
Activated carbon treated with Ammonia (C35N400)	[110]	1.7
Mesoporous carbon (CMK-3)	[111]	1.7
Ammonia treated activated carbon (RN800)	[112]	2.2
N-doped activated carbon (MFB-600)	[107]	2.3
Commercial Active Coal (G - 32H)	[108]	2.5
Porous carbon (N-doped) (RFL-500)	[113]	3.1
Activated carbon from petroleum pitch (DO-88-M)	[114]	4.7
Porous carbon sawdust-based (AS-2-600)	[90]	4.8
HCA_200 °C_120M	Current study	2.57
HCA_200 ^{0}C_0M	Current study	4.94

It is evident from the table above that both samples tested in this thesis work develop an excellent adsorption capacity, in particular the sample processed at 200 °C and zero minutes, which is higher than commercial active coals like silica gel 0.707 mmol/g and Zeolite 13X 0.669 mmol/g [101].

During comparison with the activated hydro-char obtained from eucalyptus sawdust [90] the result is extremely important as our sample has only undergone warm-up treatment to the temperature of setpoints, whereas in the (AS-2-600) case the sample has been processed for 2 hours, which is a huge advantage from the energy point of view.

4.4 Selectivity test, purity & recovery calculations

Selectivity tests were conducted at a pressure of 2 and 5 bar and results were generated by using equation (3.8) while recovery and purity calculations was done by using equations (3.9 and 3.10).

4.4.1 Selectivity test at 2 and 5 bar

Figure 4.15 shows typical adsorption curves obtained with the activated hydro-char at 2 and 5 bar (a and b, respectively) and the mixture CH_4/CO_2. Arrows signal the time of the first detection. Both diagrams show that in the blank runs the CO_2 and CH_4 signals are indistinguishable. On the contrary, in the presence of a hydro-char bed, a selectivity appears evident, as proved by the temporal separation of the arrows. Methane appears first in the column outlet regardless of the operating pressure. The delay between the two signals is an increasing function of the operating pressure, and in any case, it is sufficiently broad for envisaging the development of an industrial process. The whole of this evidence proves that hydro-char is a suitable medium for separating the mixture by selective adsorption.

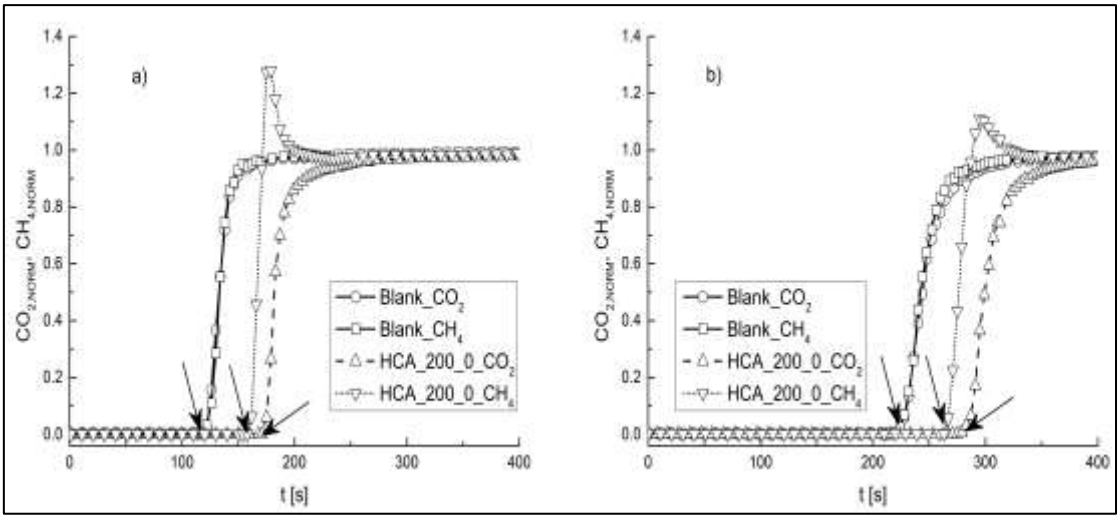

Figure 4.15: CO_2/CH_4 adsorption curves at: a) 2 bar; b) 5 bar

In particular, methane is first absorbed and then desorbed, leaving the previously occupied free. In this way, a sample is able to release CH_4 even during CO_2 absorption, indicating that it is possible to recover methane with a certain degree of purity. The selectivity results are shown in the Table 4.7.

Table 4.7: Selectivity results

Test	Average $C_{ads, CO2}$ (mmol/g)	Standard deviation	Average $C_{ads, CH4}$ (mmol/g)	Standard deviation	Selectivity (%)
2 bar	4.75	0.061	2.53	0.058	65.3
5 bar	5.27	0.086	2.51	0.056	67.7

The CO_2 selectivity figure is 65.3% this indicates a greater capacity for CO_2 adsorption compared to methane probably attributable to the different dimensions of molecular diameters. In fact, the diameter of CO_2 is about 3.4 and that of methane 3.8. However, this result is lower than commercial porous sorbents such as zeolites or activated carbons [101]. This is the possibly due to the reason that the material still has a high adsorption capacity even against methane, making the selectivity figure quite low. Table 4.8 shows data on the percentage of purity and the percentage of methane recovery.

Table 4.8: Purity and recovery results

CH_4	**2 bar**			
	Purity	95%	***Purity***	70%
	Recovery	32%	***Recovery***	60%
	5 bar			
	Purity	95%	***Purity***	70%
	Recovery	36%	***Recovery***	68%

The increase in pressure has favored CO_2 absorption, in fact the capacity has increased by about 11%, from **4.75** to **5.27** mmol/g, while it has essentially kept the methane one constant. However, this figure is much lower than the figure for the same pressure considering the $CO_2 – N_2$ mixture which was **6.4 mmol/g**. There is probably a percentage of pores still occupied by methane and therefore not available to absorb CO_2.

As evident from the Table 4.8, it is observed that at higher purity (95%) the recovery of methane decreases irrespective of the analyzed pressure selection. As the purity level decreases to 70% the recovery approaches to double figure.

5. CONCLUSION AND RECOMMENDATIONS

5.1 CONCLUSION

This work has demonstrated how it is possible to obtain porous hydro-char from lignocellulosic biomass by hydrothermal treatment and subsequent activation with potassium hydroxide. Results show that unactive samples show no adsorbent capacity for CO_2 even at higher pressures than atmospheric pressures. Only in the 5-bar test did there be a reversal of the trend, but still not acceptable for possible applications on an industrial scale. This is due to morphological properties of the sample not fit for purpose: development of inadequate porosity, very low specific surface.

The activated samples, on the other hand, show a better performance. In particular, the sample of hydro-char processed at 200 °Cand zero minutes of dwell and subsequently activated with KOH at a temperature of 600 °C shows an exceptional capacity for adsorption of CO_2 (4.94 mmol/g) at the temperature of 25 °C and the pressure of 2 bar. This figure is higher than that obtained by commercial active carbon, which makes this result extremely attractive. This notable adsorption capacity is attributable to micropores (<2 nm). The best results achieved were BET surface area of 881 m^2/g, average diameter of pore 10.9 Å, allowing to achieve 6.60 mmol/g of adsorbent capacity at 5 bar. Compared to traditional sorbents, the hydro-char showed higher CO_2 adsorption. The material retains sufficient capacity to adsorb CO_2 from the mixtures with CH_4. An additional advantage is in the ease of regeneration of the material

These results are in any case very important, since they highlight how residual material, in our case wood industries residues, can be exploited in the future to obtain a product that on the one hand preserves the environment, reducing CO_2 emissions and at the same time reducing the environmental impact related to their disposal.

5.2 FUTURE RECOMMENDATIONS

As in the results it was concluded that these tests are carried out at pressure below 5 bar so in future the tests can be carried out at greater pressure and at a large scale in a pilot plant as designed in the industrial work of this thesis. Experimental work can also investigate a wide range of operating conditions, at higher pressure and with synthetic or real biogas, in order to evaluate the optimum set of industrial plant parameters and the effect of impurities (H_2S, NH_3, etc.) and humidity in the feeding flow.

UNIVERSITY OF L'AQUILA
Department of Industrial engineering and Information & Economics

SECTION 2

Enzymatic conversion of carbon dioxide from biogas into precursors of bioplastic

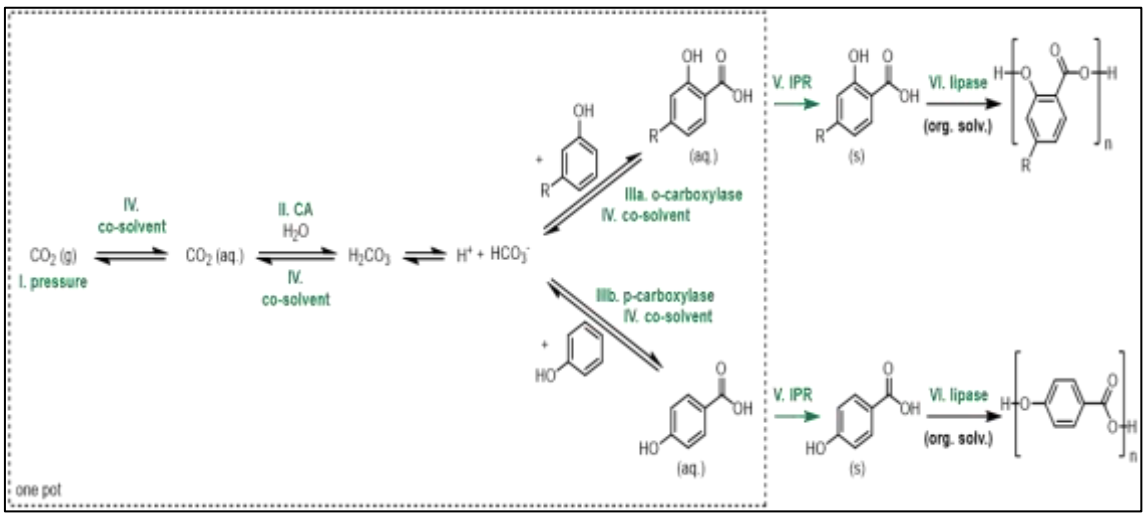

ABSTRACT

It is a new worldwide challenge to produce materials from renewable resources and to reduce greenhouse gas emissions, especially of carbon dioxide, being the main cause of the increasing ambient temperature. The Intergovernmental Panel on Climate Change (IPCC) in its latest special report on the impacts of global warming aims at a maximal temperature increase of 1.5 °C above pre-industrial levels as their main goal. The scope of the present study (PON 2014-2020 industrial PhD grant) is to upgrade biogas to bio-methane for energy purposes and to use the captured carbon dioxide, as a feed for biocatalytic production of potential monomers.

This CO_2 will be upgraded in a carboxylation reaction by the *p*-carboxylase 3,4-dihydroxybenzoic acid decarboxylase from *Enterobacter cloacae* (*Ec*AroY) to produce polymer building blocks which may serve as a raw material for bioplastic. The reaction scheme of the study is given below:

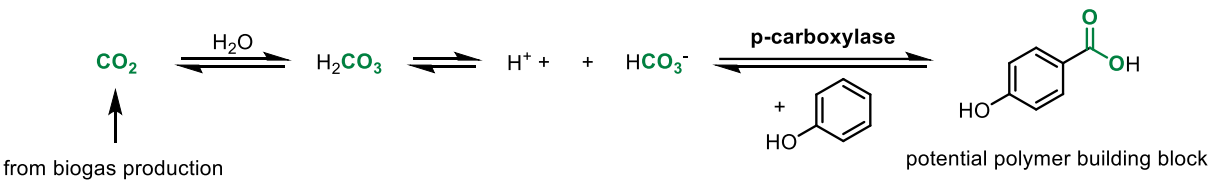

The biocatalyst was prepared and then the carboxylation reaction was engineered by considering different parameters such as pH, substrate concentration, temperature, time, co-solvent and the amount of $KHCO_3$ in order to improve conversion. Furthermore, *in-situ* product removal systems were checked.

Keywords:

p-carboxylase, carboxylation, potassium bicarbonate, carbon dioxide

6. INTRODUCTION

6.1 Research Background

With the continuous increase in fossil fuels consumption and the rapid growth of atmospheric CO_2 concentration, the harmonious state between mankind and nature faces severe challenges. Discovering green and sustainable energy resources and devising efficient methods for CO_2 capture, sequestration and utilization are urgently required. Converting CO_2 into fuels, chemicals or materials via CO_2 capture, sequestration and utilization may offer a win–win strategy to both, decrease the CO_2 emissions, and achieve the efficient exploitation of a novel carbon resource. Among the current major methods (including chemical, photochemical, electrochemical and enzymatic methods), the enzymatic method, which is inspired by the CO_2 metabolism in cells, offers a green and potent alternative for efficient CO_2 utilization due to its mild reaction conditions and sustainable processes parameters, as well as its superior, regio- and chemo-selectivity [115].

6.2 Research Motivation

The increasing ambient temperature is a hot issue nowadays which is the major effect of global warming and the main source of this issue is the emission of CO_2 and other greenhouse gasses in the air. In this work the emitted CO_2 from a biogas plant that produces electricity is captured in the process of biogas upgrading to biomethane. This CO_2 will be converted to its bicarbonate form which allows its upgrade in an enzymatic carboxylation reaction with *p*-carboxylases to produce fine chemicals or polymer building blocks for the ultimate production of bioplastic.

6.3 Aim and Objectives

Aim:

The aim of this research study is the enzymatic conversion of carbon dioxide from biogas into precursors of bioplastic.

Objectives:

The objectives of this work are the following:

1- To produce the enzyme 3,4-dihydroxybenzoic acid decarboxylase from *Enterobacter cloacae* (EcAroY, internally termed as pEG-167) as lyophilized whole *E. coli* cells.
2- To improve the conversion to the product of the carboxylation reaction with bicarbonate as CO_2-source by reaction engineering and therefore to utilize one molecule of CO_2 per molecule of product.
3- To perform analyse of the samples on HPLC to check conversion.
4- To develop an *in-situ* product removal (IPR) method.

The Methods that will be applied and the parameters that will be varied are discussed in the section “Research Methodology”.

6.4 Research Methodology

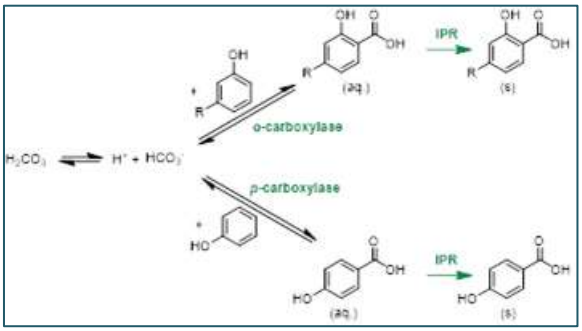

Figure 6.1: Enzymatic conversion of CO_2 into precursors of bioplastic

The following methodologies will be applied to reach the objectives:

1- **Catalyst Production**: All enzymes are heterologously expressed in *E. coli* BL21 DE3 and will be applied as lyophilized whole-cell powder
2- **Biotransformation and Reaction Engineering:** Parallel biotransformations in small scale are used to optimize the reaction procedure.
3- **Analytics**: The biotransformations are evaluated chromatographically on HPLC-UV/VIS
4- **Product Isolation**: An *in-situ* product removal (IPR) method is evaluated.

6.5 Scope of the Research

As depicted in the**Error! Reference source not found.** Figure 6.1 CO_2-gas will be upgraded to hydroxylated benzoic acids by enzymatic carboxylation. All parameters will be systematically investigated to achieve optimal productivity.

I. The enzymes preferably utilize CO_2 in the form of bicarbonate (HCO_3^-). Therefore, different forms of bicarbonate supply will be evaluated [116].

II. The performance of four different carboxylases may be evaluated, three *ortho*-carboxylases and one *para*-carboxylase. As the products obtained from the reaction catalysed by the *p*-carboxylase are more likely to serve as good polymer building blocks and the literature for this enzyme is scarce, a focus will be put onto these enzymes:

a. *o*-carboxylases [117]:
   - 2,3-Dihydroxybenzoic acid decarboxylase from *Aspergillus oryzae* (2,3-DHBD_*Ao*, pEG: 41)
   - salicylic acid decarboxylase from *Trichosporon moniliiforme* (SAD_*Tm*, pEG: 69)
   - 2,6-dihydroxybenzoic acid decarboxylase from *Rhizobium* species (2,6-DHBD_*Rs*, pEG: 68)

b. *p*-carboxylase [118]:
   - 3,4-Dihydroxybenzoic acid decarboxylase from *Enterobacter cloacae* (*Ec*AroY, pEG 167)

III. Important reaction parameters such as pH, temperature, reaction time, substrate loading, and catalyst loading will be optimized for all involved reactions.

IV. As all involved reactions are reversible and in equilibrium, the application of *in-situ* product removal (IPR) techniques may be used to boost the conversion to the product [119].

6.6 Thesis Structure (Part 2)

- ♣ Introduction: This chapter describes the research background, research motivation, aim and objectives, research methodology and scope of research.
- ♣ Literature review: In this chapter, literature review of all the related articles is described.
- ♣ Experimental design and setup: This chapter describes the experimental design and setup of the research study.

- ♣ Results, analysis, and discussions: This chapter covers the results, analysis, and discussion session.
- ♣ Conclusions and recommendations: In this chapter, conclusions and future recommendations are described.

7. LITERATURE REVIEW

7.1 What are Enzymes?

Enzymes are catalytically active proteins. As biocatalysts they can increase the speed of a reaction by up to several orders of magnitude. They have no influence on the equilibrium, because they hasten both the forward and reverse reaction [120].

7.2 Enzyme Perceptions

1- Most *enzymes are sensitive to the environmental conditions* such as temperatures greater than 50 ^{0}C and pressures beyond 10 MPa. However, if certain precautions are met, enzymes can be remarkably stable [121] [122].

2- *Enzymes are expensive,* which is true if they are bought or produced in a small scale, but the costs go down rapidly, if they are produced on a reasonable scale. Due to rapid advancement in molecular biology, now the enzymes are easily available, and their production cost is also decreasing constantly. Enzymes, if immobilized, can be reused. However, the price of a catalyst itself does not mean much, as other parameters such as turnover numbers, reusability and catalyst concentration need to be taken into account. The important question is how significantly the catalyst contributes to the cost of the product associated also considering the added value of using bio catalysis over other production methods. The added value could be attained through higher yield, milder reaction conditions, higher product purity, fewer reaction or purification steps, improved safety, reduced emissions to the environment, or the manufacture of a unique product [123].

3- *Enzymes only accept their natural substrates;* however, this statement is valid only for some of the enzymes, but majority of the enzymes do not follow this rule. In a general trend, enzymes from the primary metabolism are less flexible regarding their substrate than enzyme from the secondary metabolism. Furthermore, recent advances in enzyme engineering allow completely change the enzymes substrate scope [124].

7.3 Advantages & Disadvantages of Enzymes

Advantages and disadvantages of enzymes are as follows [125].

7.3.1 Advantages of Enzymes

1- Enzymes act under mild conditions like pH-values typically around 7 and temperatures preferably around 25-30 ^{0}C.
2- Enzymes are environmentally acceptable and do not contribute too much to pollution, as they are completely biodegradable.
3- Enzymes are compatible with each other due to similar reaction conditions. Therefore, two or more enzymes can react altogether in a single flask.
4- Enzymes exhibit high tolerance by accepting different kinds of substrates including man made molecules. They can work with organic solvents other than water if required. This makes the targeted reaction engineering feasible.
5- Enzymes are very efficient catalysts as compared to non-catalyzed reactions. Only this fact allows to perform an energetically unfavoured reaction such as carboxylation at benign conditions.
6- Enzymes are used in the industrial scale because of the mentioned abilities.
7- Enzymes can be very efficiently optimized using the methods of directed evolution.

7.3.2 Disadvantages of Enzymes

1- Enzymes display their highest catalytic activity in water. However, for most of the organic reactions water is least suitable solvent.
2- Enzymes require narrow operating parameters. Allowing only minor changes of parameters like pH, temperature, and salt concentration during the reactions, otherwise the proteins may be denatured.
3- Enzymes have the advantage in terms of flexibility for accepting non-natural substrates but depending on the reaction they may require costly natural cofactors.
4- In rare cases, enzymes may cause allergies if are not handled properly as compared to the other chemicals.
5- Enzymes may be inhibited by higher concentration of substrate or product and subsequently the rate of reaction is decreased.

7.4 Enzyme Classes

The International Union of Biochemistry (I.U.B.) introduced standards of enzyme nomenclature which endorse that enzyme names indicate both the substrate acted upon and the type of reaction catalysed. According to the enzyme commission the enzymes are divide into 7 main families:

1. oxidoreductases (EC 1)
2. transferases (EC 2)
3. hydrolases (EC 3) (have a lot of industrial applications e.g., PVC)
4. lyases (EC 4) (Industrially suitable e.g., bioplastic)
5. isomerases (EC 5)
6. ligases (EC 6)
7. translocases (EC 7)

Enzyme classes with their relevant biocatalytic reactions are briefly explained below in the Table 7.1.Whereas mostly catalysts from the EC 1 and 3 are applied in industry, decarboxylases, the enzymes applied herein, are part of the EC 4.

Table 7.1: Enzyme classes with their corresponding biocatalytic reactions

Enzyme Classes	**Biocatalytic reactions catalysed by this class**
EC 1 -Oxidoreductases	Oxidations of alcohols, aldehydes, ketones (Baeyer-Villiger), amines, thiols, sulfones, C-H bonds (hydroxylations, halogenations), alkenes (epoxidation) and aromatics Reductions of aldehydes, ketones (to aldehydes or reductive amination), carboxylic acids, alkenes, alkynes, amides, nitriles, esters and imines Dealkylations (of amines or ethers) CC bond formations or cleavages
EC 2 - Transferases	Transfer of functional groups such as aldehydes, ketones, sugars, acyl-, phosphoryl-, methyl-, and amino-groups
EC 3 - Hydrolases	Hydrolysis and formation of esters, amides, lactones, lactams, epoxides, nitriles, anhydrides, glycosides and haloalkanes
EC 4 - Lyases	Addition and elimination of small molecules such as CO_2, H_2O of HCl from C=C, CN und C=O bonds Carboxylations and decarboxylations Aldol-reactions

EC 5 - Isomerases	Racemizations Epimerizations Rearrangements
EC 6 - Ligases	ATP-dependent condensations of C-O, C-S, C-N or C-C bonds
EC 7 - Translocases	Translokases were recently added as new EC-class but are of no biocatalytic relevance.

7.5 Enzyme Sources

In organic chemistry, a large quantity of enzymes that are used for biotransformation are in the form of crude cell extracts. These are less expensive to prepare, and crude preparations may be more stable than the purified enzymes. The preparation generally contains 1-30% of actual enzyme and the remaining parts are inactive proteins, buffer salts, stabilizers and carbohydrates [126].

The major sources of enzymes for biotransformation are given below.

1- The richest and most convenient source of enzymes are derived from bacterial and fungal origins (microorganisms) by cheap fermentation. The enzymes are not necessarily native to the expression host but may have been cloned into the host.
2- Enzymes can be isolated from the slaughter waste.
3- Some enzymes that are used for biotransformation are obtained from plant sources such as fruits and vegetables.

7.6 Mechanistic aspects of enzyme catalysis

The unparalleled catalytic power of enzymes has sparked numerous studies on mechanistic theories to provide a molecular understanding of enzyme catalysis for almost a century. Among the numerous theories and rationales, the most illustrative models for the organic chemist are discussed here [127-129].

7.6.1 Induced-Fit Mechanism

This rationale, which considers that enzymes are not entirely rigid but rather represent delicate and soft structures, was developed by Koshland Jr. in the 1960s [130,

131]. It assumes that upon approach of a substrate during the formation of the enzyme-substrate complex, the enzyme can change its conformation under the influence of the substrate structure so as to wrap itself around its guest (Figure 7.1) This phenomenon was denoted as the 'induced fit'. It can be illustrated by the interaction of a hand (the substrate) and a glove (the enzyme). This advanced model can indeed explain why in many cases several structural features on a substrate are required in addition to the reactive group. These structural features may be located at quite a distance from the actual site of the reaction. The most typical 'induced-fit' enzymes are the lipases. They can convert an amazingly large variety of artificial substrates which possess structures which do not have much in common with the natural substrates – triglycerides.

No induced fit ⟶ Inactive enzyme Induced fit ⟶ Active enzyme

Figure 7.1: Schematic figures of the 'induced-fit' mechanism

A schematic representation of the 'induced-fit' mechanism is given in Figure 7.1, Whereas A represents the reactive group of the substrate, X is the complementary reactive group(s) of the enzyme – the 'chemical operator'. Substrate part B forces the enzyme to adapt a different (active) conformation. Only then are the 'active' groups X of the enzyme positioned in the right way to effect catalysis. If part B is missing, no conformational change (the 'induced fit takes place and thus the chemical operators stay in their inactive state.

7.7 Enzyme Applications

Applications of enzymes and whole cell biocatalysts for producing diverse types of chemical and biological substances have become a proven technology in chemical and pharmaceutical industries because enzyme-based processes usually lead to a reduction in

the process time, the number of reaction steps, and amount of waste [132]. Typical industrial applications of different kinds of enzymes are given in the Table 7.2.

Table 7.2: Industrial applications of enzymes

Enzymes	Use	Types of industries
Hydrolases, amidases	Synthesis of bulk chemicals such as polymer building blocks	Polymer industry [133, 134]
DNA ligase, polymerases	Manipulate DNA in genetic engineering, used in forensic science, necessary for digestion restriction and polymerase chain reaction [135].	Molecular biology
α-amylase, α-glucosidase, trans-glucosidase, sucrose phosphorylase, and dextransucrase	Arbutin is the most common skin-lightener and is known to inhibit melanogenesis without causing melano cytotoxicity [136]	Cosmetics industry
cellulase	In the textile industry, prior to conversion into fabric and yarn, cotton undergoes various processes including refining, bleaching, dyeing, and polishing (Queiroga et al., 2007). For the development of cleaner processes, the use of enzymes is rapidly growing. Typical examples include the staining of jeans using cellulase from Trichoderma viride, and a bio-carbonization process in the case of wool [137].	Textile industry
xylanase and ligninase	In the pulp and paper industries, xylanase and ligninase are used to enhance the quality of the pulp by removing lignine and hemicelluloses, which are typical impurities [138].	Pulp and paper industries
hydrolases, alcohol dehydrogenases, transaminases	Synthesis of pharmaceuticals.	Pharma industry [133, 134, 139]

7.8 Design Parameters

Parametric design was performed based on buffer solution, reaction time, reaction temperature, substrate concentration, choice of co-solvent and enzyme. The buffer solution is the mixture of a weak acid and a conjugate base in water to ensure constant pH and salt concentration. C Wuensch et al. performed the enzymatic carboxylation of phenols in a buffer solution and studied its performance [140]. Imani et al. worked on the

carboxylation of graphene oxide (GO). In the process a buffer solution is used to ensure the basic condition of the solution which resulted in efficient Nano-graphene oxide carboxylation [141]. Similarly, Ballard et al. utilized a buffers for development of a rat liver phosphoenolpyruvate carboxylase [142].

7.9 In situ Product Removal

In situ product removal (ISPR) method is allows to scavenge product that is formed and therefore to shift the reaction equilibrium. A number of processes have been carried out in utilization of this process.

Figure 7.2 shows schematic representation of the split challenges to be addressed in the design of a biocatalytic process. The circles represent the three elements present in the reactor substrate (S), product (P) and biocatalyst (B). The nodes of the circles represent the four combinations of separations required: (a) P from S; (b) P from B; (c) P from S and B; and (d) S from B. The adoption of an in-situ-product-retrieval technique requires that separations a, b and c are carried out simultaneously; separation d is necessary to make possible reuse of either the biocatalyst or unpersuaded substrate [143].

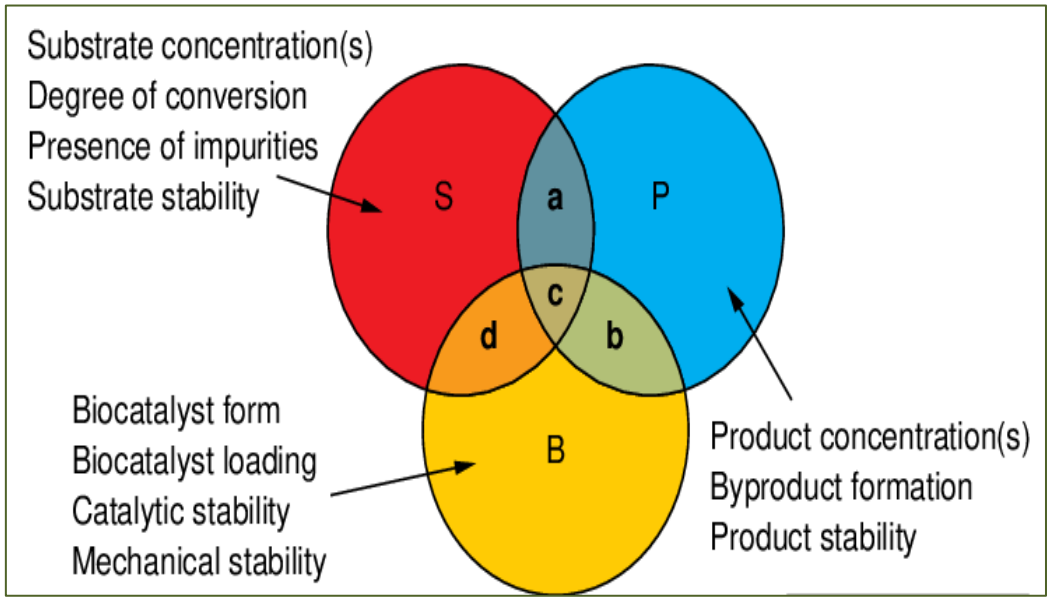

Figure 7.2: Typical biocatalyst process that needs ISPR for separation

7.10 What is Bioplastic?

Bioplastics are polymeric materials that are produced from renewable resources and ideally show good biocompatibility, biodegradability, and material properties. As such, bioplastic production has become one of the most active research areas in recent years. Bioplastic can be applied in packaging industries, spray materials, appliance materials, electronic products, agricultural products, or automation products. In the production of bioplastics, the interlinkage of biotechnology processes is a key strategy aimed at increasing the potential revenue of the entire bioprocessing chain. Given that mass generation of food waste is inevitable, the environmental burdens arising from waste disposal (e.g., water contamination and GHG emissions) should be mitigated [144].

According to the European Bioplastics Organization [145] bioplastics can be defined as plastics based on renewable resources (biobased) or as plastics which are biodegradable and/or compostable. Recently the attention in the packaging industry regarding the use of bioplastics has been shifting from compostable or biodegradable materials toward biobased materials. CO_2 that is captured from a biogas plant ultimately is derived from renewable resources. Any material (e.g., plastic) that utilizes such CO_2 as primary carbon source may therefore be regarded as bioplastic or biomaterial.

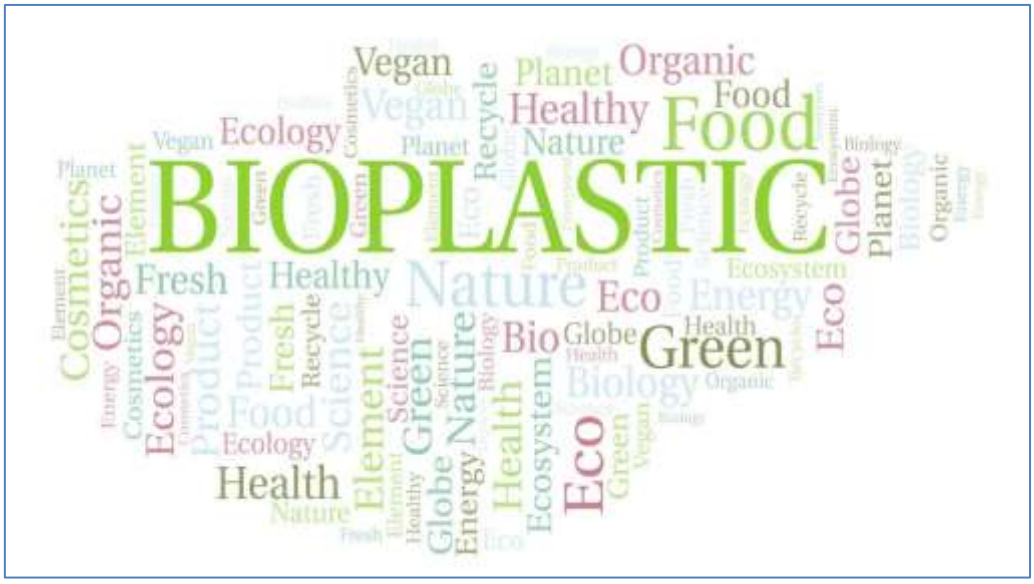

Figure 7.3: Bioplastic properties [146]

8. EXPERIMENTAL DESIGN AND SETUP

8.1 General Methods

In general, all provided data is based on at least two separately performed reactions.

In general, HPLC analysis was carried out on High pressure liquid chromatography machine (Shimadzu HPLC system: Communication Bus Module CBM-20 A, Column Oven CTO-20 AC, Degasser DGU-20 A5, Liquid Chromatograph LC-20 AD, Auto sampler SIL-20 AC, Diode Array Detector SPD-M20 A) equipped with a column Luna C18 Isis 110 °A, 150 mm × 4 mm, column temperature 30 ^{0}C.

Conversions were determined by comparison with calibration curves for substrates and products prepared with authentic reference material. All compounds were spectrophotometrically detected at 280 nm.

The method was run over 10 min with H_2O–acetonitrile (50/50) supplemented with trifluoroacetic acid (0.1%) as the mobile phase (flow rate 1 mL min^{-1}). SDS page was performed with Gene Script Express Plus^{TM} page gels. Cell disruption was carried out with a BRANSON Digital Sonifier.

8.2 Sources of Enzymes and Chemicals

The *o*-carboxylases 2,3-Dihydroxybenzoic acid decarboxylase from *Aspergillus oryzae* (2,3-DHBD_*Ao*, pEG: 41, pET21a), salicylic acid decarboxylase from *Trichosporon moniliiforme* (SAD_*Tm*, pEG: 69, pET21a) and 2,6-dihydroxybenzoic acid decarboxylase from *Rhizobium* species (2,6-DHBD_*Rs*, pEG: 68, pET21a) [117] as well as the *p*-carboxylase 3,4-dihydroxybenzoic acid decarboxylase from *Enterobacter cloacae* (*Ec*AroY, pEG 167, pET28a) [118] are available in the in-house plasmid database as well as glycerol stock in *E. coli* BL21 (DE3).

All chemicals were obtained from Sigma Aldrich in the highest available purity.

8.3 Biocatalyst Preparation as Lyophilized Whole Cells

Two types of carboxylases were produced for the different reactions.

1- ***ortho*-Carboxylases** [2,4-DHBD_*Ao*, 2,6-DHBD_*Rs* & SAD_*Tm*] [117]
2- ***para*-Carboxylase** [*Ec*AroY (pEG-167)] [118]

The following standard procedure was applied:

In order to grow cells, baffled Erlenmeyer flasks (2000 mL) were first rinsed with deionized water including their caps and then put it in the oven at a temperature of 200 °C for two hours for dry sterilization. Ingredients used for the preparation of LB medium is shown in the Table 8.1.

Table 8.1: Ingredients for LB medium.

Name	Amount
Yeast extract	5 g/L
Sodium Chloride	5 g/L
Tryptone	10 g/L

In this case yeast extract (15 g), NaCl (15 g) and tryptone (30 g) were dissolved in (3000 mL) of deionized water. Then all four sterilized vessels were filled equally with of LB medium (660 mL) and placed in an autoclave for sterilization (20 min at 120°C). Then an overnight culture (ONC) was prepared for each construct, according to standard procedure as defined bellow in the Table 8.2. This ONC was then put in a shaker at 37 ^{o}C and 120 rpm for overnight.

Inoculation of the flasks containing sterile LB-medium with the respective ONC (2 mL) was performed in the clean bench. Antibiotics (ampicillin for pEG 41, 68, & 69 and kanamycin for pEG-167) from a stock (stock: 100 mg/mL, addition: 660 µL) was added in all the four flasks in the clean bench. All four flasks were placed in a shaker at 30 °C and 120 rpm for 2 to 4 hours. Then a sample (1 mL) was taken and the optical density at 600 nm (OD600) is measured. When an OD600 of 0.6 to 1 was reached, the flasks were taken from the shaker and IPTG (660 µL from a 1 mol/L stock) was added to each flask

(660 µL) in the clean bench. Again, the flasks were placed in a shaker at 30 °C and 120 rpm for overnight.

Table 8.2: Overnight culture for each construct.

Name	LB medium general	Antibiotic (10 µL from a 100 mG/mL stock)	Cells from glycerol stock (10 µL)
2,4-DHBD_*Ao* (pEG-41)	10 mL	Ampicillin	2,3-DHBD_*Ao*
2,6-DHBD_*Rs* (pEG-68)	10 mL	Ampicillin	2,6-DHBD_*Rs*
SAD_*Tm* (pEG-69)	10 mL	Ampicillin	SAD_*Tm*
*Ec*AroY (pEG-167)	10 mL	KAN	*Ec*AroY

For harvesting, the medium was distributed in centrifuge beakers and centrifuged at 4 °C and 8000 rpm for 20 minutes to harvest the cells. The liquid phase was discarded and the cell pellet was resuspended in potassium phosphate buffer (100 mM, pH 7). Again, all the beakers were centrifuged at 4 °C and 8000 rpm for 20 minutes to wash the pellet. The liquid phase was removed, and the solid product was transferred into four round bottom flasks and frozen in liquid Nitrogen. Finally, the enzymes were lyophilized overnight. The lyophilized whole cell powder was collected in a plastic vial, weighted, labelled and stored in the freezer at -20 °C.

8.4 Decarboxylation Reaction

Decarboxylation is a chemical reaction that removes a carboxylate group and releases carbon dioxide (CO_2) [147].

$$RCO_2H \rightarrow R\text{-}H + CO_2 \qquad (8.1)$$

8.4.1 Enzyme Activity in Decarboxylation Direction

The respective enzyme in the form of lyophilized whole cells (20 mg for pEG 41, 5 mg for pEG 68, pEG 69 and pEG 167) was weighed into a microcentrifuge tube and phosphate buffer (900 µL, 100 mM, pH 7.5) was added. This mix was placed in a shaker at 30 C^o and 120 rpm for 30 minutes for rehydration. Substrate stock (100µL, 100 mM for a final concentration of 10 mM) was added to each microcentrifuge according to the Table 8.3 below:

Table 8.3: Substrates for decarboxylation.

Name	Stock in phosphate buffer (100 mM, pH 7.5)	Substrate
2,4-DHBD_*Ao* (pEG-41)	2 mL, 100 mM	2,6-DHBA
2,6-DHBD_*Rs* (pEG-68)	2 mL, 100 mM	2,6-DHBA
SAD_*Tm* (pEG-69)	2 mL, 100 mM	2,6-DHBA
*Ec*AroY (pEG-167)	2 mL, 100 mM	3,4-DHBA

The reactions set up like this were incubated at 30 C° and 120 rpm for the time given in the Table 8.4 below and then the general workup was performed to prepare samples for HPLC for analysis (see analytics). Based on the obtained conversions the enzyme preparations activity was calculated.

Table 8.4: Reaction times for the decarboxylation activity.

Enzyme [pEG]	Reaction Time [min]
2,4-DHBD_*Ao* (pEG-41)	10
2,4-DHBD_*Ao* (pEG-41)	20
2,4-DHBD_*Ao* (pEG-41)	30
2,4-DHBD_*Ao* (pEG-41)	60
2,4-DHBD_*Ao* (pEG-41)	over night
SAD_*Tm* (pEG-69)	10
SAD_*Tm* (pEG-69)	20
SAD_*Tm* (pEG-69)	30
SAD_*Tm* (pEG-69)	60
SAD_*Tm* (pEG-69)	over night
2,6-DHBD_*Rs* (pEG-68)	5
2,6-DHBD_*Rs* (pEG-68)	10
2,6-DHBD_*Rs* (pEG-68)	20
2,6-DHBD_*Rs* (pEG-68)	30
2,6-DHBD_*Rs* (pEG-68)	over night
*Ec*AroY (pEG-167)	10
*Ec*AroY (pEG-167)	20
*Ec*AroY (pEG-167)	30
*Ec*AroY (pEG-167)	60
*Ec*AroY (pEG-167)	over night

8.5 Carboxylation Reactions

Enzymatic carboxylation is a chemical reaction in which a carboxylic acid group is produced in an enzymatic reaction by treating a substrate with carbon dioxide [148].

$$R\text{-}H + CO_2 \rightarrow RCO_2H \qquad (8.2)$$

8.5.1 General Carboxylation Procedure

The respective enzyme in the form of lyophilized whole cells (either 2,4-DHBD_*Ao* (pEG-41), 2,6-DHBD_*Rs* (pEG-68), SAD_*Tm* (pEG-69) or *Ec*AroY (pEG-167), 30 mg) was weighed into a microcentrifuge tube and the respective buffer (as a standard 900 µL of a 100 mM phosphate buffer, pH 7.5 was used) was added. This mix was placed in a shaker at 30 C° and 120 rpm for 30 minutes for rehydration.
The rehydrated enzymes were poured into glass vials (5 mL) containing $KHCO_3$ (300 mg) and substrate stock (100 µL of the following stocks: resorcinol + ascorbic acid, each 100 mM in the reaction buffer for 2,4-DHBD_*Ao* (pEG-41), 2,6-DHBD_*Rs* (pEG-68) and SAD_*Tm* (pEG-69); or catechol + ascorbic acid, each 100 mM in the reaction buffer for *Ec*AroY (pEG-167); for a final substrate concentration of 10 mM) was added. The ascorbic acid was added as stabilizer for catechol to prevent autooxidation.

The samples were closed with a screw cap and a Teflon seal. The reactions were incubated at 30 C° and 120 rpm for the indicated time (standard: 24 h) before workup according to the general workup procedure and analysis on HPLC.

8.5.2 Buffer Screening

The buffer screening was performed according to the general carboxylation procedure, with the variations enlisted in the following Table 8.5.

Table 8.5: Parameters of the buffers screening.

Enzyme Type	Buffer	Substrate
2,4-DHBD_*Ao* (pEG-41)	phosphate, 100 mM, pH=5.5	resorcinol
2,4-DHBD_*Ao* (pEG-41)	TRIS-HCl, 100 mM, pH=6.2	resorcinol
SAD_*Tm* (pEG-69)	phosphate, 100 mM, pH=5.5	resorcinol

SAD_*Tm* (pEG-69)	TRIS-HCl, 100 mM, pH=6.2	resorcinol
2,6-DHBD_*Rs* (pEG-68)	phosphate, 100 mM, pH=5.5	resorcinol
2,6-DHBD_*Rs* (pEG-68)	TRIS-HCl, 100 mM, pH=6.2	resorcinol
*Ec*AroY (pEG-167)	phosphate, 100 mM, pH=5.5	catechol/ascorbic acid
*Ec*AroY (pEG-167)	TRIS-HCl, 100 mM, pH=6.2	catechol/ascorbic acid
blank	phosphate, 100 mM, pH=5.5	resorcinol
blank	TRIS-HCl, 100 mM, pH=6.2	resorcinol
blank	phosphate, 100 mM, pH=5.5	catechol/ascorbic acid
blank	TRIS-HCl, 100 mM, pH=6.2	catechol/ascorbic acid

8.5.3 Investigation of the Effect of Oxygen on the Recovery

These experiments were performed according to the general carboxylation procedure with degassed buffers and the prepared samples were overlaid with argon before the reaction vial was closed. The following Table 8.6 enlists the samples and the variations form the general carboxylation procedure.

Table 8.6: Design parameters for degassed buffers screening.

Enzyme Type	Enzyme Amount	Substrate	Substrate Amount	Buffer
*Ec*AroY (pEG-167)	20 mg	catechol / ascorbic acid	10 mM (=100µL from 100 mM stock)	phosphate, 100 mM, pH 5.5, degassed
substrate-blank	-	catechol / ascorbic acid	10 mM (=100µL from 100 mM stock)	phosphate, 100 mM, pH 5.5, degassed
product-blank	-	3,4-DHBA / ascorbic acid	10 mM (=100µL from 100 mM stock)	phosphate, 100 mM, pH 5.5, degassed

8.5.4 Screening of Different $KHCO_3$ Concentrations

The amount of added $KHCO_3$ was systematically varied from the general carboxylation procedure as enlisted in the Table 8.7 below. Furthermore, different buffers were compared.

Table 8.7: Design parameters for different $KHCO_3$ concentrations screening.

Enzyme Type	Substrate	Buffer	$KHCO_3$ [mg]
*Ec*AroY (pEG-167)	catechol / ascorbic acid	phosphate, 100 mM, pH 5.5	300
*Ec*AroY (pEG-167)	catechol / ascorbic acid	phosphate, 100 mM, pH 5.5	200
*Ec*AroY (pEG-167)	catechol / ascorbic acid	phosphate, 100 mM, pH 5.5	100
*Ec*AroY (pEG-167)	catechol / ascorbic acid	phosphate, 100 mM, pH 5.5	50
*Ec*AroY (pEG-167)	catechol / ascorbic acid	phosphate, 250 mM, pH 5.5	300
*Ec*AroY (pEG-167)	catechol / ascorbic acid	phosphate, 250 mM, pH 5.5	200
*Ec*AroY (pEG-167)	catechol / ascorbic acid	phosphate, 250 mM, pH 5.5	100
*Ec*AroY (pEG-167)	catechol / ascorbic acid	phosphate, 250 mM, pH 5.5	50
*Ec*AroY (pEG-167)	catechol / ascorbic acid	phosphate, 100 mM, pH 6.5	300
*Ec*AroY (pEG-167)	catechol / ascorbic acid	phosphate, 100 mM, pH 6.5	200
*Ec*AroY (pEG-167)	catechol / ascorbic acid	phosphate, 100 mM, pH 6.5	100
*Ec*AroY (pEG-167)	catechol / ascorbic acid	phosphate, 100 mM, pH 6.5	50
*Ec*AroY (pEG-167)	catechol / ascorbic acid	phosphate, 250 mM, pH 6.5	300
*Ec*AroY (pEG-167)	catechol / ascorbic acid	phosphate, 250 mM, pH 6.5	200
*Ec*AroY (pEG-167)	catechol / ascorbic acid	phosphate, 250 mM, pH 6.5	100
*Ec*AroY (pEG-167)	catechol / ascorbic acid	phosphate, 250 mM, pH 6.5	50
*Ec*AroY (pEG-167)	catechol / ascorbic acid	phosphate, 100 mM, pH 7.5	300
*Ec*AroY (pEG-167)	catechol / ascorbic acid	phosphate, 100 mM, pH 7.5	200
*Ec*AroY (pEG-167)	catechol / ascorbic acid	phosphate, 100 mM, pH 7.5	100
*Ec*AroY (pEG-167)	catechol / ascorbic acid	phosphate, 100 mM, pH 7.5	50
*Ec*AroY (pEG-167)	catechol / ascorbic acid	phosphate, 250 mM, pH 7.5	300
*Ec*AroY (pEG-167)	catechol / ascorbic acid	phosphate, 250 mM, pH 7.5	200
*Ec*AroY (pEG-167)	catechol / ascorbic acid	phosphate, 250 mM, pH 7.5	100
*Ec*AroY (pEG-167)	catechol / ascorbic acid	phosphate, 250 mM, pH 7.5	50
*Ec*AroY (pEG-167)	catechol / ascorbic acid	water	300
*Ec*AroY (pEG-167)	catechol / ascorbic acid	water	200
*Ec*AroY (pEG-167)	catechol / ascorbic acid	water	100

8.5.5 Recovery and Conversion After Two Hours

This experiment was performed according to the general carboxylation procedure, however, to check whether the reaction time is responsible for bad recoveries, the reaction time was shortened to 2h. The following Table 8.8 enlists all samples.

Table 8.8: Design parameters for two hours samples screening.

Enzyme Type	Substrate	Buffer	Reaction time [hr]
*Ec*AroY (pEG-167)	catechol / ascorbic acid	phosphate, 100 mM, pH 5.5	2
*Ec*AroY (pEG-167)	catechol / ascorbic acid	phosphate, 250 mM, pH 5.5	2
*Ec*AroY (pEG-167)	catechol / ascorbic acid	phosphate, 100 mM, pH 6.5	2
*Ec*AroY (pEG-167)	catechol / ascorbic acid	phosphate, 250 mM, pH 6.5	2
*Ec*AroY (pEG-167)	catechol / ascorbic acid	phosphate, 100 mM, pH 7.5	2
*Ec*AroY (pEG-167)	catechol / ascorbic acid	phosphate, 250 mM, pH 7.5	2
*Ec*AroY (pEG-167)	catechol / ascorbic acid	water	2

8.5.6 Carbonate Buffer (pH) Screening

These experiments were performed according to the general carboxylation procedure with different carbonate buffers at different pH values, to investigate the effect on conversion. The following Table 8.9 enlists all the samples.

Table 8.9: Design parameters for Carbonate buffer (pH) screening.

Enzyme Type	Substrate	Buffer	pH values of samples after 24 hours reaction time
*Ec*AroY (pEG-167)	catechol / ascorbic acid	carbonate, pH 7.99	8.56
*Ec*AroY (pEG-167)	catechol / ascorbic acid	carbonate, pH 8.50	8.87
*Ec*AroY (pEG-167)	catechol / ascorbic acid	carbonate, pH 8.99	9.20
*Ec*AroY (pEG-167)	catechol / ascorbic acid	carbonate, pH 9.49	9.69

*Ec*AroY (pEG-167)	catechol / ascorbic acid	carbonate, pH 10.00	9.97
*Ec*AroY (pEG-167)	catechol / ascorbic acid	carbonate, pH 10.49	10.56
*Ec*AroY (pEG-167)	catechol / ascorbic acid	carbonate, pH 11.01	11.01
*Ec*AroY (pEG-167)	catechol / ascorbic acid	carbonate, pH 11.48	11.35

8.5.7 Substrate Concentration Screening

These experiments were performed according to the general carboxylation procedure at different substrate concentrations, to check the conversion at different substrate concentrations. The following Table 8.10 enlists all the samples.

Table 8.10: Design parameters for Substrate concentration screening.

Enzyme Type	Substrate	Substrate conc. [mM]	Amount Substrate Stock [µL]	Buffer (Water) Amount [µL]
*Ec*AroY (pEG-167)	catechol / ascorbic acid	5	50	950
*Ec*AroY (pEG-167)	catechol / ascorbic acid	10	100	900
*Ec*AroY (pEG-167)	catechol / ascorbic acid	20	200	800
*Ec*AroY (pEG-167)	catechol / ascorbic acid	30	300	700
*Ec*AroY (pEG-167)	catechol / ascorbic acid	50	500	500
*Ec*AroY (pEG-167)	catechol / ascorbic acid	80	800	200
*Ec*AroY (pEG-167)	catechol / ascorbic acid	100	1000	0

8.5.8 Reaction Time Screening

These experiments were performed according to the general carboxylation procedure, to investigate the conversion at different reaction times. The following Table 8.11 enlists all the samples.

Table 8.11: Design parameters for reaction time screening.

Enzyme Type	Substrate	Amount substrate stock [µL]	Buffer (Water) Amount [µL]	$KHCO_3$ [mg]	Reaction time [h]
*Ec*AroY (pEG-167)	catechol / ascorbic acid	100	900	300	0.5
*Ec*AroY (pEG-167)	catechol / ascorbic acid	100	900	300	1
*Ec*AroY (pEG-167)	catechol / ascorbic acid	100	900	300	2
*Ec*AroY (pEG-167)	catechol / ascorbic acid	100	900	300	4
*Ec*AroY (pEG-167)	catechol / ascorbic acid	100	900	300	6
*Ec*AroY (pEG-167)	catechol / ascorbic acid	100	900	300	24
*Ec*AroY (pEG-167)	catechol / ascorbic acid	100	900	300	48
*Ec*AroY (pEG-167)	catechol / ascorbic acid	100	900	300	96
*Ec*AroY (pEG-167)	catechol / ascorbic acid	100	900	300	168

8.5.9 Temperature Screening

These experiments were performed according to the general carboxylation procedure to check the effect of different temperatures on conversion. The following Table 8.12 enlists all the samples.

Table 8.12: Design parameters for temperature screening.

Enzyme Type	Substrate	Amount substrate stock [µL]	Buffer (Water) Amount [µL]	$KHCO_3$ [mg]	Temperature [°C]
*Ec*AroY (pEG-167)	catechol / ascorbic acid	100	900	300	20
*Ec*AroY (pEG-167)	catechol / ascorbic acid	100	900	300	25

*Ec*AroY (pEG-167)	catechol / ascorbic acid	100	900	300	30
*Ec*AroY (pEG-167)	catechol / ascorbic acid	100	900	300	35
*Ec*AroY (pEG-167)	catechol / ascorbic acid	100	900	300	40
*Ec*AroY (pEG-167)	catechol / ascorbic acid	100	900	300	50
*Ec*AroY (pEG-167)	catechol / ascorbic acid	100	900	300	60

8.5.10 Co-Solvent Screening

These experiments were performed according to the general carboxylation procedure but with the indicated volume of different co-solvents to investigate the effect of different reaction media on conversion. *Ec*AroY (pEG: 167) enzyme (30 mg) was used with catechol and ascorbic acid (10 mM) as substrate together with potassium bicarbonate (300 mg), using water as the main solvent in combination with the different indicated co-solvents. The following Table 8.13 enlists all the samples.

Table 8.13: Design parameters for co-solvent screening.

Co-Solvent	Buffer (Water) Amount [µL]	Co-Solvent Amount [µL]	Co-Solvent Amount [%]
-	900	-	0
DMSO (dimethyl sulfoxide)	800	100	10
DMF (dimethylformamide)	800	100	10
methanol	800	100	10
ethanol (pure)	800	100	10
2-propanol	800	100	10
t-butanol	800	100	10
ethylene glycol	800	100	10
1,2-dimethoxyethane	800	100	10
acetone	800	100	10

acetonitrile	800	100	10
glycerol	800	100	10
1,4-dioxane	800	100	10
toluene	800	100	10
n-heptane	800	100	10
t-butyl methyl ether	800	100	10
DMSO (dimethyl sulfoxide)	700	200	20
DMF (dimethylformamide)	700	200	20
methanol	700	200	20
ethanol (pure)	700	200	20
2-propanol	700	200	20
t-butanol	700	200	20
ethylene glycol	700	200	20
1,2-dimethoxyethane	700	200	20
acetone	700	200	20
acetonitrile	700	200	20
glycerol	700	200	20
1,4-dioxane	700	200	20
toluene	700	200	20
n-heptane	700	200	20
t-butyl methyl ether	700	200	20

8.5.11 Water Immiscible Co-Solvents Screening

In these experiments the previous screening was extended to water immiscible co-solvents. The screening was performed as before, but with the modified workup-procedure. The following Table 8.14 enlists the design parameters of all the samples.

Table 8.14: Design parameters for water immiscible co-solvents.

Name	Water	Co-Solvent
positive blank	900µL	-
10% *t*BME	800 µL	100 µL *t*-butyl methyl ether
10% *n*-heptane	800 µL	100 µL *n*-heptane
10% *t*BME negative blank	800 µL	100 µL *t*-butyl methyl ether
10% *n*-heptane negative blank	800 µL	100 µL *n*-heptane
20% *t*BME	700 µL	200 µL *t*-butyl methyl ether
20% *n*-heptane	700 µL	200 µL *n*-heptane
20% *t*BME negative blank	700 µL	200 µL *t*-butyl methyl ether
20% *n*-heptane negative blank	700 µL	200 µL *n*-heptane

8.5.12 Higher Enzyme and Substrate Concentration Screening

*Ec*AroY (pEG: 167) enzyme (30 mg, 45 mg or 60 mg) was used with the substrate (catechol / ascorbic acid, each 10 mM) and water as a buffer. The experiments were performed to check the conversion at higher enzyme and substrate loadings. The following Table 8.15 enlists all the samples.

Table 8.15: Design parameters for higher enzyme and substrate.

Enzyme [mg]	Substrate [mmol/L]	Substrate stock [µL]	Buffer (water) [µL]
30	10	100	900
45	10	100	900
60	10	100	900
30	30	300	700
45	30	300	700
60	30	300	700
30	50	500	500

45	50	500	500
60	50	500	500

8.6 Analytics

Calibration in broad sense is the process of bringing a method, procedure and operation in general to confirm with set of objectives and goals that are established and highly reliable [149].

In measurement sciences, calibration is an operation that establishes a relationship between an output quantity with an input quantity for a measuring system under specified conditions. The result of calibration is a model that may have the form of a conversion factor, a mathematical equation, or a graph. By means of this model, then it is possible to estimate input values from measured output values.

8.6.1 Chromatographic Methods

Chromatography is based on the principle that molecules can be separated via interaction with a stationary and a mobile phase. The intermolecular interactions between molecules of the sample and the stationary phase determine their time on the column. HPLC uses a moderate to high pressure to achieve the desired flow rate of the solvent through the chromatographic column as small particles have greater resistance to flow. There are different solvents used in HPLC such as aqueous solvents (water) and organic solvents (methanol, acetonitrile, or propanol). To improve the chromatographic peak shape, acids can be used such as acetic acid, formic acid, trifluoroacetic acid. A pump aspirates the mobile phase from the solvent reservoir and moves it through the system's column and detector. An injector for an HPLC system should provide injection of the liquid sample within the range of 0.1-100 µL of volume with high reproducibility and under high pressure (up to 4000 psi). The HPLC detector, located at the end of the column detects the analytes as they elute from the chromatographic column. Commonly used detectors are UV-spectroscopy, fluorescence, mass-spectrometric and electrochemical detectors. Measurements are usually on columns made of polished stainless steel, that are between 50 and 300 mm long and have an internal diameter of between 2 and 5 mm. They are commonly filled with a stationary phase with a particle size of 3–10 µm. [150, 151].

8.6.1.1 HPLC Method

A Shimadzu HPLC system (Communication Bus Module CBM-20 A, Column Oven CTO-20 AC, Degasser DGU-20 A5, Liquid Chromatograph LC-20 AD, Auto sampler SIL-20 AC, Diode Array Detector SPD-M20 A) was used to analyse the samples on a Luna C18 Isis 110 °A, 150 mm × 4 mm, column, at a column temperature of 30 ^{0}C.The retention times were as follows: methyl-2 benzoic acid: 8.20 min; methyl-2 catechol: 8.51 min. For the quantification, a calibration for the substrate and product was established.

8.6.2 Calibrations

Standards were freshly prepared, following the same procedure that was used for the preparation and workup of the reactions and measured on the regular basis. Below are the latest calibrations for all compounds shown in the Figure 8.1 below.

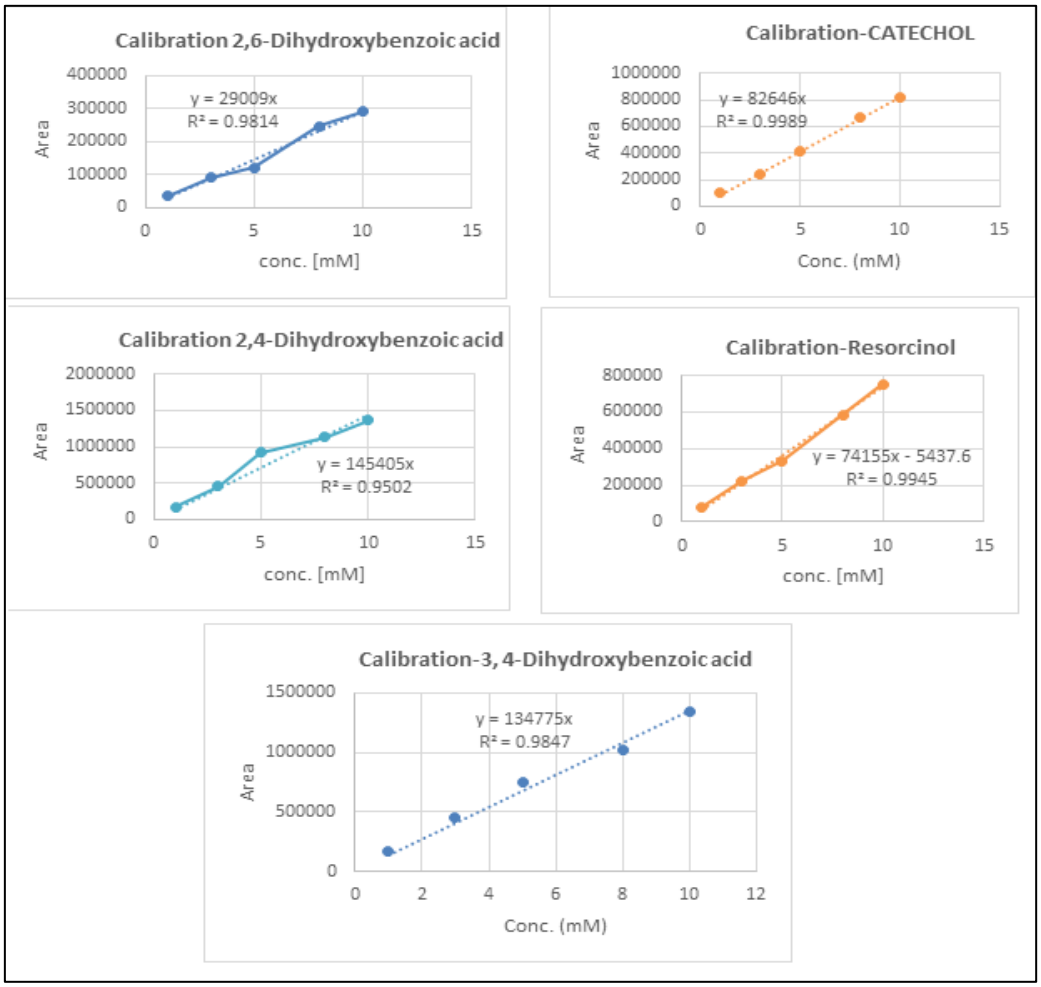

Figure 8.1: Calibration curves of the substrates and products on HPLC.

8.7 Sample preparation for HPLC analysis

If the reaction was performed in HPLC glass vials, the content was transferred into 2 mL microcentrifuge vials, which were centrifuged at 13000 rpm for 15 minutes. If the reaction was performed in microcentrifuge vials, the mixture was directly centrifuged at 13000 rpm for 15 minutes. In both cases, part of the supernatant (100 µL) was transferred into microcentrifuge vials (1.5 mL), a mix of water, acetonitrile and trifluoroacetic acid (total 1000 µL; 50/50/1) was added and the mixture was centrifuged again at 13000 rpm for 15 minutes. The supernatant was transferred to HPLC glass vials, closed, labelled analyzed on aqueous HPLC.

8.7.1 Modification for water-immiscible co-solvents

In case water-immiscible cosolvents were used, the cosolvent was evaporated using a gentle airstream prior to the general workup.

9. RESULTS, ANALYSIS AND DISCUSSION

9.1 Introduction

Basically, this focusses around two reactions, carboxylation & decarboxylation. For the reactions catalysed by the three *o*-carboxylases 2,3-DHBD_*Ao* (pEG: 41), SAD_*Tm* (pEG: 69), 2,6-DHBD_*Rs* (pEG: 68), generally resorcinol was applied as test-substrate, yielding a mix of the regio-isomers 2,6-dihydroxybenzoic acid (major product) and 2,4-dihydroxybenzoid acid. For the reversed (decarboxylation) reaction, 2,6-dihydroxybenzoic acid was converted back to resorcinol Figure 9.1.

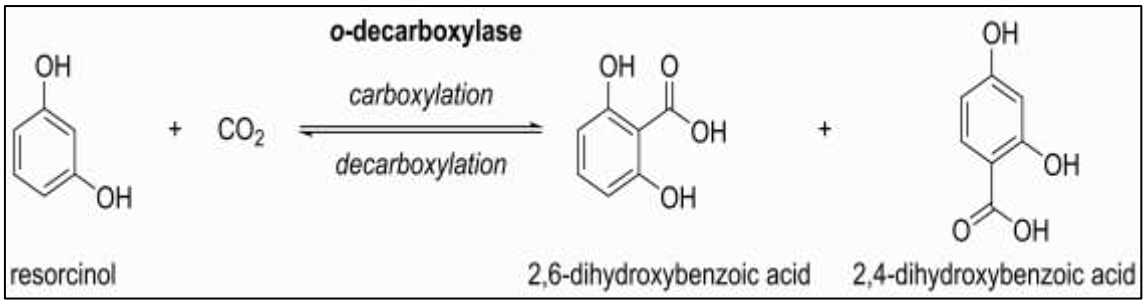

Figure 9.1: o-carboxylation of resorcinol and decarboxylation of 2,6-dihydroxybenzoic acid by o-carboxylases.

In case of the *p*-carboxylase *Ec*AroY (pEG 167) catechol serves as substrate and is carboxylated to form 3,4-dihydroxybenzoic acid. Decarboxylation of 3,4-dihydroxybenzoic acid again yields catechol Figure 9.2.

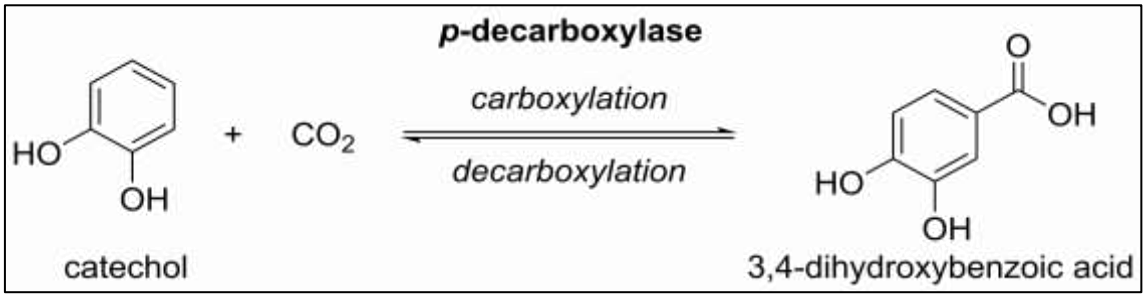

Figure 9.2: p-carboxylation of catechol and decarboxylation of 3,4-dihydroxybenzoic acid by p-carboxylases.

9.2 Results

Results of the experiments and their analysis are briefly explained in the figures and tables.

9.2.1 Enzyme Preparation

Two types of enzymes in the form of lyophilised whole cells were produced. The yields obtained from 660 mL of culture is shown in the Figure 9.3 and Table 9.1.

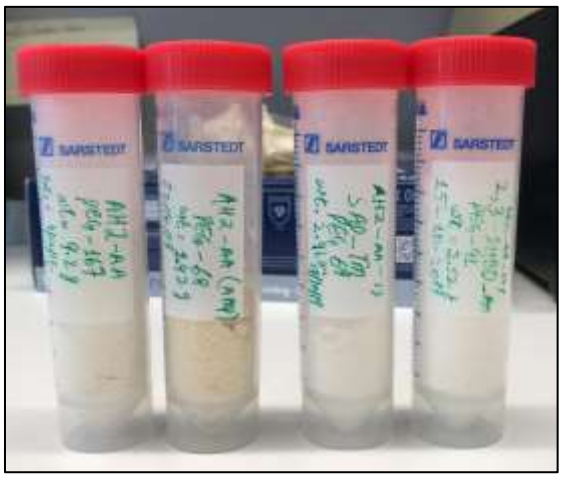

Figure 9.3: Lyophilized whole cells of 2,3-DHBD_Ao (pEG: 41), SAD_Tm (pEG: 69), 2,6-DHBD_Rs (pEG: 68) and EcAroY (pEG 167).

Table 9.1: Yield of lyophilized whole cells.

Biocatalyst/ Enzyme		**Yield [lyophilized cells, mg]**
o-carboxylases	2,3-Dihydroxybenzoic acid decarboxylase from ***Aspergillus oryzae*** (2,4-DHBD_Ao), **pEG: 41**	2.52
	2,6-dihydroxybenzoic acid decarboxylase from **Rhizobium species** (2,6-DHBD_*Rs*), p**EG: 68**	2.42
	salicylic acid decarboxylase from ***Trichosporon moniliiforme*** (SAD *Tm*), **pEG: 69**	2.96
p-carboxylase	3,4-Dihydroxybenzoic acid decarboxylase from ***Enterobacter cloacae*** (*Ec*AroY), p**EG: 167**	9.2

Furthermore, the SDS-gel Figure 9.4 of the four constructs shows good overexpression for all target enzymes except SAD*Tm* (pEG: 69).

Scale	Standard	-	2,4-DHBD_Ao (pEG 41)	2,6-DHBD_*Rs* (pEG 68)	SAD_*Tm* (pEG 69)	*Ec*AroY(pEG 168)
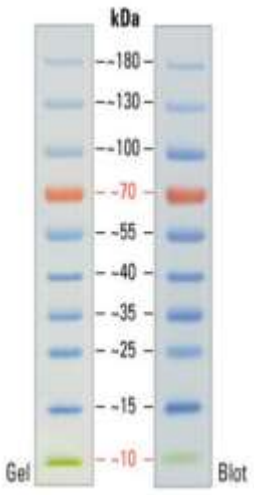	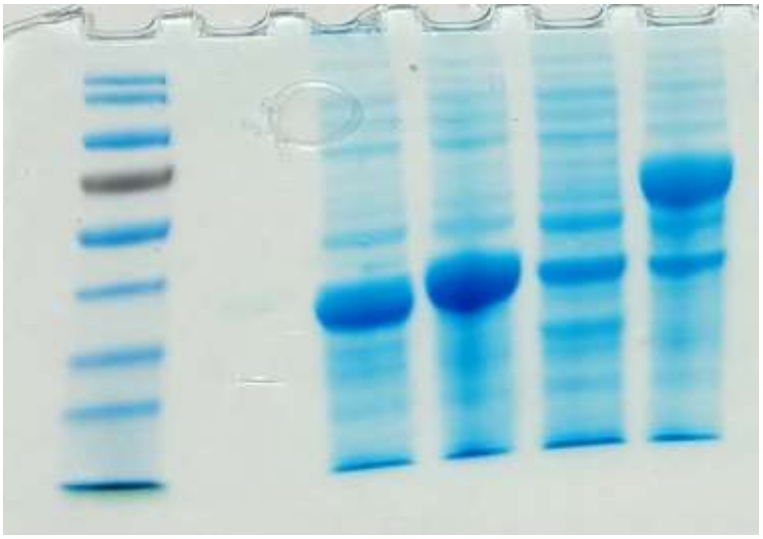					

Figure 9.4: SDS-gel of whole cell of the four constructs.

The sizes of the bonds showing overexpression fit to the calculated enzyme masses as shown in the Table 9.2 given below.

Table 9.2: Calculated mass of all the enzymes.

Enzyme type	Calculated mass
2,4-DHBD_*Ao* (pEG: 41)	21 kDa
2,6-DHBD_*Rs* (pEG: 68)	37 kDa
SAD_*Tm* (pEG: 69)	39 kDa
*Ec*AroY (pEG: 167)	53 kDa

As 3,4-dihydroxybenzoic acid decarboxylase from *Enterobacter cloacae* (*Ec*AroY), has not been investigated in literature as deeply as the other enzymes and as the obtained *p*-hydroxybenzoic acid has potential to serve as monomer for polymerization, this work mainly focuses on this enzyme.

9.2.2 Determination of the Enzyme Activities in the Decarboxylation Reaction

These experiments were performed to check which enzyme is more active and from the results it was clear that *Ec*AroY (pEG: 167) was more active than the other three with 24 U/g lyophilized whole cells as shown in the Table 9.3.

Table 9.3: Activity of the enzyme preparations.

Enzyme type	**Activity** U/g catalyst	**Conversion after 24h [%]**
2,4-DHBD_*Ao* (pEG: 41)	**3.9**	**>99**
2,6-DHBD_*Rs* (pEG: 68)	**11**	**>99**
SAD_*Tm* (pEG: 69)	**20**	**>99**
*Ec*AroY (pEG: 167)	**24**	**98**

The corresponding time curves are also given in the Figure 9.5 below. From the figure it is clear that EcAroY (pEG-167) is showing promising results as compared to the others.

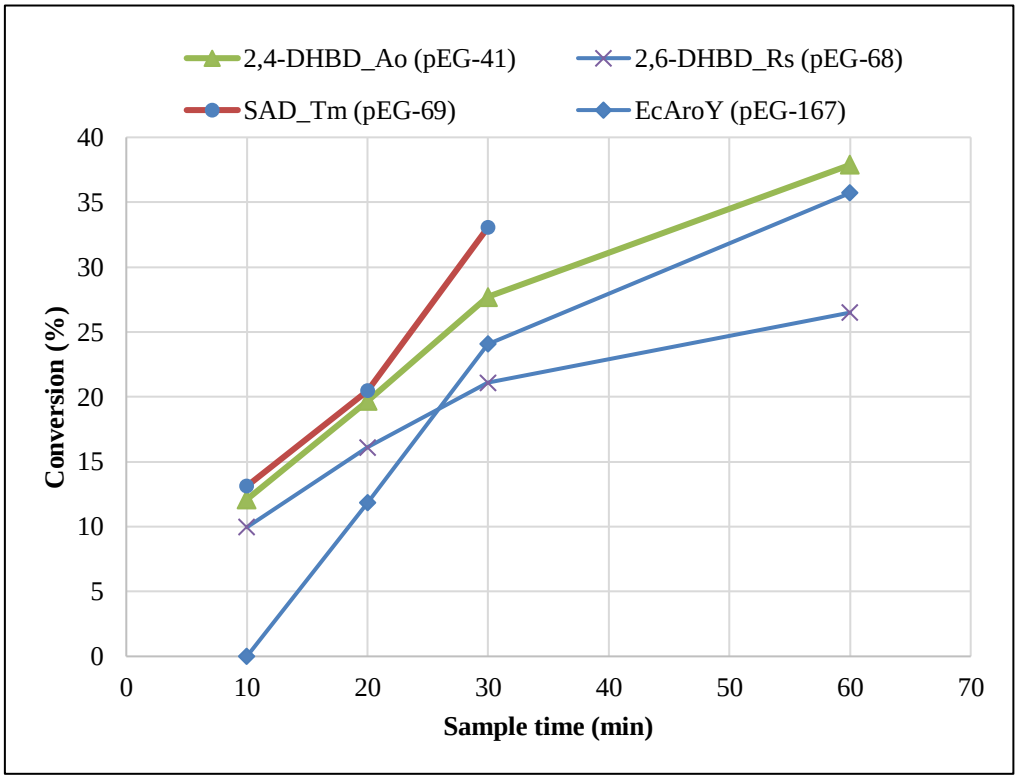

Figure 9.5: Time curves for the activity measurements.

9.2.3 Buffer Screening in the Carboxylation Reaction

The influence of the buffer salt (TRIS-HCl buffer vs. phosphate buffer, both 100 mM) on the conversion was tested with resorcinol for the *o*-carboxylases and catechol with ascorbic acid for the *p*-carboxylase. The ascorbic acid was added as stabilizer for catechol to prevent autooxidation.

Recovery is troublesome but results are reproducible when conversion is calculated based on recovery. Recovery refers to analytical recovery. As both, the substrate and the product are calibrated using external standards, the recovery is the sum of detected substrate and product. As can be seen in the Figure 9.6, the two buffers perform comparably for all enzymes.

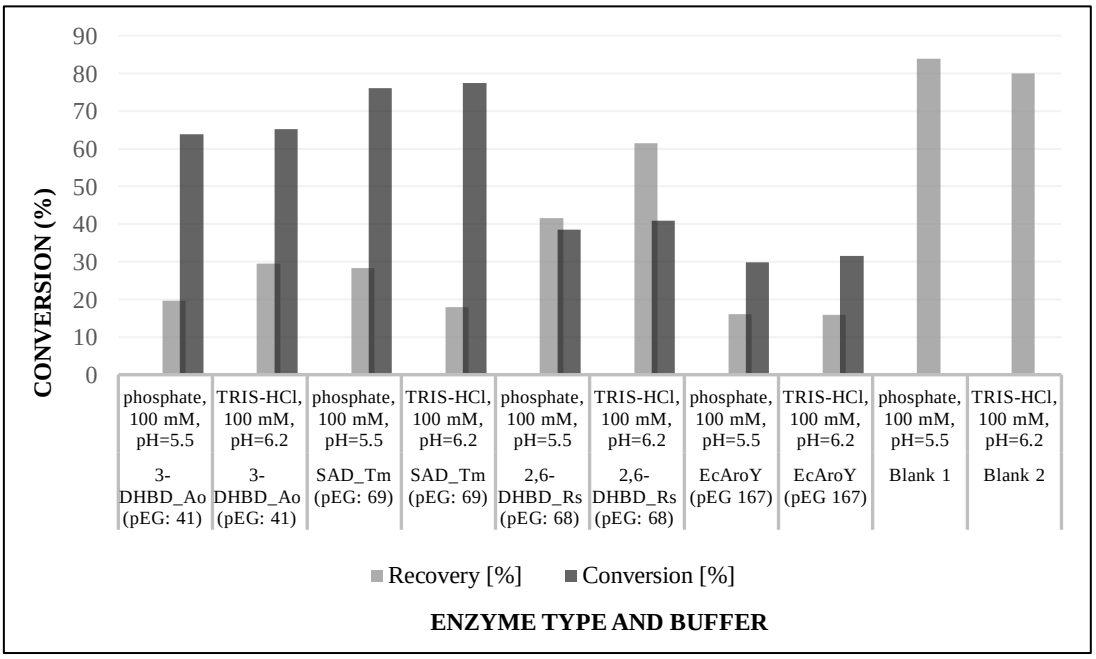

Figure 9.6: Recovery and conversion in the screening of different buffer salts in the carboxylation of catechol and resorcinol.

9.2.4 Influence of Oxygen on the Recovery

These experiments were performed to check if the recovery improves, when the samples are degassed and therefore oxygen-free. The substrate catechol (with ascorbic acid) was used for *p*-carboxylase *Ec*AroY (pEG: 167). Phosphate-buffer (100 mM, pH 5.5, degassed) was used for all the experiments with 300 mg potassium bicarbonate. However,

the recovery did not improve, so oxygen seems not to affect the recovery as shown in the Figure 9.7 given below.

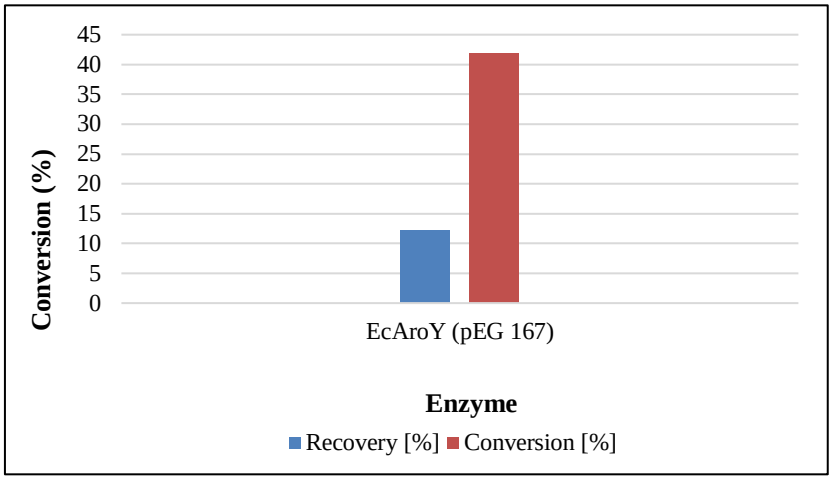

Figure 9.7: Recovery and conversion in the carboxylation of catechol using EcAroY, in the absence of oxygen

9.2.5 Evaluation of Different KHCO3 Concentrations and Buffers in the Carboxylation Reaction

All the experiments were performed three times with the *p*-carboxylase to see what amount of $KHCO_3$ is required for good conversion and what is the effect of the $KHCO_3$ concentrations on the recovery. In addition, different buffers and buffer concentrations were checked. In general, the higher the $KHCO_3$ concentration, the lower was the recovery. Accordingly, also all the buffers, performed similar, however, the best results were obtained with the phosphate buffer at a concentration of 250 mM at pH 5.5.

Recovery refers to analytical recovery. As both, the substrate and the product are calibrated using external standards, the recovery is the sum of detected substrate and product while conversion is the percentage of formed product from the sum of analytically recovered substrate and product.

It was interesting to see that the use of sole water gave a very comparable conversion. Buffer concentrations of 250 mM are obviously not enough to buffer the effect of 3M $KHCO_3$ on pH. Furthermore, the pH of all samples after the reaction was quite similar. For future screenings water was used as solvent. The results are given in the Figure 9.8 and Figure 9.9.

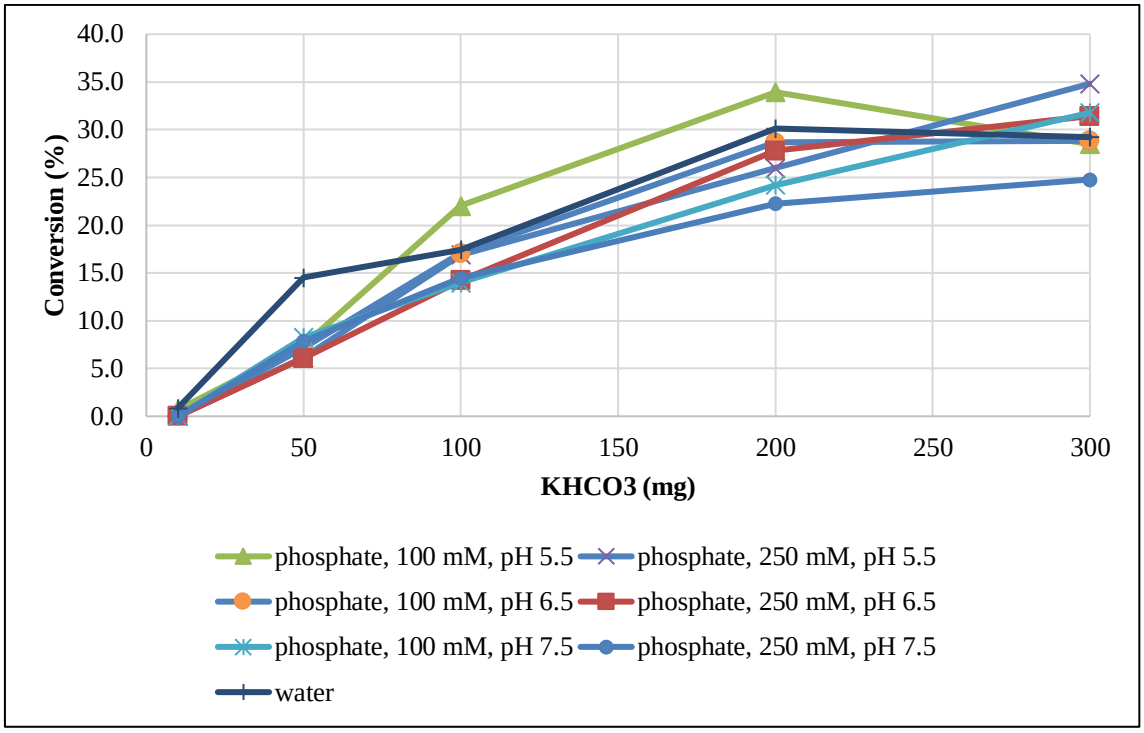

Figure 9.8: Carboxylation of catechol using EcAroY in different buffers and at different concentrations of $KHCO_3$.

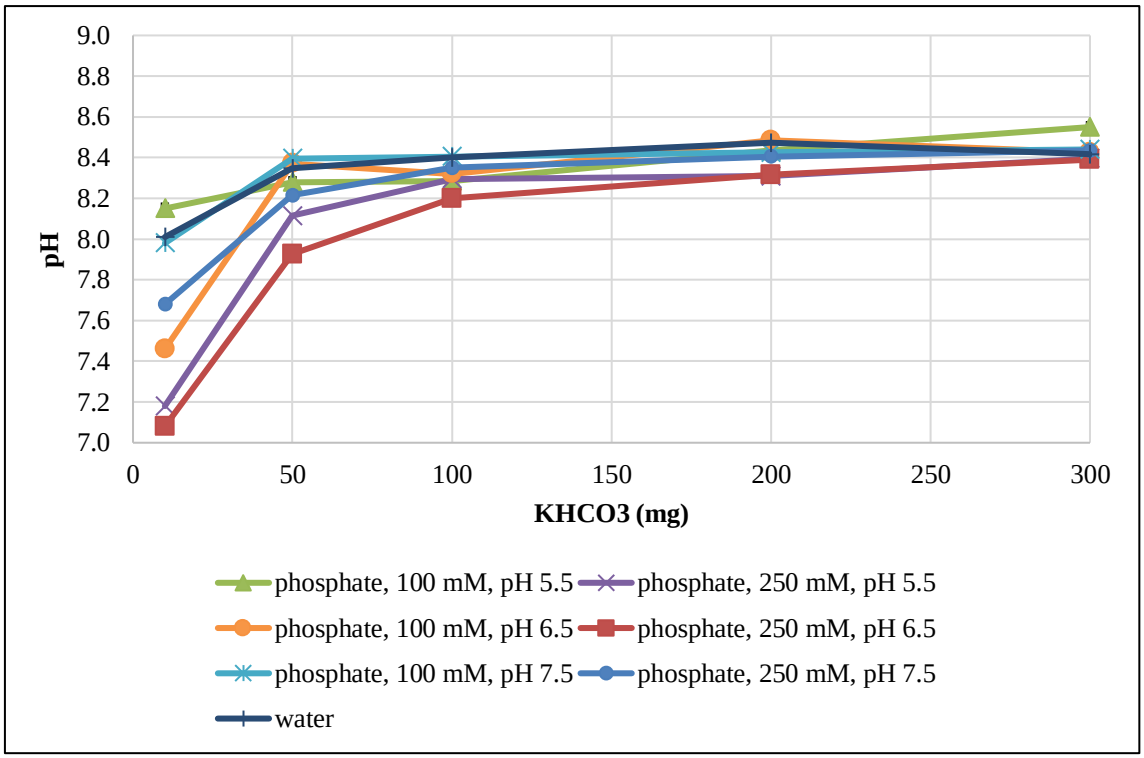

Figure 9.9: Effect of in different buffers and different concentrations of $KHCO_3$ on the pH.

9.2.6 Effect of Shorter Reaction Rimes on the Recovery and Conversion in the Carboxylation of Catechol

These experiments were performed to check the recovery and conversion if the samples are placed in the shaker for a shorter reaction time (two hours instead of 24 hours). Recovery refers to analytical recovery. As both, the substrate and the product are calibrated using external standards, the recovery is the sum of detected substrate and product while conversion is the percentage of formed product from the sum of analytically recovered substrate and product.

The substrate catechol (with ascorbic acid) was used with the *p*-carboxylase *Ec*AroY (pEG: 167). 300 mg Potassium bicarbonate were used with the same biocatalyst amount (30 mg). The pH of the samples was measured after the reaction.

From the results it was clear that the conversion was lower as compared to the 24 hours samples and the recovery was still insufficient as shown in the Figure 9.10.

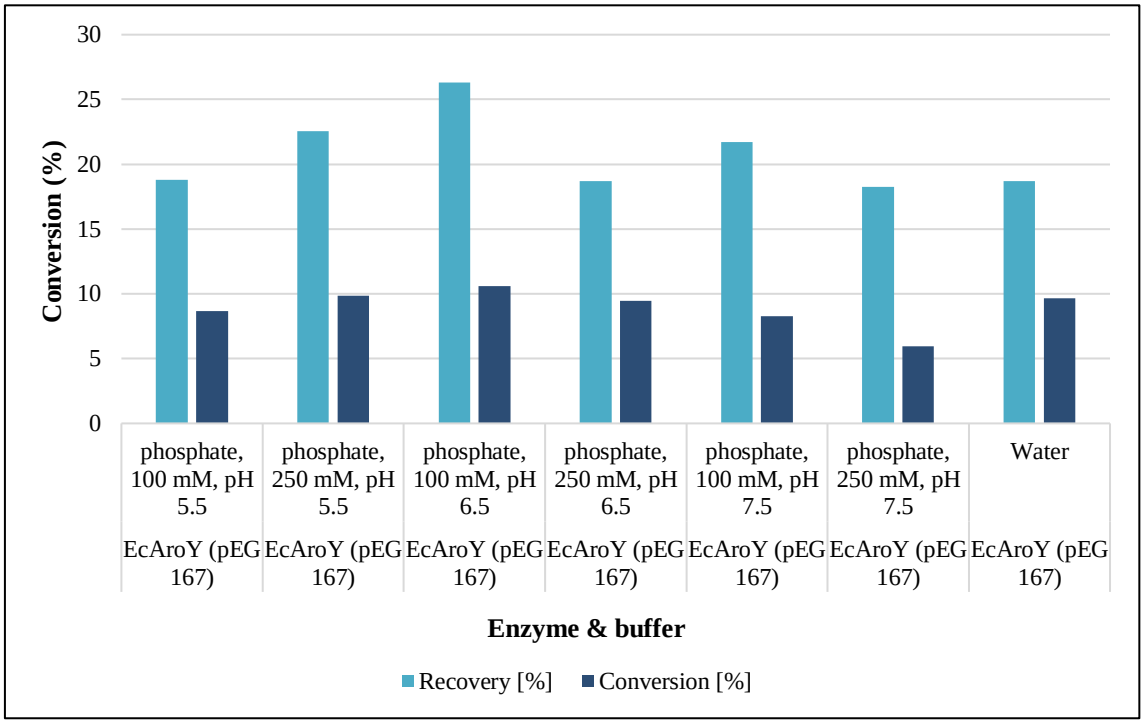

Figure 9.10: Recovery and conversion after two hours of reaction time using catechol as substrate for carboxylation with EcAroY (pEG: 167).

9.2.7 Evaluation of Carbonate Buffers at Different pH in the Carboxylation of Catechol

These experiments were performed to check the conversion at different pH values in carbonate buffers. The substrate catechol (with ascorbic acid) was used for the *p*-carboxylase *Ec*AroY (pEG: 167). The conversion is the percentage of formed product from the sum of analytically recovered substrate and product.

The pH of the samples was measured after the reaction for the comparison and analysis.

From the results it was clear that there was a good conversion at pH values between 7.99 and 8.50 and conversion goes to zero at pH values above 9.49 (Figure 9.11).

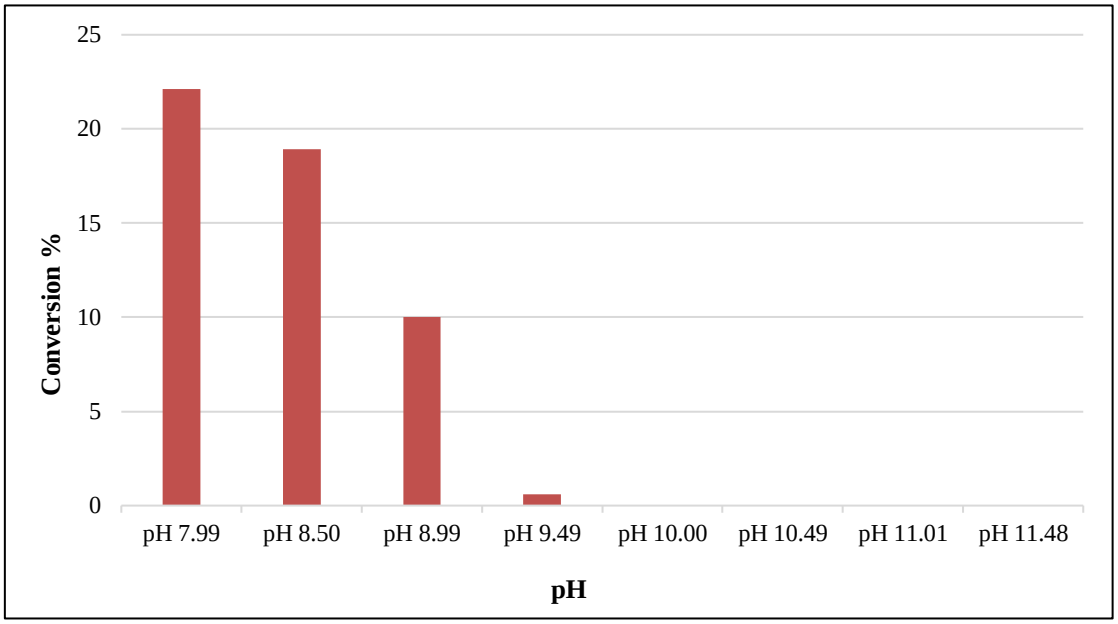

Figure 9.11: Carboxylation of catechol using EcAroY in different carbonate buffers at constant carbonate concentration (3M).

9.2.8 Evaluation of Different Catechol Concentrations in the Carboxylation Reaction

These experiments were performed to check the recovery and conversion based on different concentrations of the substrate according to general carboxylation method. Water was used as a buffer and the pH values of the samples were measured after the reaction (24 hours). Recovery refers to analytical recovery. As both, the substrate and the

product are calibrated using external standards, the recovery is the sum of detected substrate and product while conversion is the percentage of formed product from the sum of analytically recovered substrate and product.

From the results it was clear that conversion was highest at 100 mM amount of the substrate as shown in the graph below (Figure 9.12).

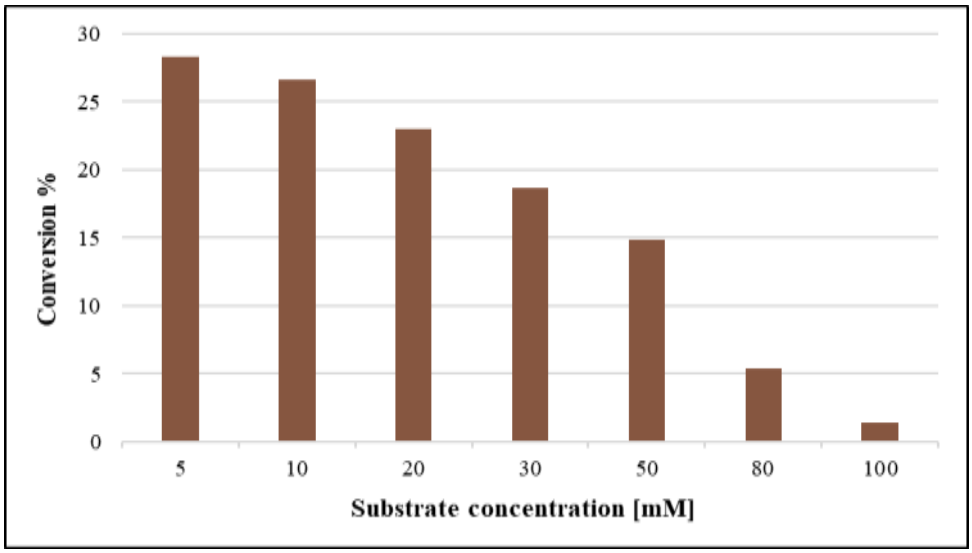

Figure 9.12: Carboxylation of catechol using EcAroY at different substrate concentrations.

Although the conversion was only 14% when a concentration of 50 mmol/L catechol was applied, this translates to 7 mmol/L of formed product as depicted in Figure 9.13.

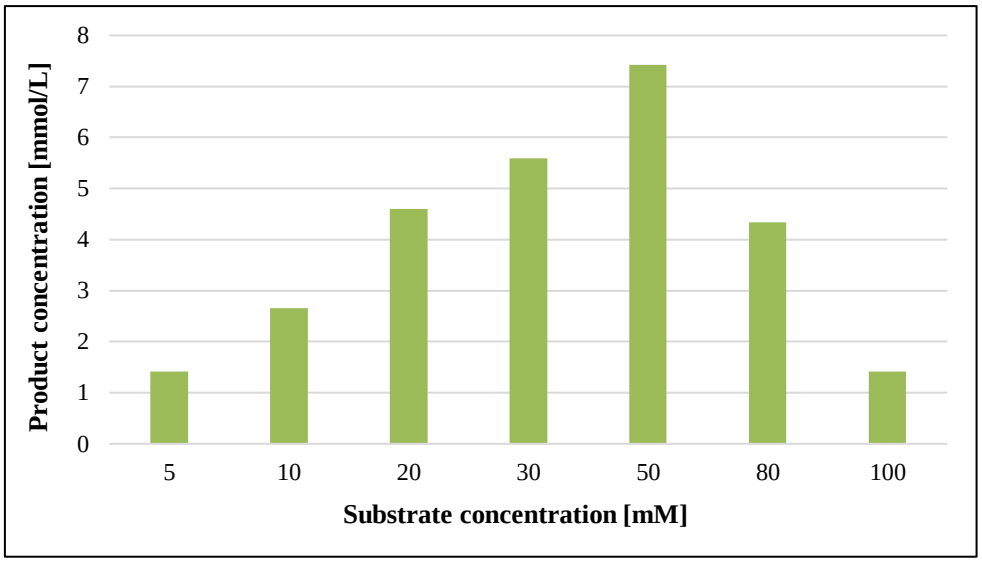

Figure 9.13: Product formation using EcAroY for the carboxylation of catechol at different substrate concentrations.

9.2.9 Effect of Prolonged Reaction Time on the Carboxylation of Catechol

These experiments were performed to check conversion if an increase of the reaction time has a beneficial effect on the carboxylation. Water was used as a buffer and the pH values of the samples were measured after the reaction (24 hours). The conversion is the percentage of formed product from the sum of analytically recovered substrate and product.

From the results it was clear that highest conversion (up to 52%) was recorded after 168 hours (one week) of time as shown in the graph below (Figure 9.14).

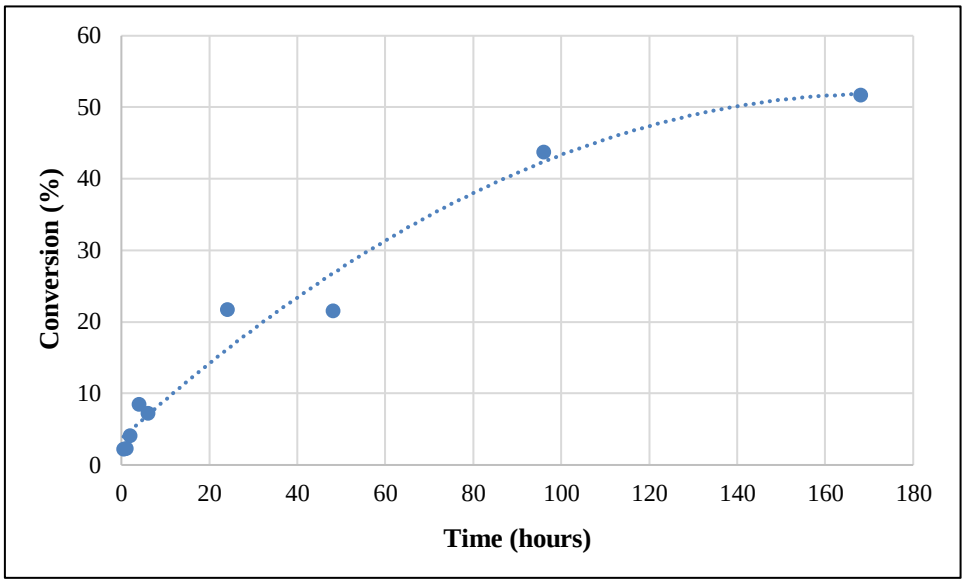

Figure 9.14: Carboxylation of catechol using EcAroY at prolonged reaction times.

9.2.10 Evaluation of Different Reaction Temperatures in the Carboxylation Reaction

These experiments were performed to investigate the conversion at different temperatures during the reaction, according to general carboxylation method. Water was used as a buffer and the pH of the samples was measured after the reaction (24 hours). The conversion is the percentage of formed product from the sum of analytically recovered substrate and product.

From the results it was clear that conversion was recorded highest at 35 to 50 ^{0}C as shown in the graph below (Figure 9.15).

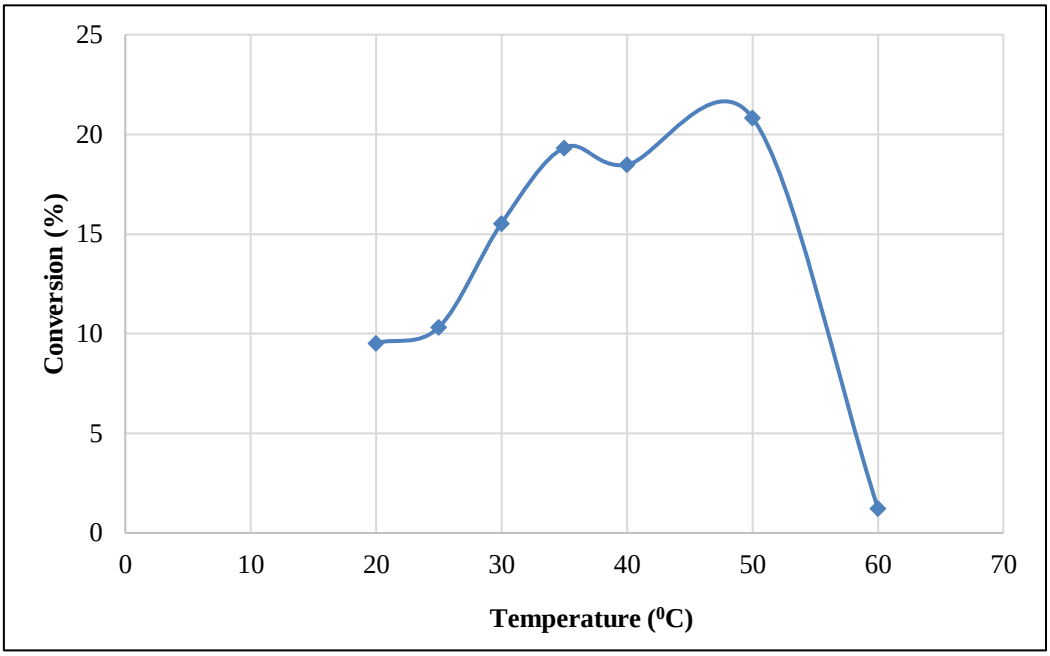

Figure 9.15: Carboxylation of catechol using EcAroY at different reaction temperatures.

9.2.11 Investigation of Different Co-Solvents for the Carboxylation Reaction.

These experiments were performed to check the effect of different co-solvents on the conversion of a reaction according to general carboxylation method. Water was used as a buffer and the pH values of the samples was measured after the reaction (24 hours).

The results suggest that the highest conversion was recorded using *t*-butyl methyl ether as a co-solvent as shown in the graph below (Figure 9.16). However, it needs to be mentioned, that the conversion of the positive blank reaction could not be reproduced in this screening. Therefore, only relative conversions are reported. Furthermore, the extraction procedure that was applied in the standard workup method could not be used for the water-immiscible solvents glycerol, n-heptane and using *t*-butyl methyl ether. These values can therefore not be compared to the others. The conversion is the percentage of formed product from the sum of analytically recovered substrate and product.

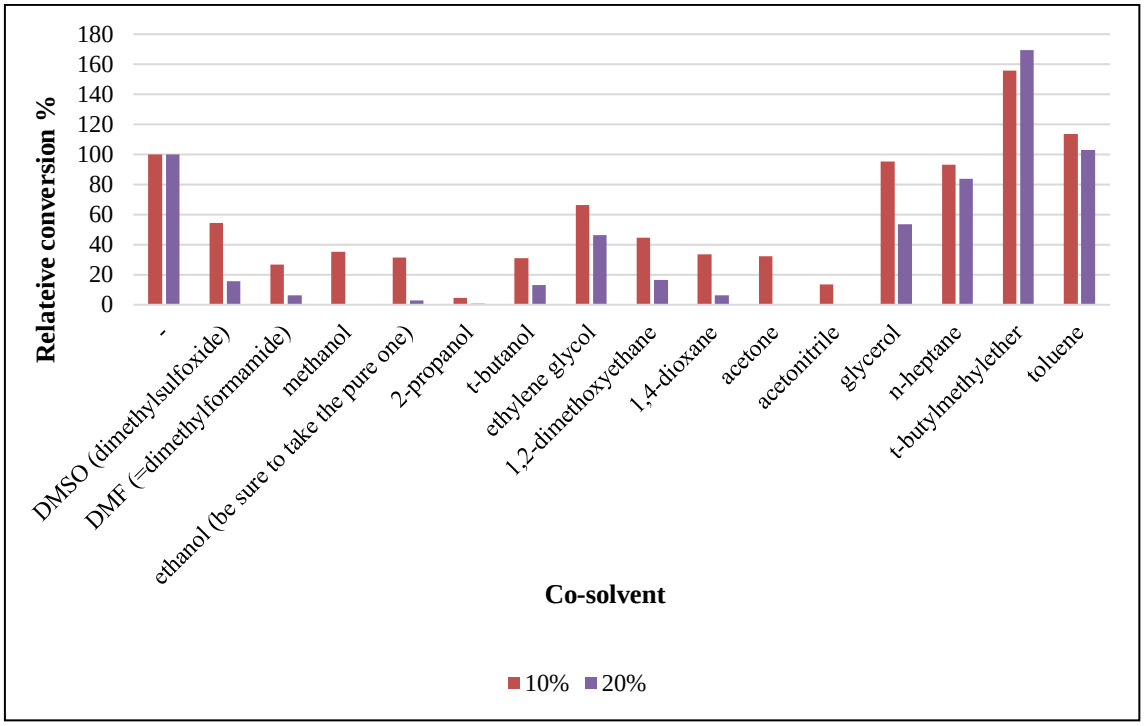

Figure 9.16: Carboxylation of catechol using EcAroY in different co-solvents.

For this reason, the workup procedure was altered, and the water-immiscible co-solvents were evaluated again. The highest conversion was recorded when using 20 % *t*-butyl methyl ether or 10% *n*-heptane as a water immiscible co-solvents as shown in the graph below (Figure 9.17).

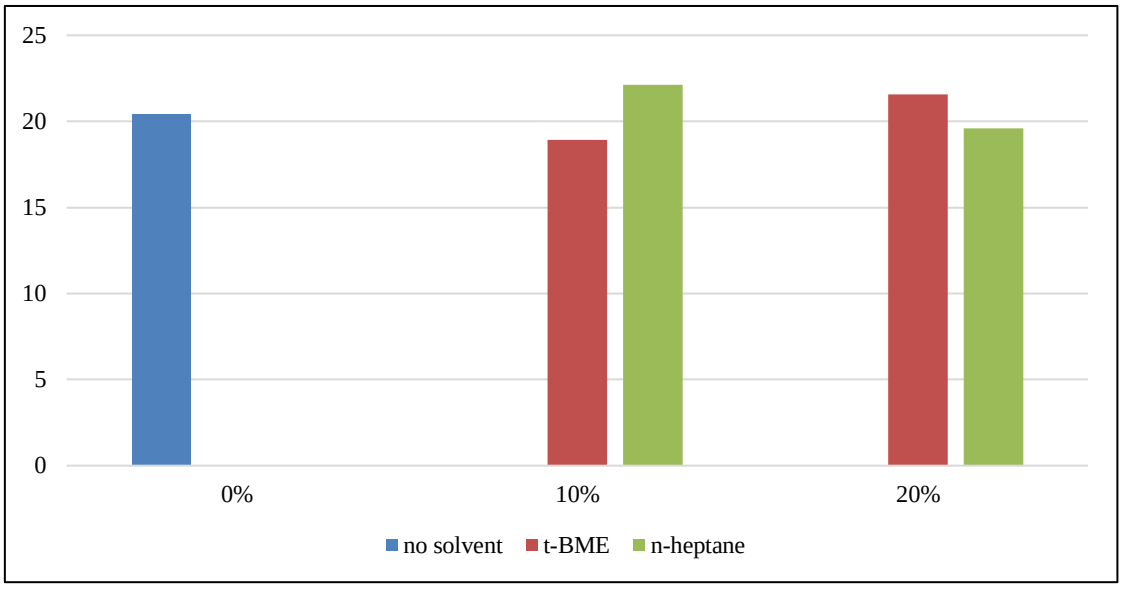

Figure 9.17: Carboxylation of catechol using EcAroY in different water immiscible co-solvents.

9.2.12 Effect of higher Enzyme and Substrate Loadings on the Conversion of the Carboxylation Reaction.

In a final screening the beneficial effects of enzyme and substrate loading was investigated. The conversion increases to up to 27% as shown in the Figure 9.18 given below. As the natural reaction of the applied decarboxylase is decarboxylation rather than carboxylation, the whole reaction features an unfavourable equilibrium for C-C bond formation. Different strategies to push the equilibrium (especially: high bicarbonate concentrations) allowed to perform the reaction in the carboxylation direction. Additionally, a higher substrate concentration proved beneficial, as up to 7 mmol/L of product were formed at 50 mmol/L substrate concentration and 6 mmol/L at 30 mmol/L substrate concentration. Further methods to shift the equilibrium would include pulling, by removing the formed product in situ. This was recently demonstrated by coupling the carboxylation reaction with an enzymatic redcution of the formed carboxylate to the corresponding aldehyde [152].

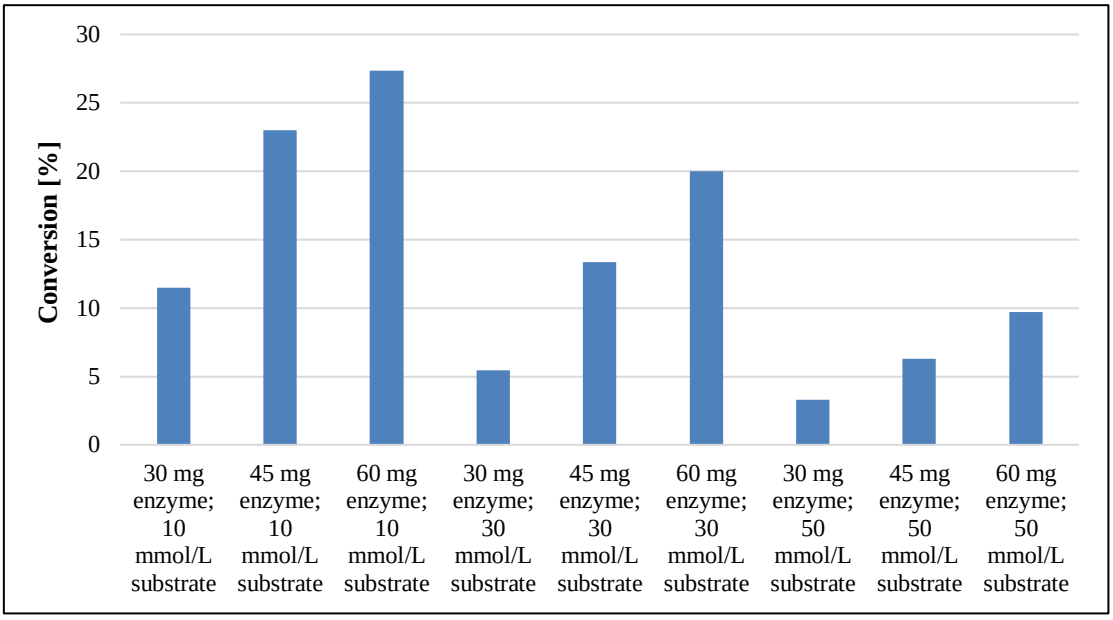

Figure 9.18: Effect of higher enzyme loading on the conversion in the carboxylation of catechol using EcAroY.

As shown in the Figure 9.19 below, the highest productivity of up to 6 mmol/L product concentration is reached when 60 mg of the enzyme preparation were used together with a substrate concentration of 30 mmol/L.

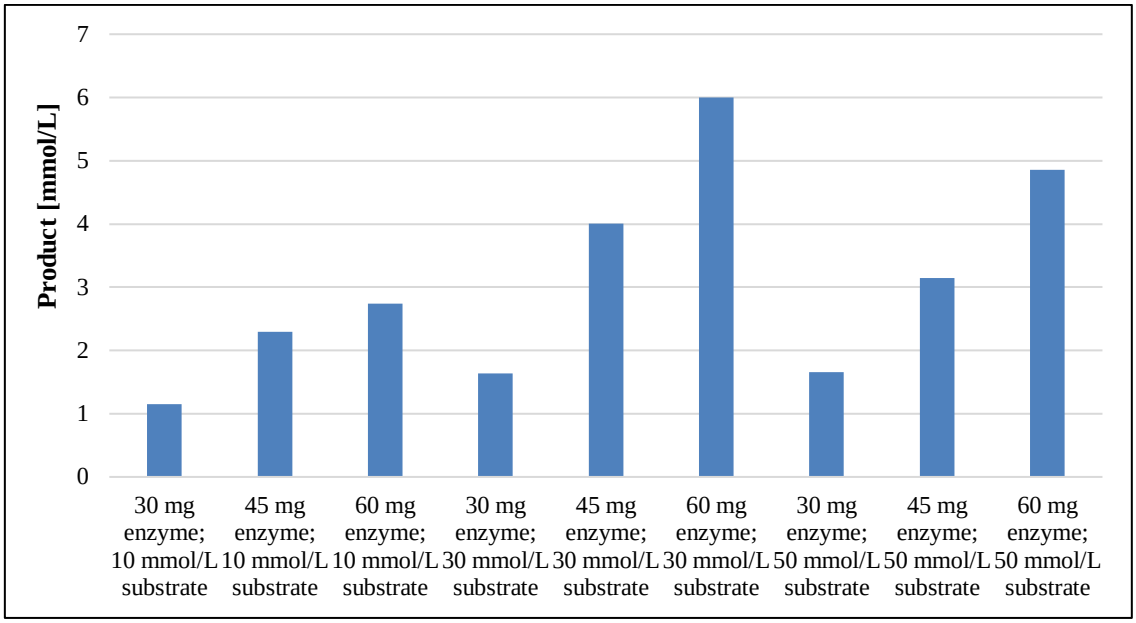

Figure 9.19: Effect of higher enzyme loading on the product formation in the carboxylation of catechol using EcAroY.

9.2.13 In Situ Product Removal to Pull the Equilibrium of the Carboxylation Reaction

In order to pull the equilibrium of the carboxylation reaction towards the product side, the potential of different quaternary ammonia salts to scavenge the product was evaluated. As recently demonstrated, such quaternary ammonia ions may form insoluble salts with the product`s carboxylate moiety, that then precipitate and therefore force the reaction towards completion [119].

Seven different precipitants (namely: tetrabutylammonium bromide, hexadecyltrimethylammonium bromide, benzyl triethyl ammonium chloride, *n*-octyl trimethyl ammonium chloride, dodecyl trimethyl ammonium chloride, benzyl trimethylammonium chloride, benzyl dimethyl dodecyl ammonium chloride), were evaluated at 20 mmol/L concentration. However, this resulted in decreased conversions in any case.

In future, either further salts might be evaluated, or alternative ISPR techniques, such as the combination of the carboxylation reaction with a second enzyme in an enzymatic cascade might be tested [152].

10. CONCLUSION AND RECOMMENDATIONS

10.1 Conclusion

It can be concluded that the best reaction conditions for the investigated *p*-carboxylase enzyme (*Ec*AroY, pEG 167) with catechol as substrate are at a potassium bicarbonate ($KHCO_3$) concentration of 3 mol/L. Prolonged reaction times (up to 7 days) and increased catalyst loading resulted in increased conversions. The effect of cosolvents was minimal, but the overall productivity could be boosted when higher substrate concentrations were applied. Throughout the study, diminished recoveries were a problem.

There were two ways seen during literature review and also during experiments analysis about extraction of the product by using in situ.

First one is the use of formation of insoluble ammonia salts [119] and more such salts should be tested.

The second one is the combination with a further reaction, as for example the reduction of the carboxylate with a carboxylic acid reductase [152]. An alternative further reaction would be also the direct polymerization in situ.

The results are promising, but far from industrial scale ad feasibility. Argue, that more research is needed to reach this ambitious goal.

10.2 Recommendations

In the future different in situ product removal techniques or other follow up reactions can be used to drive the reaction to higher conversions. Precedence for this can be found in literature.

UNIVERSITY OF L'AQUILA
Department of Industrial engineering and Information & Economics

SECTION 3

Plant Design for producing electricity and bioplastic (A.P.S. S.p.A. Rome, Italy)

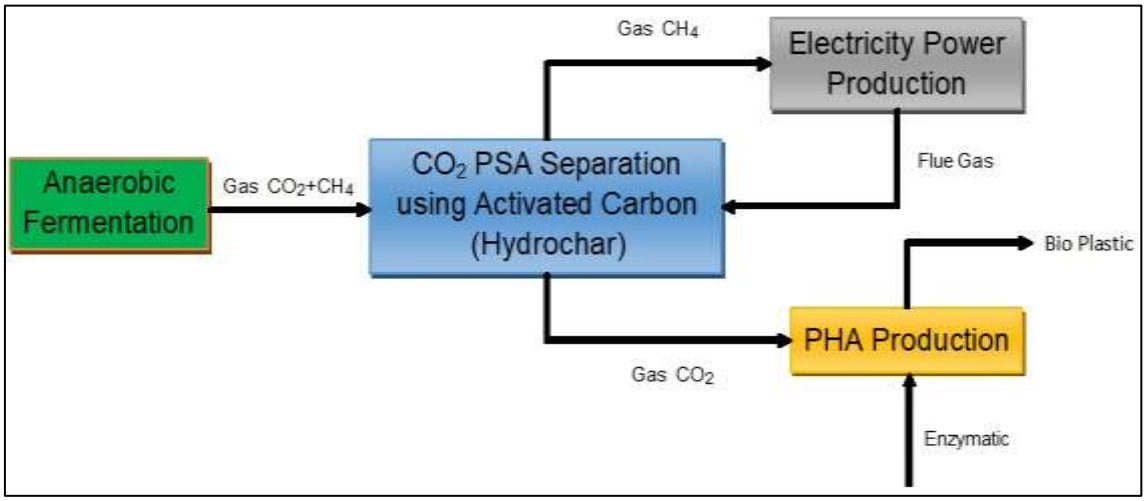

ABSTRACT

The new worldwide challenge is to increase energy power production, produce bio plastic and to reduce the atmosphere gas emission, especially Carbon dioxide that is the main cause of the ambient increasing temperature. The scope of the present study (PON 2014-2020 industrial PhD grant) is to upgrade the biogas to bio methane for energy and cooking purposes and also to optimize the process configuration for upgrading the biogas from a fermentation using the various technologies studied in L'Aquila University, Italy. To use the carbon dioxide, that is a pollutant gas, as a feed for bio plastic produce is the part of study in the University of the Graz, Austria.

Lab-scale experimental results for CO_2 capture from biogas by Pressure Swing Adsorption method using Hydro-char (activated and non-activated carbon) and the purity was 95 (vol %) and recovery was 68 (vol %) [87].
The process design of an industrial plant configuration has been developed in the APS, an Italian engineering company, in order to:

- Define and optimize the process configuration
- Define heat material balance
- Preliminary size of the various equipment, using the process software simulation
- HYSYS and HTRI for dimensioning the heat exchangers.

Block flow diagrams (BFDs) with the use of the "Draw.io" program and process flow diagrams by hand and by using the "AutoCAD" software have been realized at this point. The sizing of the equipment was carried out in some cases with calculations made with Excel.

Finally, an economic analysis has been carried out using the "CapCost" spreadsheet for the biogas plant. The final objective was to analyze the best from an economic point of view, considering the net cash flow evaluating the plant costs, management costs, utilities expenses and revenues from the sale of the final product.

Keywords:
Hydro char, biogas upgrading, CO2 capture, Pressure Swing Adsorption, CapCost

11. INTRODUCTION

11.1 Research Background

Human modern activities have a keen effect on the environment in terms of climate change, particularly by the transportation and energy generation. CO_2 emission in the air due to enormous use of fossil fuels is one of the main issue that is affecting the global warming which needs attention and solution.

Alternative to the fossil fuels are the biofuels (fuels produces with biomass), which looks like an attractive way out for the replacement or at least partially. By using this source of energy will subsequently reduce the emission of greenhouse gasses [153] and the effect of global warming [154, 155]. In the recent and past time, considerable interest has been taken to develop the inventive solutions for the improvement of the biofuel's sustainability, for plant engineering solutions and biomass transformation processes that are essential to operate such processes on a broader scale.

The economic activities has a major role in the production of global greenhouse gas emissions [156] as shown in the Figure 11.1.

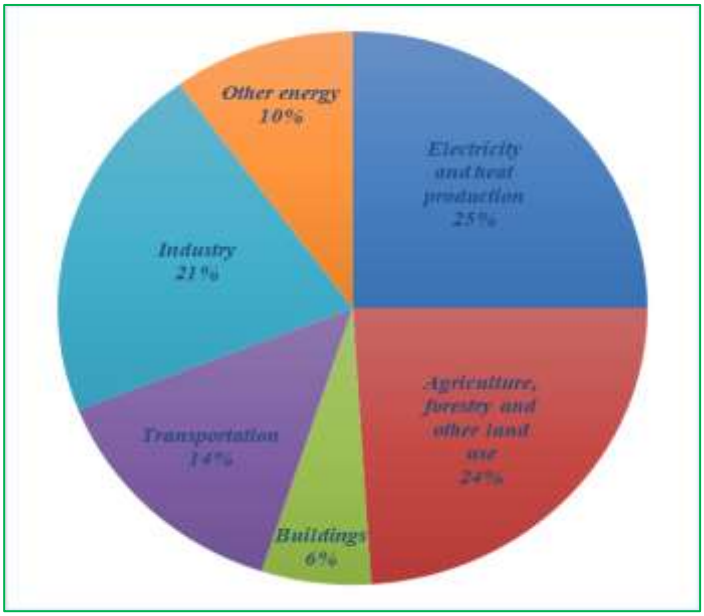

Figure 11.1: Global greenhouse gas emission by economic sector

It is mandatory to find and use the new renewable sources of the energy in order to minimize the consumption of fossil fuels and the GHG emission. These type of energy resources can be found out anywhere in the world and are cleaner than conventional sources of energies. There are five major groups of renewable energy resources: solar, wind, hydro, geothermal and biomass. Except geothermal all other energy sources exist because of the energy of the sun [157].

In this work, the design, simulation, and cost of all the system components of a biogas plant fed with biogas from the fermentation process was carried out by considering scoring model and lifecycle analysis from the four proposed schemes.

The study reported here was carried out in collaboration with APS S.p.A., an Italian company that works in the field of designing and installation of biogas plants.

11.2 Research Motivation

Renewable energy has ample benefits like less dependency on fossil fuels which are more costly and are easily available with infinite amount in the worldwide. Another advantage is that it reduces the GHG levels, especially CO_2 which is affecting the climate change a lot [158]. The motivation of this research is to design a biogas plant for the rural areas of the poor countries where it is also a source for the peoples that will boost their lives through employability and infrastructure.

11.3 Aim and Objectives

Aim:

Semi-industrial plant design for producing electricity and bioplastic from biogas

Objectives:

1. To design best plant configurations by considering scoring model and life cycle assessment techniques.
2. To design, simulate, and analyze all the equipment used in the semi-industrial plant.
3. To estimate and calculate equipment cost and final capital cost of the plant.

11.4 Research Methodology

The Figure 11.2 represents the research methodology of the research work performed.

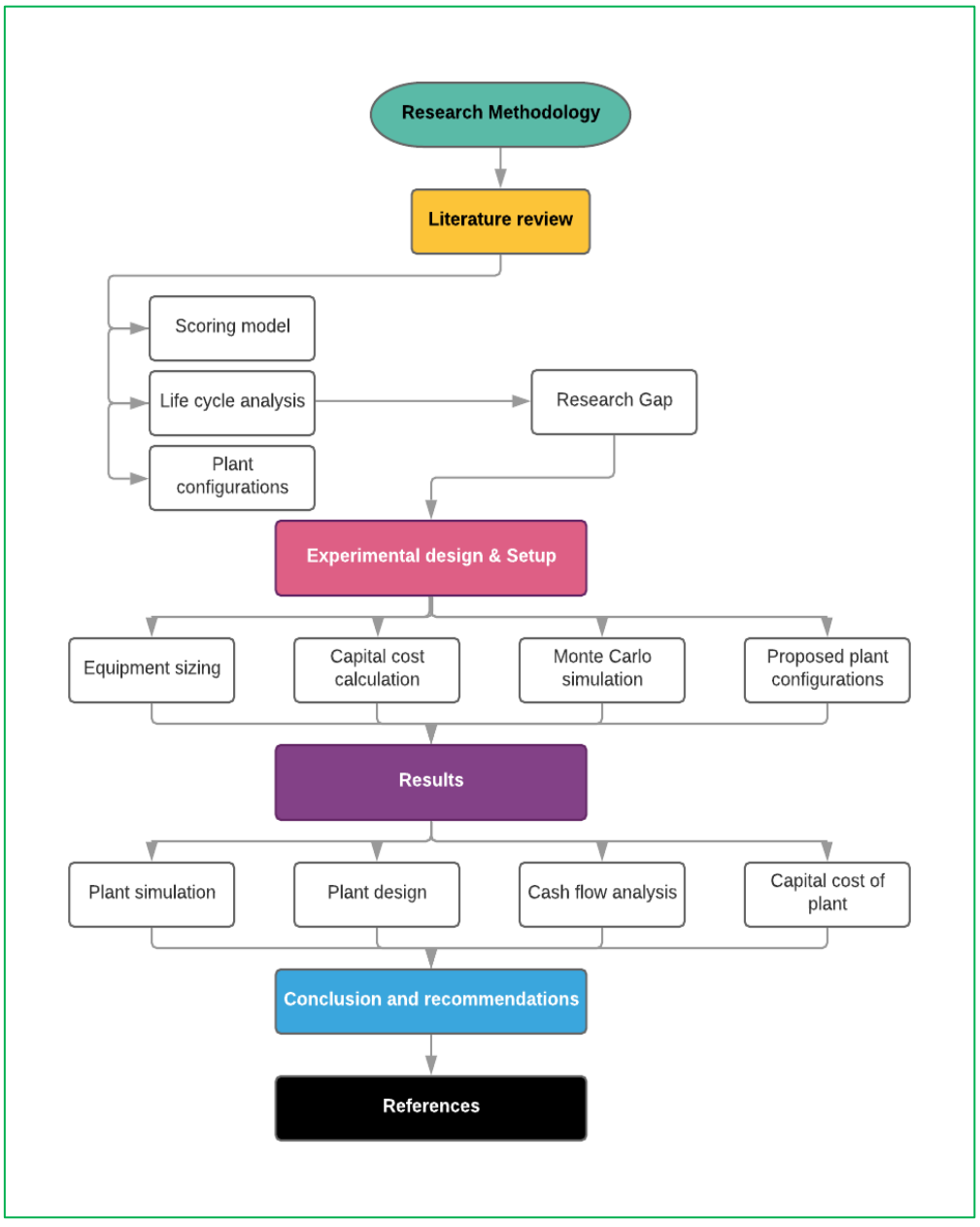

Figure 11.2: Research methodology

11.5 Scope of the research

To understand the trend of energy revolution it is crucial in the future to use the renewable energy due to depletion of the natural resources for the development and betterment of our society. The scope of this research is to provide step by step approach to design a

biogas electricity generation plant by keeping in mind the research gap identified in the literature and to take a step in the direction of defining standards and benchmarks for the energy sector.

11.6 Thesis structure (Part 3)

- Introduction: This chapter describes the research background, research motivation, aim and objectives. research methodology and scope of research.
- Literature review: In this chapter, literature review of all the related articles is described.
- Design of experiments: This chapter describes the experimental design and setup of the research study.
- Results, analysis, and discussion: This chapter covers the results, analysis, and discussion session.
- Conclusions and recommendations: In this chapter, conclusions and future recommendations are described.

12. LITERATURE REVIEW

12.1 Introduction

Energy demand for energy increasing with population growth and the natural reserves of fossil fuels and biomass are depleting at a very fast rate and increase the use of fossil fuels will cause in the increase in global warming, which restrains the use of fossil fuels on a large scale. As energy extract from fossil fuels cause air pollution which results in the depletion of ozone layer at faster rate. To overcome energy shortage and to minimize hunger of energy, the need of the hour is to thus switch to other alternative sources the hour of need is thus to switch an alternative source of energy which would be environmentally friendly. The research will help to mitigate the pressure on the natural reserves.

The influence of human lives on climate and eventually on overall temperature of the planet earth is very threatening with the passage of time. The anthropogenic activities of human such as transportation, deforestation, industrialization, urbanization, burning of fossil fuels, burning of renewable fuels, organic wastes are playing an important role in increasing the temperature of the earth. It is because the gasses produce because of these activities generate a large amount of greenhouse gasses which then add up to the harmful gasses which are present in the environment already naturally and cause an increase in the global warming. For the socio-economic green healthy environment, the climate change and global warming are very great threats. The main factors of the phenomenon in environment that occurs global warming and climate change are wind changes, water level and pure water availability, perception regime, temperature change etc. [159]. So, the need is to minimize the factors affecting the environment due to increase number of factors causing climate change or global warming in order to establish socio-economic green healthy human friendly environment. The greenhouse gasses (GHG) percentage with respect to the human activities are shown in the Figure 12.1, because of these gasses, the production of greenhouse gasses increasing day by day and that need to be addressed [160]

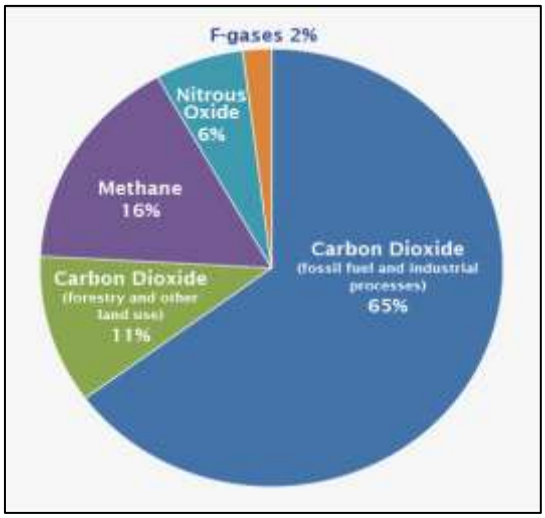

Figure 12.1: GHG distribution by a gas

Emission of carbon dioxide because of the burning of fossil fuels are the reason if dramatic increment in the amount of carbon dioxide in the atmosphere. With the industrialization especially in small range of countries the green house effects are increasing. European countries, China, and United States are the biggest hub of the production of carbon dioxide as the greenhouse effect per capita are highest in these countries especially Russia and USA [2].

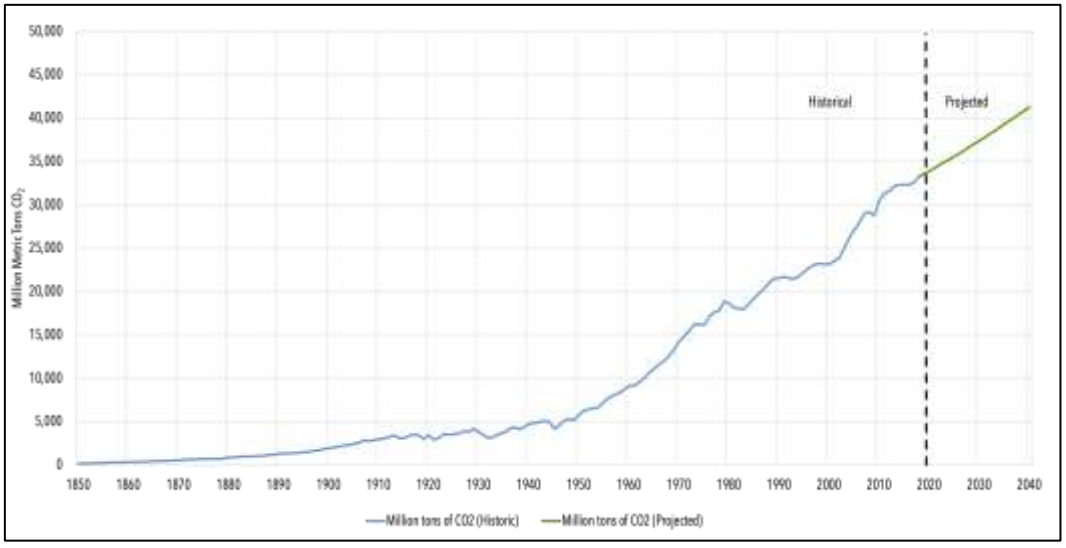

Figure 12.2: Global Carbon Dioxide Emissions, 1850–2040

To avoid the production of harmful gasses and its exposure to the atmosphere it is however necessary to divert the attention from the usage of fossil fuels and to focus on the other resources to produce energy. One of the best sources of energy with zero

greenhouse effects is renewable energy resources. The best advantage of the renewable energy is that these sources are available everywhere in the world and is cleaner than other sources of energy production. The main renewable energy sources are: wind, geothermal, hydro, biomass and solar. These all resources are present abundantly in the atmosphere [161]. The main utilization of renewable energy is to capture heat and then utilize the heat in any useful application for the production of electricity or mechanical power.

12.2 Biogas plant for producing electricity

In order to use the biogas in the vehicle as a fuel the upgrading of biogas to biomethane is increasing and the fuel is the added in the natural grid system. Walla et al. used biogas plant in its study to produce electricity from the maize silage. Author conducted a survey to find out the best suitable plant size to achieve the maximum amount of efficiency [18]. Biogas plants comes with different shape and sizes according to the demand and process requirements.

In underdeveloped countries, the applications of biogas are bound to the purpose of lightening and for cooking or in other small scale applications, whereas, in developed countries the biogas are used on largescale commercial based industries for electricity supply [162, 163].

In 2014, there were almost 100,000 latest equipped modern biogas plants in China and 4,300,000 small scale residential digesters which generate 15-million cubic meter volume of biogas which sums up to 9 million cubic meter volume of biomethane (324 TJ primary energy).

The plan for the development of the renewable energy at a long term and medium term scale requires to reach the target of 80 million plants of biogas on a small scale house hold digesters and 8000 biogas plans on a large scale with the capacity of the production of at least 3000 MW[164].

In 2017, at United States, the number of biogas plants installed were almost more than 2100 whereas, the energy production from the utilization of biogas was recorded with

18.5 million cubic meter of volume of per year biogas production and the power generation was recorded as 41.2 TWh [1].

In 2015, at Europe, there were almost 17,400 plants installed of biogas production which were mostly utilized for the production of electricity. The other applications of biogas utilization at Europe also involves other heat consuming applications in order to save the efforts for the improvement of economic of country. One of the application of biogas are gas engines which are used for the electricity production and has reached to the range of 35 to 40 % of the electricity efficiency on the basis of engine specifications and type [165].

Figure 12.3 shows the biogas plants installed in different parts of world and their capacity for the comparison analysis.

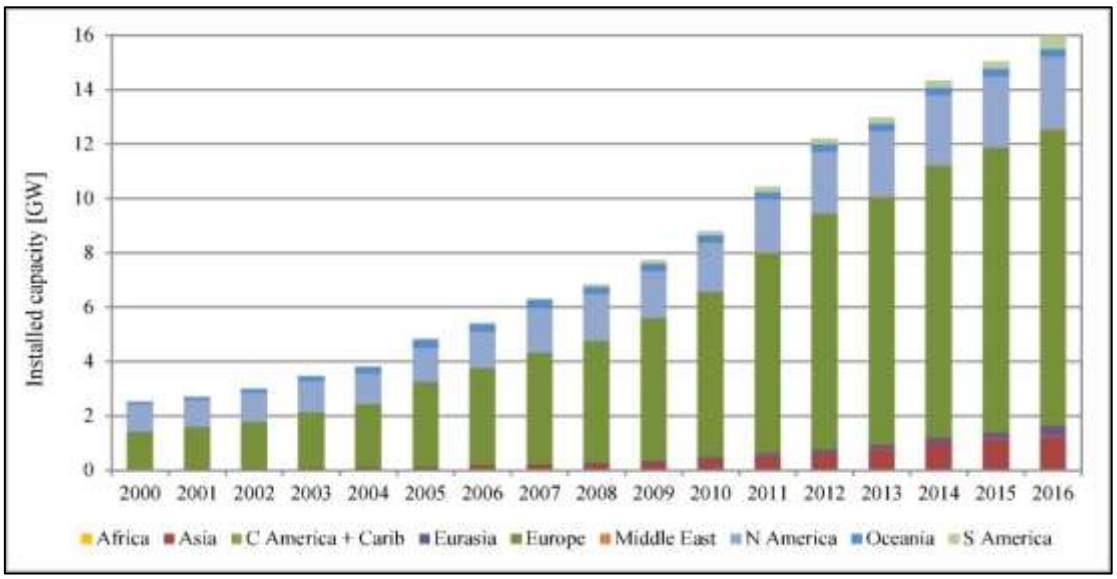

Figure 12.3: Evolution of global installed electricity biogas plant capacity [1]

12.3 Life cycle assessment

The process for the evaluation of the burdens in related with environment during the process or activities involved during the production is called life cycle assessment. It also involves the quantification and identification of materials and the handling of exhaust gasses exposed to the environment. The assessment also carried out for the calculation of the waste handling and from the utilization of that waste in order to improve the environment by utilize the waste in better way. So overall in short the transportation,

extraction of raw material, process activities, manufacturing, final disposal, reuse, distribution, recycling, raw material process etc. type of all stages are assessed in the life cycle assessment [166].

The life cycle assessment is dived into different stages which involves; extraction of raw material stage, processing, product manufacturing, commercialization, transportation, usage, and the maintenance stages are involved. The last stage is of the final management [167]. Figure 12.4 shows all the main stages involved in the life cycle assessment.

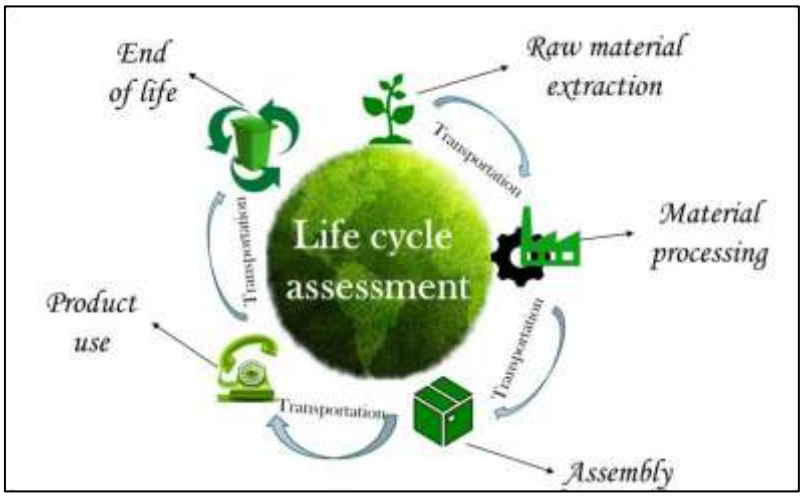

Figure 12.4: Main stages of the LCA

The overall assessment of the utilization of biogas to produce power and electricity and their environmental impact is analysed with the utilization of life cycle assessment technique. Many researchers performed LCA on different domain. Similarly, Ishikawa et al. studies the different types of biogas plants. Authors evaluated the different type of biogas plants on the basis of their life cycle assessment [168].

12.3.1 Limitations of LCA

One of the strengths of LCAs is a holistic approach, that considers the whole production chain and considers that the emission reductions in some areas, cause an increase in another part of the chain. Conversely, one of the noticeable drawbacks of the LCA, is the subjective choice of the observed systems' boundaries which creates obstacles in the direct comparison of the seemingly similar LCAs. In the same way, policies focusing mainly on specific environmental benefits, such as decreasing fossil carbon emissions,

may create unexpected side effects regarding all-round sustainability. For instance, Germany's experience show that economic incentives for renewable energy production (Renewable Energy Sources Act) which have increased biogas production, are counterpoised by local conflicts related to changing agricultural landscapes, increasing land prices and experienced loss for quality of life [169].

12.4 Process simulation

For decision making of chemical engineering processes in the design, optimization, and operation the chemical processes simulation is a significant tool. The results produced after suitable model formation is superb. The simulations can easily analyze the design or operation of new equipment or plant using laboratory (experimental) or real time data.

Zhou et al. studies the technology for the separation of biogas and carbon dioxide by using the Hysys software simulations [170]. Similarly, Lionzio et al. worked on the upgradation of biogas by using the absorption process. Authors performed experimental studies and simulations studies to validate the results. The software used for the simulation studies was Chem cad [171].

The scope of process simulation spreads for away in the different fields including research and development, process design, training, optimization of processes, production planning, and process design. Process simulation in all the disciplines of chemical engineering and general engineering is applied now a days. A wide palette of simulation solutions is mentioned below in the Figure 12.5.

Figure 12.5: Process simulation scope [172]

12.5 Monte Carlo simulation

For the analysis of the large dimensions and data basically two techniques have been developed since many years. First technique is called analytical methodology that is based on the account of the situations that illustrate the complete system which was established in some European countries and also in the north America. The second technique was created in the Italy, France, and a lot of other countries based on the Monte Carlo simulation for the system analysis.

In the analytical methodology only critical issues are entertained that are specified in each case study while as in the Monte Carlo simulation whole cases are considered. In case of wind turbine every particular placement of the cluster, which we have in our disposal, can be the ideal one. This is the reason for selecting the Monte Carlo simulation method instead of the analytical method [173].

A sample Monte Carlo simulation example is shown in the Figure 12.6.

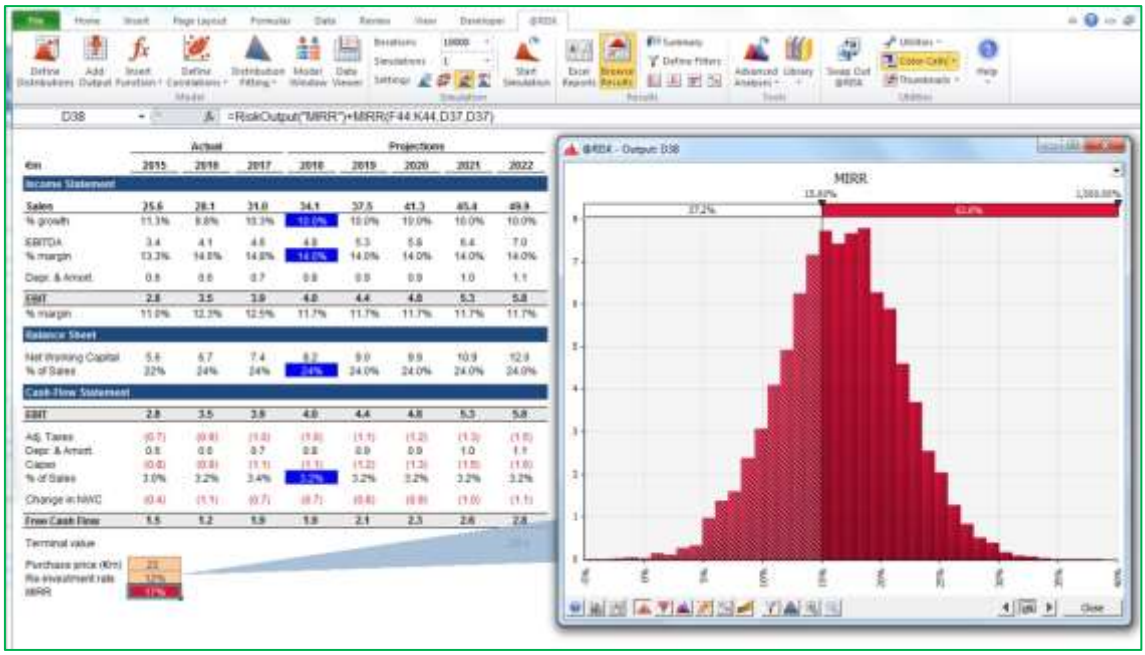

Figure 12.6: Monte Carlo simulation excel example

13. EXPERIMENTAL DESIGN AND SETUP

13.1 Introduction

In this chapter proposed plant configurations, design of process flow diagram and equipment used, simulation of plant design and cost analysis techniques are discussed in detail.

13.2 Proposed schemes (Plant configurations)

The four-plant configurations were prepared by considering environmental and design issues and are described here below in detail.

13.2.1 Base case (Scheme 1)

Biogas from anaerobic fermentation was sent directly to the gas turbine to produce energy, only H_2S removal in order to incorporate equipment life and environmental specification. The CO_2 was emitted into the air as shown in the Figure 13.1.

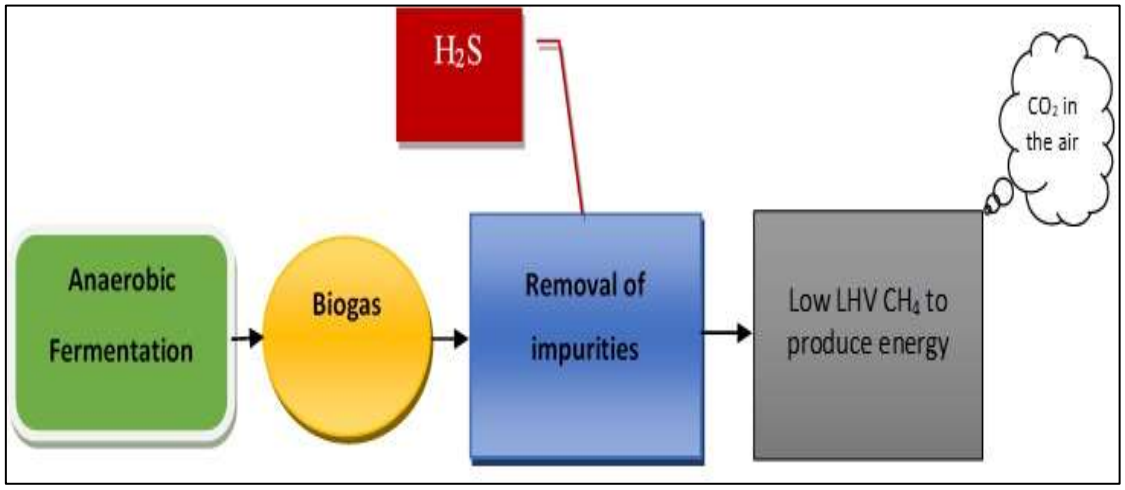

Figure 13.1: Removal of H2S only

13.2.1.1 Advantages and disadvantages of base case (Scheme 1)

Pros and cons of the scheme 1 are shown in the Table 13.1 below.

Table 13.1: Pros and cons of scheme 1

Advantages	Disadvantages
Very easy to perform plant turndown	Void waste heat recovery
Very low maintenance cost and frequency	Very high environmental impact
Overall small plant lay out	Very low preliminary RAM Study
Very low capital cost and operating cost	Very low profit

13.2.2 Biogas pre-treatment (Scheme 2)

Biogas from anaerobic fermentation was treated with pressure swing adsorption method using activated carbons (hydro char) where CH_4 and CO_2 was separated. CH_4 was sent to the gas turbine to produce energy, but CO_2 was sent to the atmosphere as shown in the Figure 13.2.

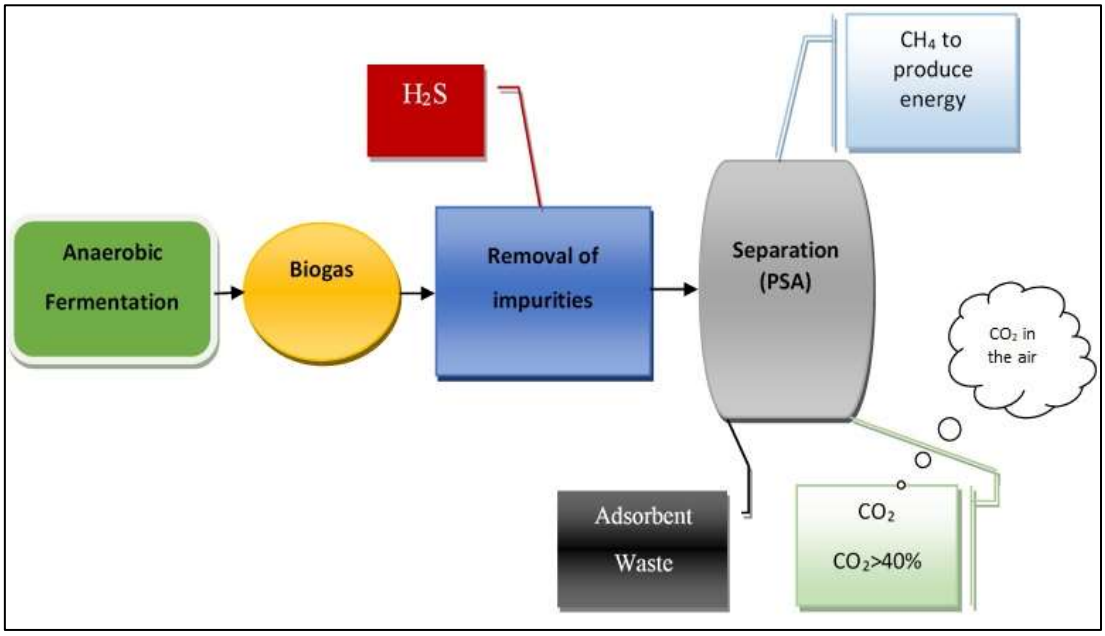

Figure 13.2: biogas pretreatment Using PSA to separate Ch_4 and CO_2

13.2.2.1 Advantages and disadvantages of biogas treatment (Scheme 2)

Pros and cons of the scheme 2 are shown in the Table 13.2 below.

Table 13.2: Pros and cons of scheme 2

Advantages	Disadvantages
Easy to perform plant turndown	Void waste heat recovery
low maintenance cost and frequency	Very high environmental impact
Small overall plant lay out	Very low preliminary RAM study
Low capital cost and operating cost	Low profit

13.2.3 CO_2 from biogas sent to bioplastic production (Scheme 3)

Biogas from anaerobic fermentation was treated with pressure swing adsorption method using activated carbons (hydro char) where CH_4 and CO_2 were separated. CH_4 was sent to the Gas turbine to produce energy and CO_2 was sent to the PHA for enzymatic reuse to produce bioplastic material as shown in the Figure 13.3.

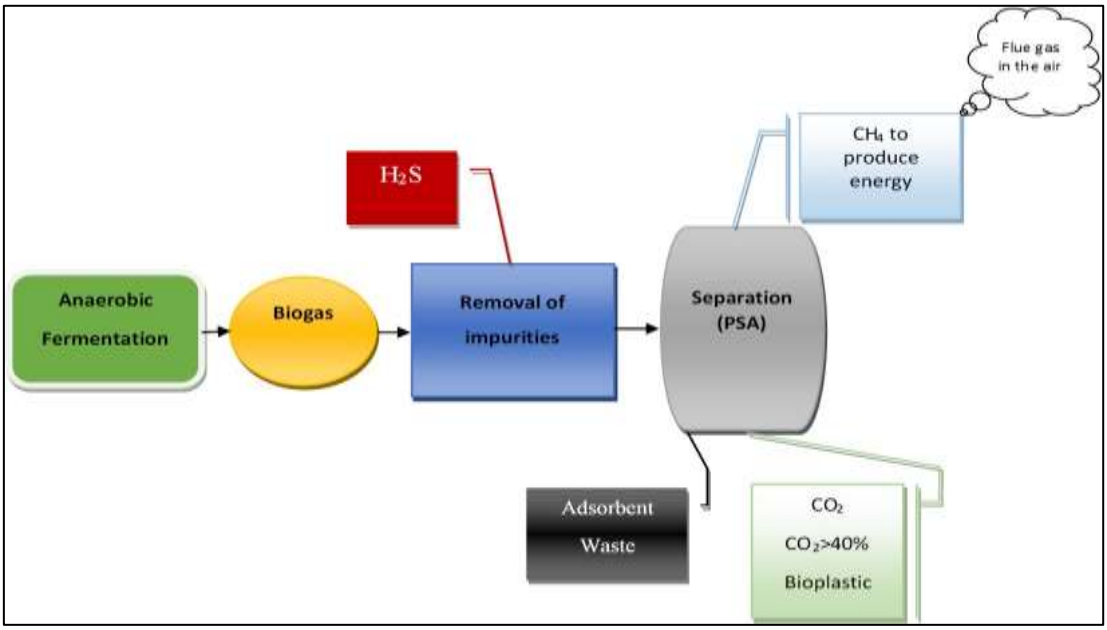

Figure 13.3: CO_2 recovery from biogas sent to produce bioplastic

13.2.3.1 Advantages and disadvantages of CO_2 from biogas sent to bioplastic production (scheme 3)

Pros and cons of the scheme 3 are shown in the Table 13.3 below.

Table 13.3: Pros and cons of scheme3

Advantages	Disadvantages
Easy to perform plant turndown	Void waste heat recovery
Medium maintenance cost and frequency	High capital and operating cost
Medium profit	High overall plant layout
Medium preliminary RAM study	
Medium environmental impact	

13.2.4 CO2 from Biogas and flue gas recovery sent to Bioplastic production (Scheme 4)

Biogas from anaerobic fermentation was treated with pressure swing adsorption method using activated carbons where CH_4 and CO_2 was separated. CH_4 was sent to the Gas turbine to produce energy and CO_2 was sent to the PHA for enzymatic reuse to produce bioplastic. Flue gas from Gas turbine was sent to another pressure swing adsorption method using activated carbons (hydro char) to separate CO_2 from other gases in order to feed for bio plastic production. This stream is provided with a steam boiler in order to recover the waste heat as shown in the Figure 13.4.

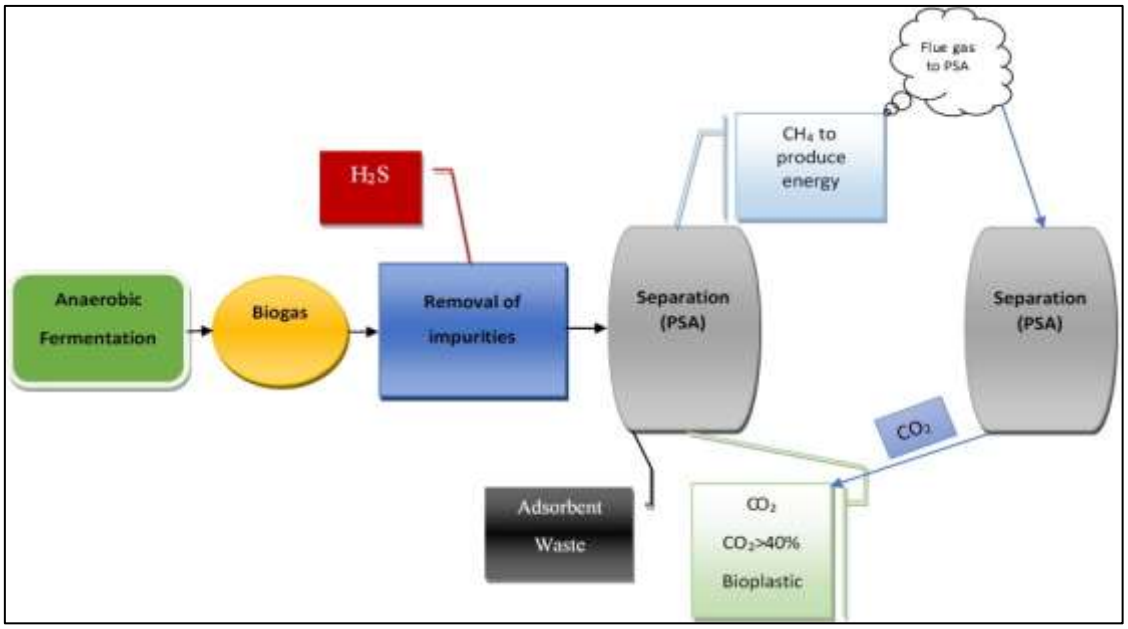

Figure 13.4: Flue gas was treated to feed more CO_2 to bioplastic production

13.2.4.1 Advantages and disadvantages of CO2 from Biogas and flue gas recovery sent to Bioplastic production (scheme 4)

The pros and cons of scheme 4 are shown Table 13.4 below.

Table 13.4: Pros and cons of scheme 4

Advantages	Disadvantages
Medium to perform plant turndown	High maintenance cost and frequency
High profit	High capital and operating cost
High waste heat recovery	
Ver high preliminary RAM study	
High environmental impact	

13.3 Scoring model

For the 4 selected schemes a scoring model has been prepared considering the main **"Q"** factors as described below:

The main **"Q"** Factors of the Scoring Model are defined below:

- **Q1**: Waste Heat Recovery (10%)
- **Q2**: Environmental impact (19%)
- **Q3**: Plant Turn Down (2 %)
- **Q4**: Preliminary RAM Study (4%)
- **Q5**: Maintenance cost and frequency (8%)
- **Q6**: Overall Plant Dimensions (5%)
- **Q7**: Main Equipment Delivery and Installation Time (9%)
- **Q8**: CAPEX and OPEX (18%)
- **Q9**: Profit in terms of IRR and ROI (25 %)

The shown values reward the more profit and the less environment impact plant. Those value will be multiplied for 1,2,3 or 4 corresponding to the score,1 is the worst 4 is the best, in case that the configuration has not considered the voice it is considered equal to 0.

13.4 Life cycle analysis

A lot of specific software that are used to carry out the life cycle analysis such as OpenLCA, SimaPro, Gemis and Gabi. SimaPro is one of the most popular software and is being used in more than eighty countries for almost 25 years in the academic and industrial level. The environmental, social, and economical aspects of the service, product, and organization that are produced throughout the whole life cycle can be easily computed by using SimaPro tool.

By applying this software program, it is feasible to make assemblies, establish processes, scenarios of waste and complicated life cycles as an illustration of what could occur in a in real life scenario [174] as shown in the Figure 13.5.

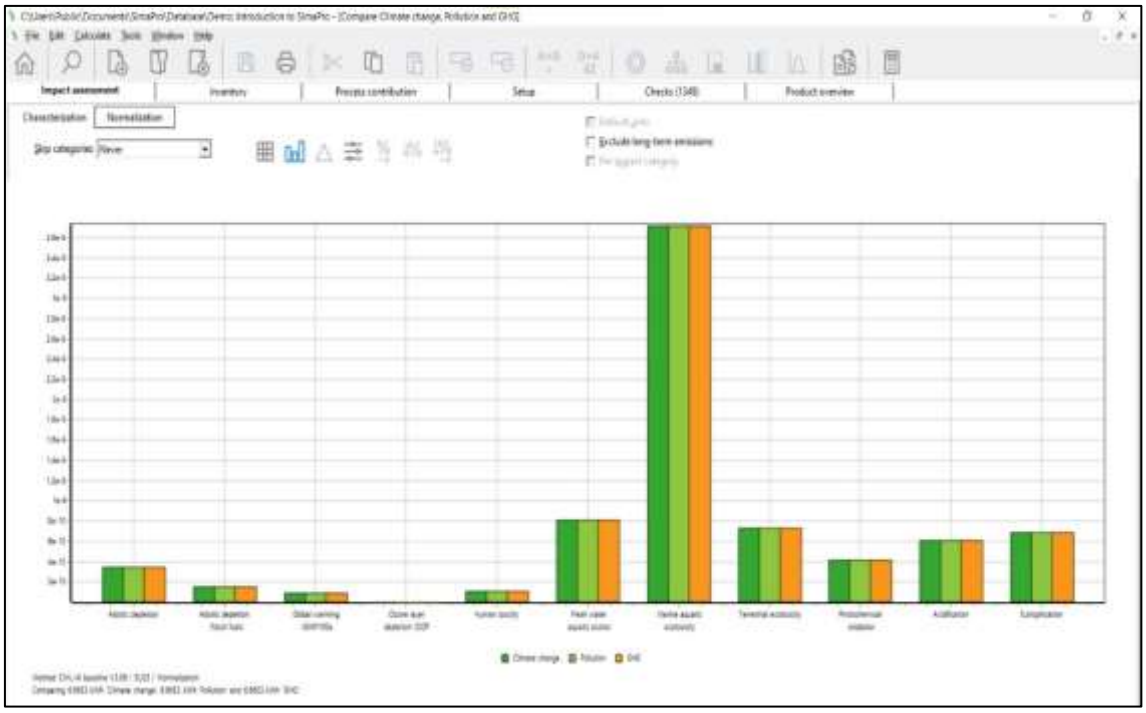

Figure 13.5: Simapro software example

13.5 Process flow diagram

The simplified flow chart of all the plant is shown in the Figure 13.6. In the block diagram it can be seen that the biogas is subjected to pre-treatment. In pre-treatment the first step is to remove humidity. This can be achieved by compressing biogas in the reciprocating compressor. The dehumidified biogas was then sent to the sulphur guard bed for the removal of sulphur contents from the gas. Now, this gas is composed of carbon dioxide and methane with minor amount of environment friendly nitrogen gas. The gas is then sent for the split of methane and carbon dioxide through pressure swing adsorption method (PSA) by using hydrochar (carbon rich adsorbent material). Now we have two streamlines; one is rich methane and second is carbon dioxide.

The enriched methane was then sent to the gas turbine for the electricity production. The exhaust flue gasses were utilized to produce steam and this steam were then utilized for the electricity generation through steam turbine and the remaining condensed steam which is in the form of water is supplied back to the steam drum through feed water pump. The flue gasses which were obtained from the exhaust of steam boiler were then treated again through PSA for the separation of methane and carbon dioxide.

Separated methane is sent back to the main methane streamline whereas, carbon dioxide joins the main carbon dioxide streamline and sent to the laboratory for the production of bioplastics.

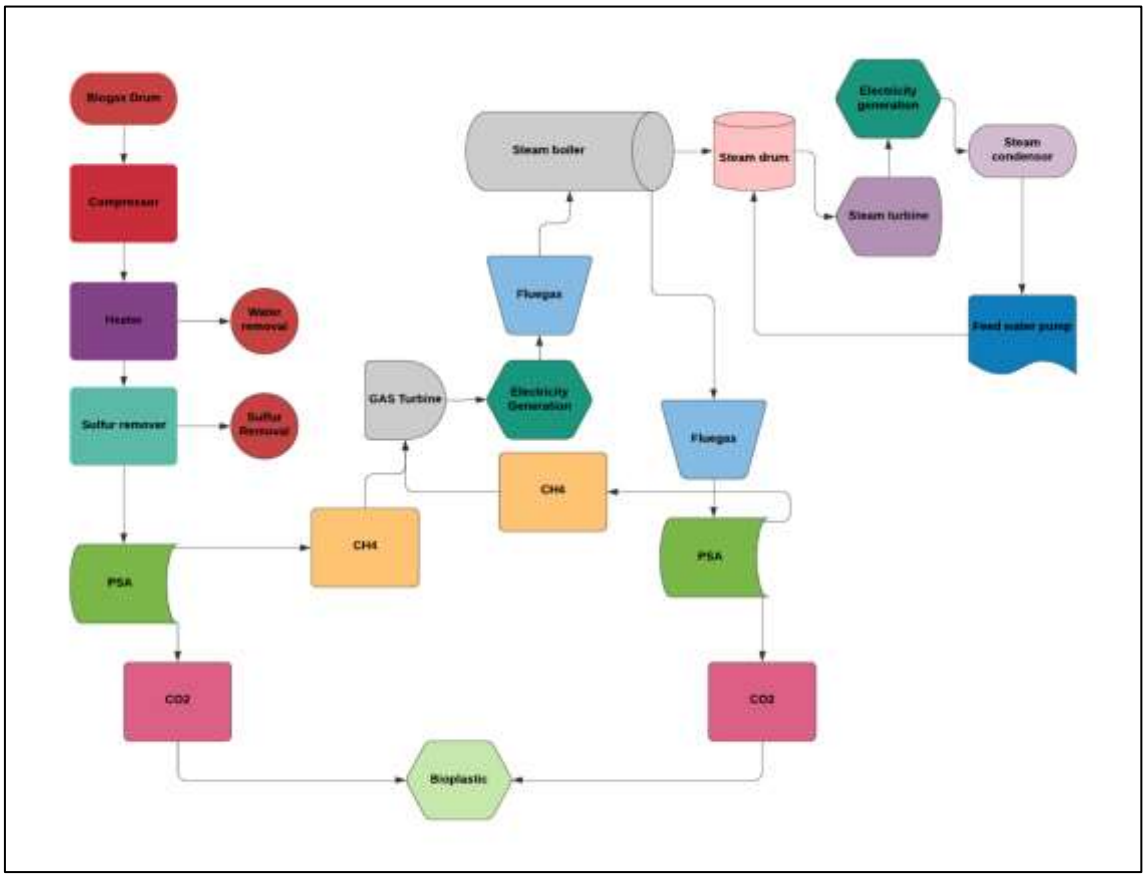

Figure 13.6: Flow chart of biogas plant

The process flow diagrams of all the plant were prepared by hand and also with the help of AutoCAD software. In this case starting from biogas reservoir to electricity generation there were total six process flow diagrams were prepared by hand using drawing sheets and also by using AutoCAD software. First process flow diagram from biogas to humidity removal step is shown in the Figure 13.7. While PSA drawing made by the AutoCAD software is shown in the Figure 13.8.

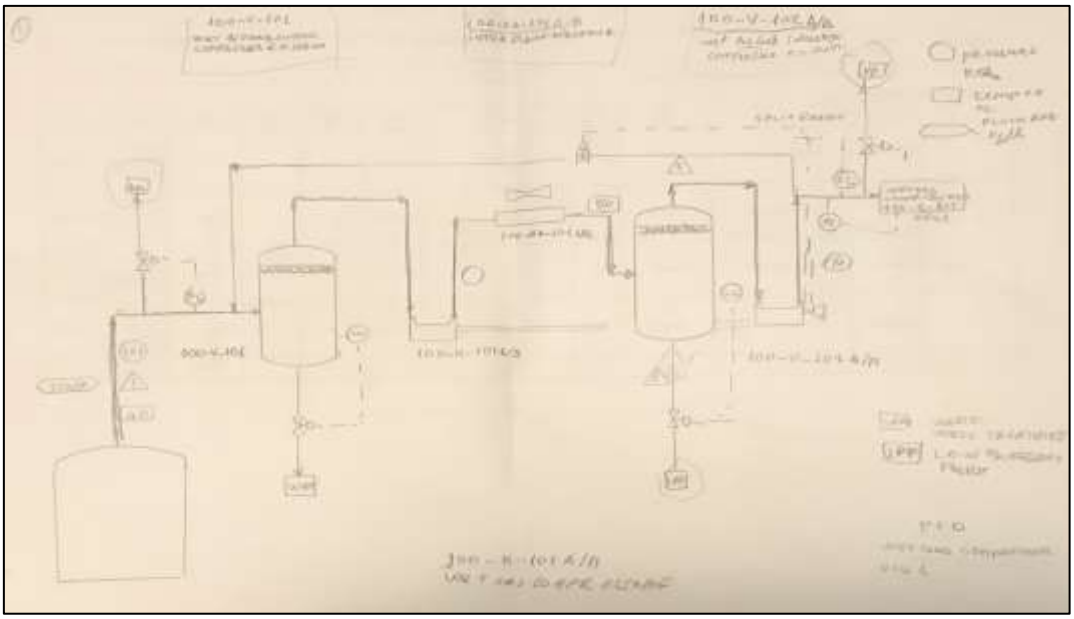

Figure 13.7: process flow diagram (by hand drawing)

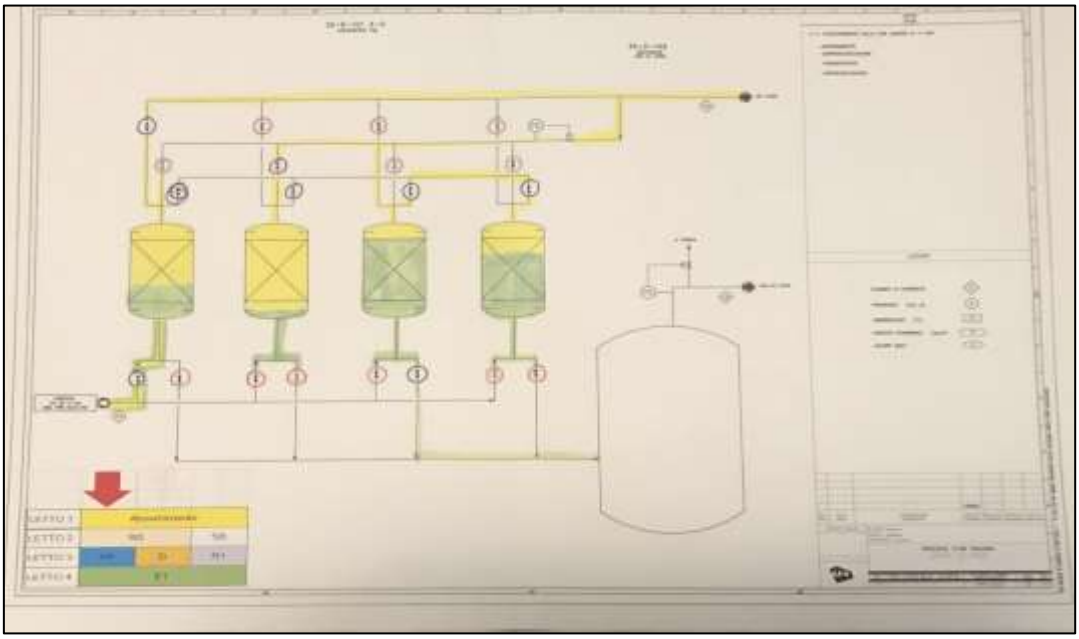

Figure 13.8: Process flow diagram by AutoCAD

13.6 Process simulation

Design, optimization, and operation of chemical processes can be carried out through effective process simulation tool for the assistance of decision making. After suitable making of the thermodynamic model the results that are achieved are the superb.

To analyze the operation of chemical plant or to design new equipment or plant simulation is used based on experimental or real time data.

For analyzing chemical systems or processes there are very convenient simulators like MATLAB Simulink, Aspen HYSYS, PRO II, and Chemcad because their structure consists of many unit operations which can be interconnected to simulate process or system.

An AspenTech a software making firm has launched his Aspen software (Advanced System for Process Engineering) in 1980 in the market. Chemical processes flowsheets can be simulated by using this software and the description of process design, Process variables sensitivity analysis, properties estimation of the compound, mass and energy balance and economical calculation and analysis cab be performed also [175].

The method to incorporate simulation in AspenPlus® contains the following steps [176].

1 Problem identification and description
2 Flowchart diagram making
3 Introduction of specific general description of the simulation
4 Component's selection
5 Model selection (thermodynamic)
6 Specification of process streams
7 Equipment selection and specification
8 Achievement of the simulation result report
9 Analysis of the results

The simulation bundle consists of three major blocks: visual , physical belongings and simulation engine.

13.7 Equipment summary/sizing

13.7.1 Pump

Boiler Feed water pump of centrifugal type (high discharge) is used in the scheme/plant to supply condense water to the steam drum in which design capacity, density of fluid,

design temperature and pressure, material for casing and impeller are already pre-defined and calculated. Typical pump diagram is shown in the Figure 13.9 below.

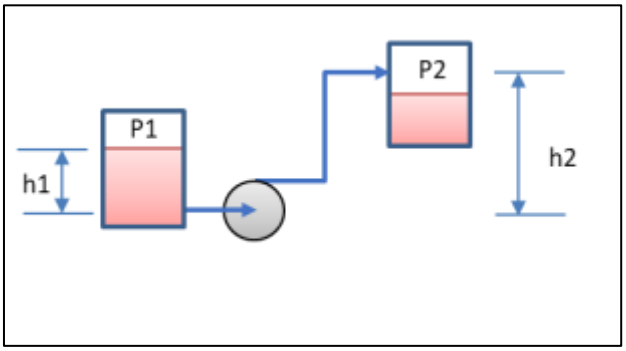

Figure 13.9: Typical pump diagram

Differential head, net present suction head, and minimum required power needed to be calculated [177].

- Differential head can be calculated by using equation (13.1) .

$$H = h_d - h_s \tag{13.1}$$

Where, differential head is H, total discharge head (h_d) and total suction head is (h_s).

- Net present suction head can be calculated from the equation (13.2).

$$NPSH=(p_i/\rho g+v_i^2/2g)-p_v/\rho g \tag{13.2}$$

Where, absolute pressure at inlet is p_i, v_i^2 is average velocity at inlet, ρ is fluid density, g is acceleration of gravity, and p_v is vapor pressure of fluid.

- Minimum power required by the pump can be calculated by using equation (13.3).

$$Power= Q\rho gh/\eta \tag{13.3}$$

Where, Q is flow rate of pump, h is head of the pump and η is efficiency of pump

- Efficiency of the centrifugal pump with corresponding impellor size and speed as shown in the Figure 13.10.

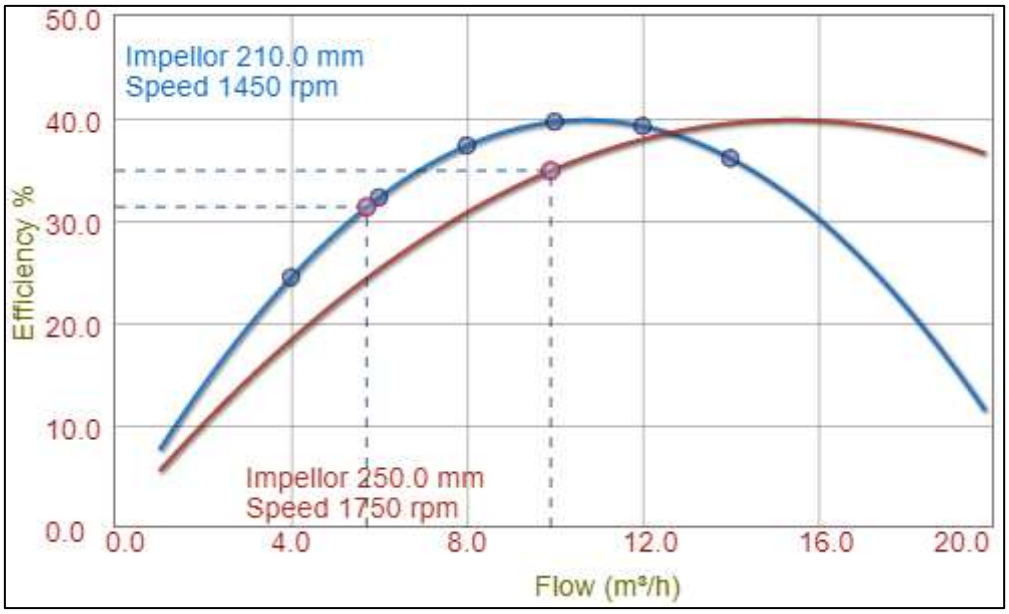

Figure 13.10: Efficiency v/s flow (Centrifugal pump)

13.7.2 Heat exchanger

The calculations have been distinguished with the use of a simulator for the design of heat exchangers "HTRI Xchanger Suite". The results obtained from these simulations are used for the sizing of the head capacitors and bottom boilers of plant. In particular, the global heat exchange coefficients that the HTRI software calculates have been used. The geometric configuration of the exchanger according to the TEMA standard, of the BEM type, has therefore been defined. A number of other features have been set up concerning mantle geometry, tube geometry and whether or not baffles, the building material for mantle and tubes, are present. Once the simulation is done, the software provides the following results in the Figure 13.11.

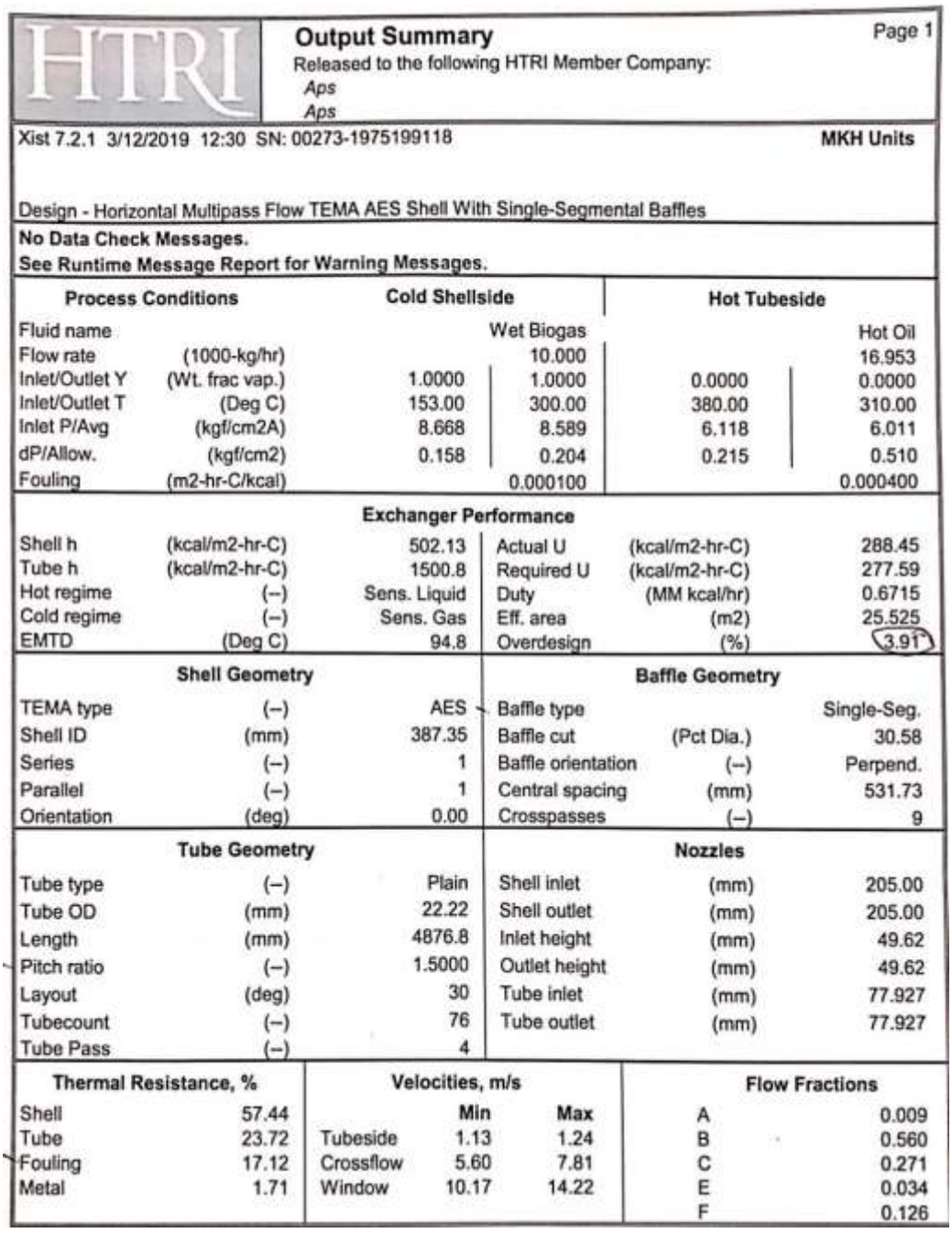

Output Summary Page 1

Released to the following HTRI Member Company:
Aps
Aps

Xist 7.2.1 3/12/2019 12:30 SN: 00273-1975199118 **MKH Units**

Design - Horizontal Multipass Flow TEMA AES Shell With Single-Segmental Baffles

No Data Check Messages.
See Runtime Message Report for Warning Messages.

Process Conditions		Cold Shellside		Hot Tubeside	
Fluid name			Wet Biogas		Hot Oil
Flow rate	(1000-kg/hr)		10.000		16.953
Inlet/Outlet Y	(Wt. frac vap.)	1.0000	1.0000	0.0000	0.0000
Inlet/Outlet T	(Deg C)	153.00	300.00	380.00	310.00
Inlet P/Avg	(kgf/cm2A)	8.668	8.589	6.118	6.011
dP/Allow.	(kgf/cm2)	0.158	0.204	0.215	0.510
Fouling	(m2-hr-C/kcal)		0.000100		0.000400

Exchanger Performance

Shell h	(kcal/m2-hr-C)	502.13	Actual U	(kcal/m2-hr-C)	288.45
Tube h	(kcal/m2-hr-C)	1500.8	Required U	(kcal/m2-hr-C)	277.59
Hot regime	(--)	Sens. Liquid	Duty	(MM kcal/hr)	0.6715
Cold regime	(--)	Sens. Gas	Eff. area	(m2)	25.525
EMTD	(Deg C)	94.8	Overdesign	(%)	3.91

Shell Geometry			Baffle Geometry		
TEMA type	(--)	AES	Baffle type		Single-Seg.
Shell ID	(mm)	387.35	Baffle cut	(Pct Dia.)	30.58
Series	(--)	1	Baffle orientation	(--)	Perpend.
Parallel	(--)	1	Central spacing	(mm)	531.73
Orientation	(deg)	0.00	Crosspasses	(--)	9

Tube Geometry			Nozzles		
Tube type	(--)	Plain	Shell inlet	(mm)	205.00
Tube OD	(mm)	22.22	Shell outlet	(mm)	205.00
Length	(mm)	4876.8	Inlet height	(mm)	49.62
Pitch ratio	(--)	1.5000	Outlet height	(mm)	49.62
Layout	(deg)	30	Tube inlet	(mm)	77.927
Tubecount	(--)	76	Tube outlet	(mm)	77.927
Tube Pass	(--)	4			

Thermal Resistance, %		Velocities, m/s			Flow Fractions	
			Min	Max		
Shell	57.44	Tubeside	1.13	1.24	A	0.009
Tube	23.72	Crossflow	5.60	7.81	B	0.560
Fouling	17.12	Window	10.17	14.22	C	0.271
Metal	1.71				E	0.034
					F	0.126

Figure 13.11: HTRI results

It was therefore decided to create a horizontal exchanger in which the two fluids pass countercurrent, the process current condenses the mantle side at the expense of the cooling water circulating inside the pipes as shown in the Figure 13.12.

HTRI

Final Results Page 2

Released to the following HTRI Member Company:

Aps

Aps

Xist 7.2.1 3/12/2019 12:30 SN: 00273-1975199118 **MKH Units**

Design - Horizontal Multipass Flow TEMA AES Shell With Single-Segmental Baffles

Process Data		Cold Shellside		Hot Tubeside	
Fluid name			Wet Biogas		Hot Oil
Fluid condition			Sens. Gas		Sens. Liquid
Total flow rate	(1000-kg/hr)		10.000		16.953
Weight fraction vapor, In/Out	(--)	1.0000	1.0000	0.0000	0.0000
Temperature, In/Out	(Deg C)	153.00	300.00	380.00	310.00
Skin temperature, Min/Max	(Deg C)	253.49	351.11	280.89	364.51
Wall temperature, Min/Max	(Deg C)	257.87	353.16	260.46	354.38
Pressure, In/Average	(kgf/cm2A)	8.668	8.589	6.118	6.011
Pressure drop, Total/Allowed	(kgf/cm2)	0.158	0.204	0.215	0.510
Velocity, Mid/Max allow	(m/s)	7.27		1.17	
Mole fraction inert	(--)				
Average film coef.	(kcal/m2-hr-C)		502.13		1500.8
Heat transfer safety factor	(--)		1.0000		1.0000
Fouling resistance	(m2-hr-C/kcal)		0.000100		0.000400

Overall Performance Data

Overall coef., Reqd/Clean/Actual	(kcal/m2-hr-C)	277.59	/	348.05	/	288.45
Heat duty, Calculated/Specified	(MM kcal/hr)	0.6715	/			
Effective overall temperature difference	(Deg C)	94.8				
EMTD = (MTD) * (DELTA) * (F/G/H)	(Deg C)	95.13	*	0.9963	*	1.0000

See Runtime Messages Report for warnings.

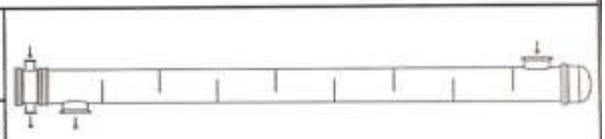

Exchanger Fluid Volumes

Approximate shellside (L)	453.2
Approximate tubeside (L)	171.2

Shell Construction Information

TEMA shell type	AES		Shell ID	(mm)	387.35
Shells Series	1 Parallel	1	Total area	(m2)	25.879
Passes Shell	1 Tube	4	Eff. area	(m2/shell)	25.525
Shell orientation angle (deg)	0.00				
Impingement present	No				
Pairs seal strips	1		Passlane seal rods (mm)	22.225	No. 2
Shell expansion joint	No		Rear head support plate	No	
Weight estimation Wet/Dry/Bundle	2287.1	/	1663.0 /	667.62	(kg/shell)

Baffle Information

Type	Perpend.	Single-Seg.	Baffle cut (% dia)	30.58	
Crosspasses/shellpass		9	No. (Pct Area)	(mm) to C.L	
Central spacing	(mm)	531.73	1 27.91	75.20	
Inlet spacing	(mm)	558.61	2 0.00	0.00	
Outlet spacing	(mm)	529.41			
Baffle thickness	(mm)	9.52			
Use deresonating baffles		No			

Tube Information

Tube type		Plain	Tubecount per shell		76
Overall length	(mm)	4876.8	Pct tubes removed (both)		6.58
Effective length	(mm)	4810.	Outside diameter	(mm)	22.225
Total tubesheet	(mm)	66.67	Wall thickness	(mm)	2.108
Area ratio	(out/in)	1.2341	Pitch (mm) 33.337	Ratio	1.5000
Tube metal		Carbon steel	Tube pattern (deg)		30

Figure 13.12: HTRI results and figure of horizontal heat exchanger

13.7.3 Compressor

Maximum permissible operating pressure for the reciprocating and centrifugal compressor is calculated by adding maximum differential pressure in the compressor with maximum pressure at the inlet.

Maximum discharge temperature shall be maximum allowable temperature for centrifugal and reciprocating compressor during operation for inclusion of some deviation values [178]. The power required to derive the compressor is given by using equation (13.4).

$$P=W*N_w/60 \tag{13.4}$$

Where W is work done, N_w is speed of the compressor in rpm.

13.8 Equipment design

CHECALC is a chemical engineering calculations web software used to assist process and plant, operation and maintenance and is available online [179]. This software is used in this research work for the detail calculations of the static equipment used in the biogas plant and one calculation procedure for the design of vessel is shown in the Figure 13.13 below.

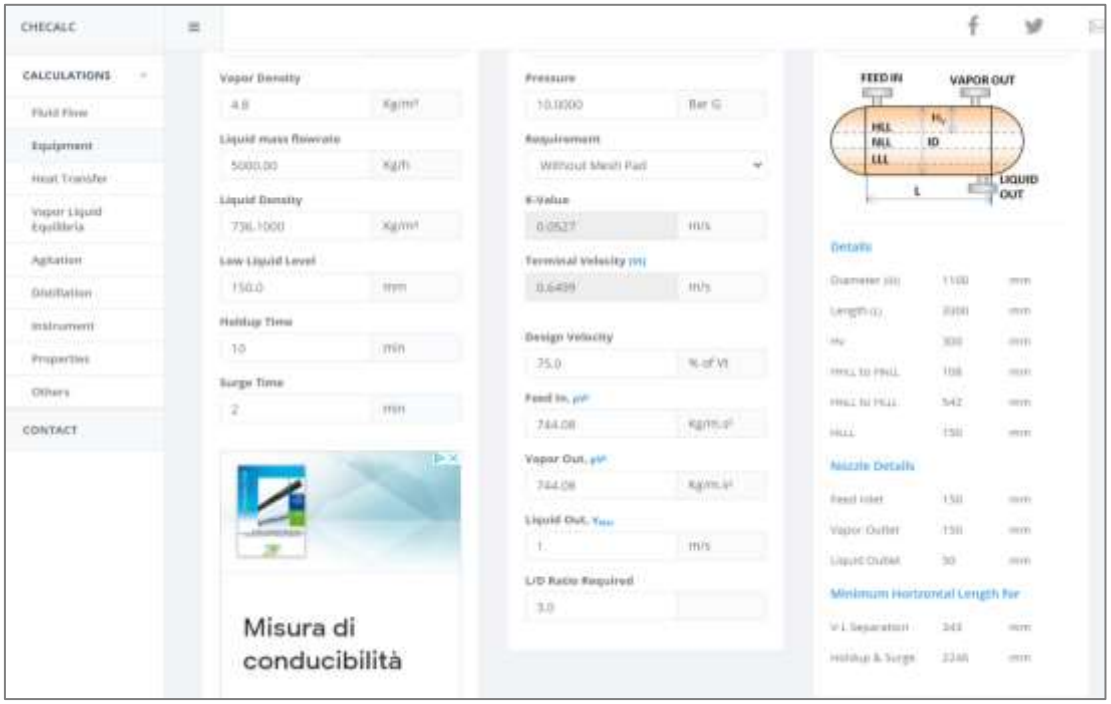

Figure 13.13: Design of vessel by using CHECALC web software

13.9 Package's calculations

There were two packages one is from biogas to electricity generation and second one is from flue gas to electricity generation.

13.9.1 Case without dryer (Biogas)

In this scenario process feed conditions are supplied with corresponding permeate and residual conditions selection which are given below in the Table 13.5.

Table 13.5: Process feed, permeate and residual conditions

Name	Unit	Process Feed conditions	Permeate Condition (CO_2)	Residual Condition (rich CH_4)
Flowrate	Kg/h	11,083.60	7494.3	3589.3
Operating Pressure	Barg	7.2	0	6.7
Operating Temperature	°C	40	40	40
MW	Kg/Kmole	23.81	30.33	16.43
CO_2	% mol.	26.94	50.34	0.49
H_2O	% mol.	1.02	1.92	0
Methane	% mol.	70.48	46.48	97.62
Nitrogen	% mol.	1.56	1.26	1.89
Viscosity	cp	0.013	0.01	0
Zeta		0.9822	0.9967	0.9873

13.9.1.1 Membrane dimension parameters

For CO_2 removal from biogas a membrane technique was suggested, and input parameters are given below in the Table 13.6.

Table 13.6: Membrane dimension parameters

Membrane Dimension parameters		
Name	**amount**	**unit**
Diameter	200	mm
Length	20	m
Molecular Sieve bulk Density	600	Kg/m3
Water absorption on mass MS	21	% mass

CO_2 adsorption	0.8	mole/kg MS
CH_4 adsorption	0.25	mole/kg MS
N_2 adsorption	0.68	mole/kg MS
Number of elements	80	
Diameter of Particle	1	mm
Void fraction of bed	37%	

13.9.2 Case without dryer (Flue gas)

In this scenario process feed conditions are supplied with corresponding permeate and residual conditions selection which are given below in the Table 13.7.

Table 13.7: Process feed, permeate and residual conditionsS

Name	Unit	Process Feed conditions	Permeate Condition (CO_2)	Residual Condition (rich CH_4)
Flowrate	Kg/h	86,000	15400	70600
Operating Pressure	Barg	7.6	0	7.1
Operating Temperature	°C	40	40	40
MW	Kg/Kmole	29.51	30.33	28.52
CO2	% mol.	7.5	47	0.12
H2O	% mol.	1	7	0
Methane	% mol.	0	0	0
Nitrogen	% mol.	91.5	46	99.88
Viscosity	cp	0.013	0.01	0
Zeta		0.9822	0.9967	0.9873

13.9.2.1 Membrane dimension parameters

For CO_2 removal from biogas a membrane technique was suggested, and input parameters are given below in the Table 13.8.

Table 13.8: Membrane dimension parameters

Membrane Dimension parameters		
Name	**amount**	**unit**
Diameter	250	mm
Lenght	8	m
Molecular Sieve bulk Density	600	Kg/m3

Water absortion on mass MS	21	% mass
CO2 adsorbition	0.4	mole/kg MS
CH4 adsorbtion	0.25	mole/kg MS
N2 adsorbition	0.15	mole/kg MS
Number of elements	85	
Diameter of Particle	1	mm
Void fraction of bed	37.00%	

Pressure drop was calculated in both cases with the equation (13.5) [98].

$$\frac{\Delta P}{\Delta z} = \frac{u}{D_p} \cdot \frac{1-\varepsilon}{\varepsilon^3} \cdot \left(\frac{150\ (1-\varepsilon)\mu}{D_p} + 1.75\rho u \right) \tag{13.5}$$

where $\Delta P/\Delta z$ is the pressure drop per unit length of the column, u is the gas speed equal to the ratio of gas flow to the pipe area, D_p is the diameter of the glass particles, ε the void fraction of the bed and is equal to 0.37, μ and ρ respectively the viscosity (0.01) and density of the gas (7.64 kg/m^3).

13.10 Equipment cost/ Capital cost of plant

Capital and operating cost of the main equipment e.g., compressors, pumps, turbines, reactors, vessels, heat exchangers, and heaters was analyzed through rough economic estimation. The operation, maintenance and insurance cost related to capital investment was 1.1%, 2.3% and 2% respectively. The total cost of the upgraded biogas (biomethane) per tonne could be computed from annual operating and capital cost and the amount of the upgraded biogas produced (tonnes).

Total capital cost of the plant was calculated by using CAPCOST, a capital cost estimation software based on the equipment module approach [180]. The capital cost calculated with CAPCOST comprises the direct and indirect project costs by multiplying a bare module factor with the equipment cost. The bare module factor is correlated with the installation of equipment including material and labour for installation, the transportation, insurance and taxes, construction overhead and contractor engineering expenses. Bare module cost includes labour and materials, inspection, structure (foundation, etc.), piping, instrumentation, painting and insulation, utility hook up (electrical, water, steam, sewer, etc.), and engineering supervision.

The approach of CAPCOST is given below in the Figure 13.14.

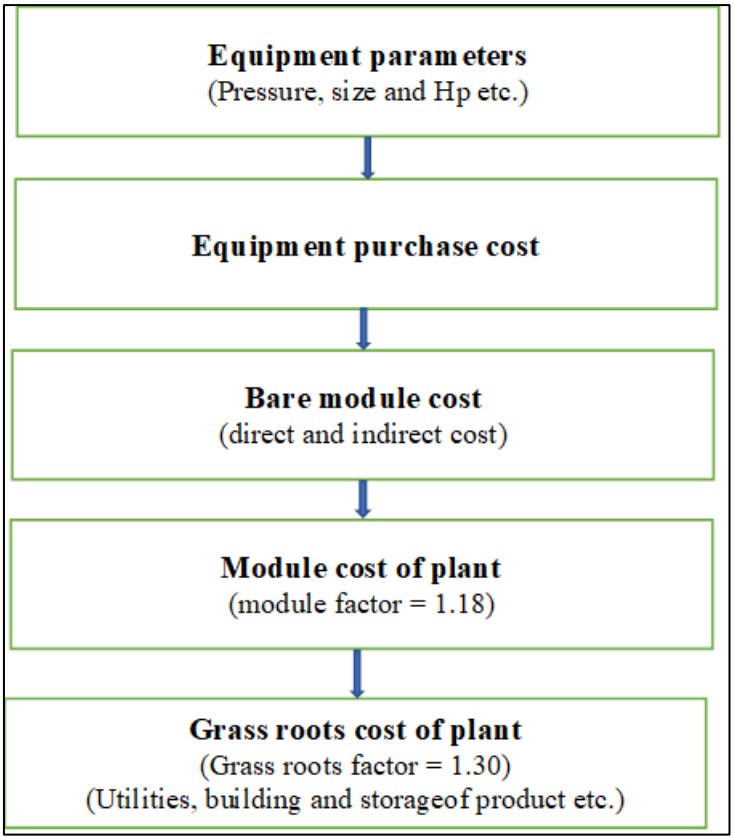

Figure 13.14: CAPCOST approach

13.11 Cash flow analysis

CAPCOST software was also used to analyze the cash flow and the input values including cost of land, salvage value (project end life value), cost of equipment and facilities (FCI_L), revenue, raw material cost, cost of utilities (calculated from given data), cost of labor, and waste treatment cost are given in the Table 13.9 below.

Table 13.9: Input parameters for CFD

Economic Options	
Land purchased cost ($)	1250000
Rate of taxation	30%
Rate of interest (annual)	2%
Salvage/ project end life Value ($)	30520000
FCI_L ($)	305200000
Factor of module (total)	1.18
Factor of grass root	0.50

Product sale revenue ($)	141806880
Cost of raw material (C_{RM}) ($)	83220000
Cost of Utilities (C_{UT})) ($)	3858400
Cost of waste treatment (C_{WT}) ($)	0
Labor operating cost (C_{OL}) ($)	158700

The plant has total life of 22 years including project life (after startup) of 20 years and 2 years of construction life. Fixed capital investment was distributed at the end of first year 60% and remaining 40% at the end of second year.

13.11.1 Cost of manufacturing and working capital

The cost of manufacturing was calculated from the equation (13.6) provided by the CAPCOST software.

$$\text{Cost of Manufacturing } (COM_d) = 0.18*FCI_L + 2.76*C_{OL} + 1.23*(C_{UT} + C_{WT} + C_{RM}) \quad (13.6)$$

The cost of working capital was calculated by using equation (13.7).

$$\text{Working Capital} = A*C_{RM} + B*FCI_L + C*C_{OL} \quad (13.7)$$

13.12 Monte Carlo simulation

The parameters and their base values used for Monte Carlo simulation including upper a lower limit is shown in the Table 13.10 below.

Table 13.10: Key Parameters over Plant Life

Parameters	Lower Limit	Upper Limit	Base Value
FCIL	-20%	30%	$ 305,200,000
Product price	-10%	10%	$ 141,806,880
Working Capital	-50%	10%	$ 38,900,000
Income Tax Rate*	-20%	20%	30%
Rate of interest*	-10%	20%	2%
Cost of raw material	-10%	15%	$ 83,220,000
Salvage Value	-80%	20%	$ 30,520,000

14. RESULTS, ANALYSIS AND DISCUSSION

14.1 Introduction

This chapter includes all the results and analysis that are designed in the previous chapter.

14.2 Plant configuration

From the four proposed plant configurations each one has their own pros and cons. By analyzing all four the fourth proposed scheme has high environmental impact, medium to perform plant turndown, high profit, high waste heat recovery, and very high preliminary RAM study. The scheme four uses the flue gas also, which in other cases emitted to the air is not good regarding climate change as shown in the Figure 14.1.

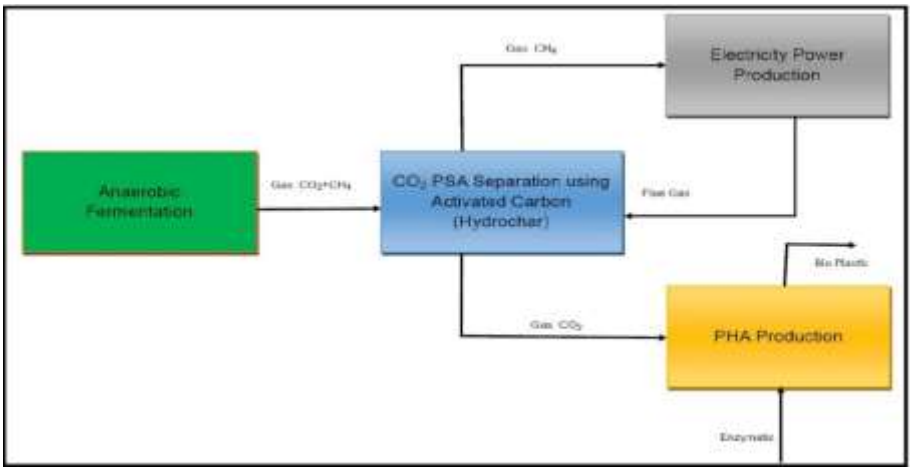

Figure 14.1: Plant configuration of scheme 4

By keeping detail comparison between all the proposed schemes, scheme four looks promising but this is not enough so more analysis are required to choose the best option.

14.3 Scoring model analysis and results

The results of the scoring model technique based on "Q" factors clearly shows that scheme four is the best because it has score 2.58 which is highest as compared to the other schemes as shown in the Table 14.1 below.

Table 14.1: Scoring model technique results

Cases/Schemes	Waste heat recovery	Environmental impact	Plant turn down	Preliminary RAM study	Maintenance cost and frequency	Overall plant dimensions	Main equipment delivery and installation time	CAPEX & OPEX	IRR & ROI	Score
Base case **(Scheme-01)**	0	0	0.08	0.04	0.32	0.2	0.36	0.72	0.25	1.97
Biogas pretreatment **(Scheme-02)**	0	0	0.08	0.08	0.24	0.15	0.27	0.54	0.5	1.86
Biogas CO2 recovery **(Scheme-03)**	0	0.45	0.04	0.12	0.16	0.1	0.18	0.36	0.75	2.16
Biogas and flue gas recovery **(Scheme-04)**	0.4	0.6	0.02	0.16	0.08	0.05	0.09	0.18	1	**2.58**

14.4 Life cycle analysis results

Life cycle analysis results by using Simapro software shows that scheme four has best figures by considering climate change, global warming, GHG, pollution, human toxicity, and ozone layer depletion parameters as compared to the others as shown in the Figure 14.2.

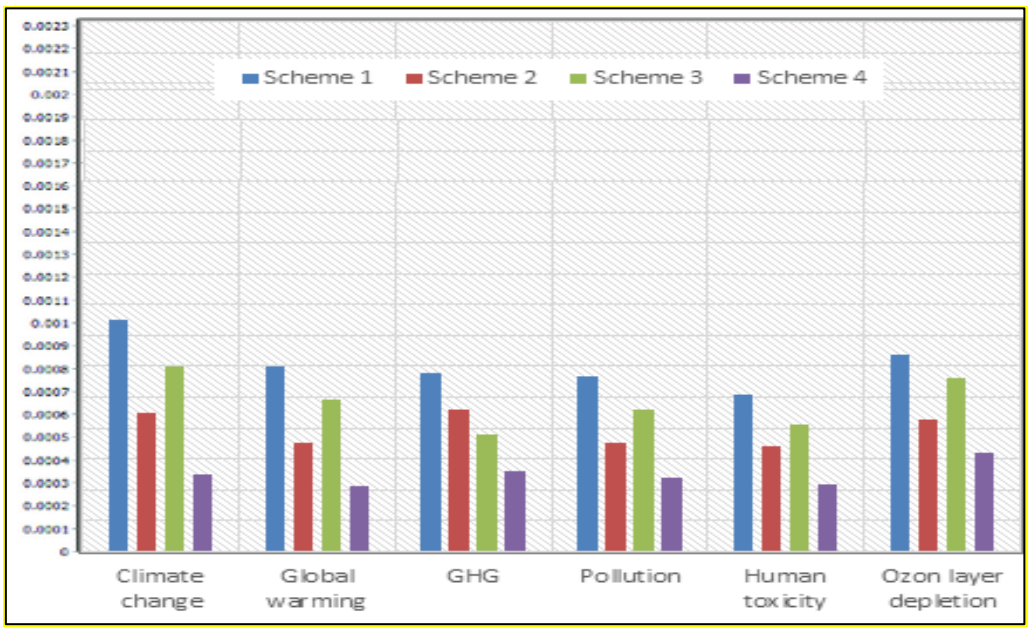

Figure 14.2: Life cycle analysis results by using Simapro software

14.5 Process simulation results (Aspen HYSYS)

Process simulation is done by using Aspen HYSYS software as shown in the

Figure ***14.3***. From the figure it is shown that biogas obtained from anaerobic fermentation is sent to the vessel (100-V-101) having flowrate of 10,000 kg/h, temperature 35 ºC and pressure 101.3 kPa having the following composition: Methane 57 %, Carbon Dioxide 36 %, Nitrogen 5%, Oxygen 1%, H_2S, Siloxanes, Aromatics, H_2, etc balanced. Water saturated at operating temperature and pressure. Composition has been taken from [101]

Power required to induce the biogas into the vessel is 298 kW. The first step is to dehumidify the wet biogas. For that purpose, the wet biogas is first sent to the double acting reciprocating compressor (100-k-101A/B) to achieve the input requirement of the heater. An air cooler (100-EA-101) is used between the two stages of the double acting compressors in order to decrease the temperature of biogas during the process. After the compressors, the biogas having temperature reached to 153.4 ºC and pressure 850 kPa is sent to the heater (100-E-101). After passing through the heater, the temperature of dry biogas has reached 300 ºC and slight pressure drop of 820 kPa is observed. The second step is to remove the Sulphur contents from the dry biogas. For that purpose, the incoming dry biogas is passed through the Sulphur guard bed (100-X-101). At this point the properties of dry biogas are 298 ºC and 780 kPa pressure. The third step is to separate the methane and carbon dioxide gasses from the Sulphur free dry biogas. The biogas is first passed through the air cooler (100-EA-102) to decrease the temperature to the normal ambient temperature of 40 ºC. After achieving the required conditions, the separation of methane and carbon dioxide is carried out by using pressure swing adsorption (PSA) (100-X-102) technique in which hydro char (activated carbon) is used as an adsorbent material. At this point, the temperature and pressure of biogas is 40 ºC and 700 kPa respectively. Now, we have two streamlines; one is methane that will be used for the electricity generation purposes and the second is carbon dioxide which will be used to produce bioplastic material in the laboratory.

Methane achieved from the PSA separation is sent to the heavy-duty multi-stage reciprocating compressor (101-K-101) to pressurize the biogas to 2100 kPa and corresponding temperature has also increased to 151.7 ºC. The pressure at this stage is suitable but the temperature is too high for the gas turbine which is needed to be cooled

down. So, an air cooler (200-EA-101A/B) is added to lower the temperature to the normal ambient temperature of 40 ºC. Now, pure oxygen is required for the burning purpose in the gas turbine. For this purpose, air (wet) is captured from the open environment and is treated in the separator (TEE-100) with the help of reciprocating compressor (200-K-101A) to extract the pure oxygen from the air (wet) and the other gasses are sent directly to the exhaust streamline of the gas turbine i.e., flue gas. Now, the methane having flow rate of 193.9 kg/h and pure oxygen is sent to the gas turbine (200-R-100) for combustion purposes in order to produce electricity through generator attached (200-XP-101) which is achieved to be 16 MW of electricity.

The next step is to treat the flue gas streamline which is sent to the steam boiler (300-E-100) for steam generation having properties of 1247 ºC temperature and 160 kPa pressure. The steam obtained from the steam boiler is used to produce electricity through steam generator (200-XP-102). The electricity obtained is 6 MW at this stage. The steam after passing through steam generator is condensed by using an air cooler (300-EA-101). The condensed water is then supplied to the steam drum (300-E-102) with the help of centrifugal pump (P-100). This condensed water is again sent to the steam boiler for steam generation and hence the cycle continues.

The exhaust flue gas from the steam turbine having carbon dioxide contents is again treated with similar procedure as applied before through pressure swing adsorption technique (400-X-100) for the separation of carbon dioxide. This carbon dioxide is then added to the mainstream line of carbon dioxide.

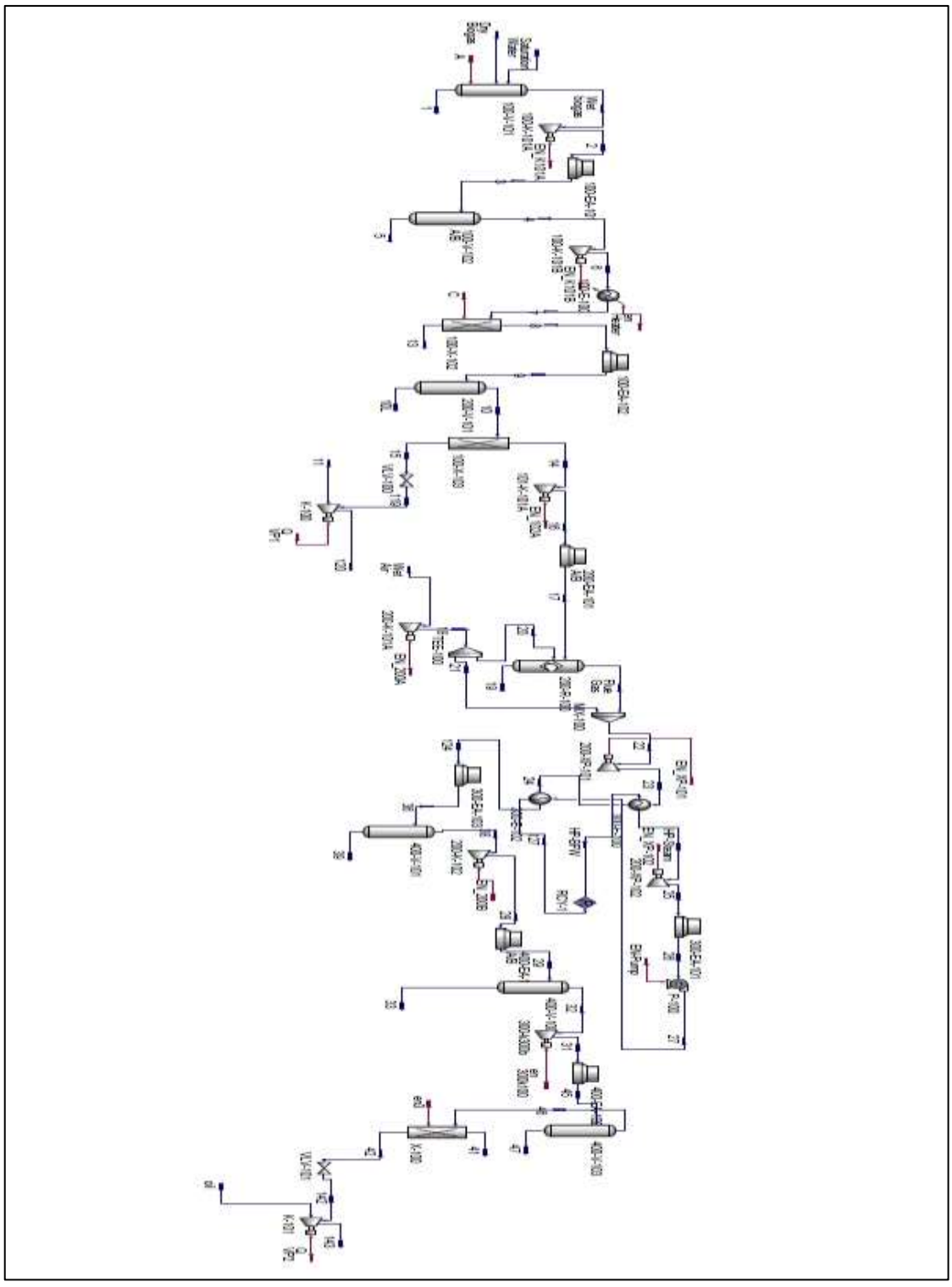

Figure 14.3: Process simulation by using Aspen HYSYS software

14.6 Equipment summary

Equipment summaries of all the equipment used in the plant design were prepared by using the formulas that were discussed briefly in the previous chapter and Microsoft excel sheets were used for the calculations.

14.6.1 Compressor

Total five compressors were used in the scheme and the detail of each is shown in the Table 14.2 below.

Table 14.2: Equipment summary of the Compressors

COMPRESSORS															
Item	Service	Oper / Stand-by	Type	Design Capacity	MW	K	Inlet		Discharge		Material		Driver type	Minimum Required power	Notes
							Temp.	Press.	Oper. Pressure	Design Pressure	Casing	Rotor / Piston			
				M^3/h		C_p/C_v	^0C	Bar (g)	Bar (g)	Bar (g)				KW	
100-K-101 A/B	wet biogas compressor	"1/1	Rec	11620	23.54	1.256	35	0	7.5	10	KCS (1)	KCS (1)	Elect	1000	(1) NACE requirement
200-K-101 A/B	Rich Methane suction compressor	"1/1	Rec	800	16.43	1.31	40	6	20	30	KCS	KCS	Elect	260	
400-K-101 A/B	Flue gas compressor	"1/1	Cent	63965	28.93	1.386	40	0.05	8.1	12	KCS	KCS	Elect	6800	
100-K-102 A/B	Biogas PSA Vacuum pump	"1/1	VP	7800	30.33	1.29	40	0	50	1.3	KCS	KCS	Elect	98	
400-K-102 A/B	Flue Gas PSA Vacuum pump	"1/1	VP	14000	35.15	1.326	40	0	50	1.3	KCS	KCS	Elect	170	

14.6.2 Heat exchanger

Five heat exchangers were used, and the calculations was done by using HTRI software as shown in detail in the Table 14.3 below.

Table 14.3: Equipment summary of heat exchangers

HEAT EXCHANGERS											
Item	Service	Type	Duty	Surface	Shell side			Tube side			Notes
					Design Temp.	Design Press.	Material	Design Temp.	Design Press.	Material	
			Kcal/hr	m^2	^0C	Bar (g)		^0C	Bar (g)		
100-E-101	Biogas heater	AES	671500	26	330	8.5	CS	420	7	CS	NASE Requirement for both sides
100-E-102	Biogas Vacuum Pump Cooler	AES	890000	56	450	8	CS	400	7.5	CS	Included in the package 100-K-102 A/B
300-E-101	Flue gas boiler feed water preheating	(1)	840000	1100	1300	3.5	CS	260	35	CS	Included in the package 100-K-102 A/B
300-E-102	Flue gas steam boiler	(1)	2200000	860	600	3.5	CS	260	35	CS	Included in the package 200-GT-101 (2) estimated finned area
400-E-102	Flue gas Vacuum Pump Cooler	AES	1200000	650	700	3	CS	360	8	CS	Included in the package 100-K-102 A/B

14.6.3 Air cooler

Seven air coolers were used in the scheme and their function was to cool down the biogas and the flue gas. The detail sizing of all the air coolers is shown in the Table 14.4 below.

Table 14.4: Equipment summary of the air coolers

AIRCOOLERS										
Item	Service	Duty	Bare surface	Design Temperature	Design Pressure	Tube Material	Minimum Required power	Fan number	Estimated plot area	Notes
		Kcal/h	m^2	°C	Bar (g)		KW		m^2	
100-EA-101 A/B	Interstage wet biogas compressor air cooler	654000	112	200	6	Carbon Steel	12	2	7X5	Two air cooler and one in spare (1) NACE requirement
100-EA-102	Sweet Biogas air cooler	1338700	62	330	8.5	Carbon Steel	6	2	7X1.5	
200-EA-101 A/B	Fuel gas air cooler	234410	24	180	23	Carbon Steel	3	2	8.5X1.5	Two air cooler and one in spare
300-EA-101	Steam condenser	22407000	276	100	3.5	Carbon Steel	78	12	11X250	
300-EA-103	Flue gas final air cooler	7200000	211	250	3.5	CS	40	2	11X13.5	
400-EA-101 A/B	Flue gas interstage compressor air cooler	4400000	168	200	5	CS	80	4	10X10	Two air cooler and one in spare
400-EA-102	Flue gas discharge compressor air cooler	3500000	125	200	10	CS	40	4	8.5X7.5	

14.6.4 Reactor

There was only single reactor was used and its function was to remove sulfur from the biogas and the detail sizing of the reactor is shown in the Table 14.5.

Table 14.5: Equipment summary of the reactor

Reactor											
Item	Service	Type	Height / Length	Diameter	Design Temperature	Design Pressure	Material	Catalyst Volume	Corrosion Allowance	Insulation	Notes
			mm	mm	°C	Bar (g)		m^3	mm		
100-R-101 A/B	Sulphur guard bed	Verticle	9500	1900	330	8.5	Carbon Steel	19	3	Yes hot	Catalyst ZnO

14.6.5 Pump

Boiler water feed pump was used in the scheme/plant to supply condense water to the steam drum and the sizing detail is given in the Table 14.6 below.

Table 14.6: Equipment summary of the pump

Pump														
Item	Service	Oper / Stand-by	Type	Design Capacity	Density	NPSH	Design Temp.	Design Press.	Differential head	Material		Driver type	Minimum Required power	Notes
										Casing	Impeller			
				m^3/h	Kg/m^3	m	°C	Bar (g)	m				KW	
300-P-101 A/B	Boiler Feed water pump	*1/1	CT	48	950	3.6	120	40	400	CS	CS	Elect	70	

14.6.6 Vessel

There were many vessels required to hold the gas after the reactions and equipment summary of all the seven vessels are given in the Table 14.7 below.

Table 14.7: Equipment summary of the vessels

Vessels										
Item	**Service**	**Type**	**Height or Length**	**Diameter**	**Design Temperature**	**Design Pressure**	**Material**	**Corrosion Allowance**	**Insulation**	**Notes**
			mm	mm	°C	Bar (g)		mm		
100-V-101	Wet biogas suction compressor K.O. Drum	Vertical	6600	2200	85	3.5	Carbon steel	3	No	Provide with demister
100-V-102 A/B	Wet biogas interstage compressor K.O. Drum	Vertical	3900	1300	85	6	Carbon steel	3	No	Provide with demister NACE requirement is necessary
200-V-101	Rich Methane compressor K.O. Drum	Vertical	3000	1000	85	10	Carbon steel	3	No	Provide with demister
300-V-101	Steam Drum	Horizontal	6900	2300	85	8	Carbon steel	3	No	Provide with demister
300-V-102	Low pressure Condensate boiler water K.O. Drum	Horizontal	5100	1700	85	3.5	Carbon steel	3	No	Provide with demister
400-V-101	Cold flue gas compressor K.O. Drum	Vertical	1000	3900	85	3.5	Carbon steel	3	No	Provide with demister
400-V-102	Flue gas interstage compressor K.O. Drum	Vertical	6000	2500	85	6	Carbon steel	3	No	Provide with demister
400-V-103	Flue gas discharge compressor K.O. Drum	Vertical	6000	2400	85	10	Carbon steel	3	No	Provide with demister

14.6.7 Turbine

There were two turbines was used one was gas turbine to produce electricity from the biogas and the second one was the steam turbine to produce electricity from the flue gas. The sizing of them is given in the Table 14.8.

Table 14.8: Equipment summary of the turbines

Turbines								
Item	Service	Type	Inlet Stream		Exhaust Stream		Produced Energy Power	Notes
			Temperature °C	Pressure Bar (g)	Temperature °C	Pressure Bar (g)	KW	
200-GT-101	Gas turbine	GT	1745	11	1247	0.6	8200	Estimated Turbine ISO horsepower 13800 to be defined during detailed Engineering, Gas turbine provide with flue gas steam heat exchanger recovery.
300-TK-101	Steam turbine	ST	235	29.5	60	0	5800	

14.6.8 Package

There were two packages used one from biogas to electricity and second from flue gas to the electricity and their detail sizing is shown in the Table 14.9 below.

Table 14.9: Equipment summary of the packages

MISCELLANEOUS & PACKAGES						
Item	Service	Design Temperature	Design Pressure	Material	Flow	Description
		°C	Bar (g)		Kg/hr	
100-X-101	Biogas CO2 PSA	85	10	Carbon Steel	11000	Package composed by 90 tubes of 8" diameter and length 20 m each with Hydro char. Each element needs 376 kg in total 30.2 ton
400-X-101	Flue Gas CO2 PSA	85	10	Carbon Steel	86000	Package composed by 85 tubes of 10" diameter and length 8 m each with hydro char. Each element needs 236 kg in total 20.2 ton

14.7 Equipment design

In depth detail design of the equipmets was done by using CHECALC web software and the results are given below.

14.7.1 Air cooler design

Based on the equipment summary of all the equipment used in the plant design the input parameters were set in the CHECALC web software and the results were achieved and were compiled in the tabular form of the excel sheets. Table 14.10 shows the design of the air cooler and similarly design of all the other equipment was done.

Table 14.10: Air cooler design

AIRCOOLER (100.EA-101 A/B)											
Tube length	Tube rows	Heat duty	U value	Process side		Air side			Efficiency		
				Inlet Temperature	Outlet Temperature	Inlet Temperature	Face velocity	Site elevation	Fan	Motor	
m		Kcal/h	W/m2.°K	°C	°C	°C	m/s	m	%	%	
9.144	6	654000	200	129	40	35	27	50	75	95	
RESULTS											
Air outlet temperature	LMTD	Correction factor	LMTD corrected	Finned area	Face area	Air cooler width	Tube detail						Power detail			
							OD	Fin Height	Layout	Pitch	Total	Per row	Air flow rate	Pressure drop	Break power	Motor power
°C	°C		°C	m²	m²	m	Inch	Inch		Inch			M³/h	Inch H₂O	KW	KW
58.03	24.84	0.9	22	170	1.1	0.12	1	0.6	30°	2.5	11	2	10287 6	44.24	413	455

14.8 Package's calculations

The results of membrane design for pressure swing adsorption method are given below in the Table 14.11 and Table 14.12.

Table 14.11: Case without dryer (biogas)

Membrane dimension with PSA		
Diameters	200	mm
Length	20	m
Number of elements	80	
Weight of Molecular Sieve for each elements	376.99	Kg
Total Molecular Sieve	30159.3	Kg
Pressure drop calculated	282.92	Kpa
Velocity	0.12034	m/s

Table 14.12: Case without dryer (Flue gas)

Membrane dimension with PSA		
Diameters	250	mm
Length	8	m
Number of elements	85	
Weight of Molecular Sieve for each elements	235.62	Kg

Total Molecular Sieve	20027.7	Kg
Pressure drop calculated	51.64	Kpa
Velocity	0.55	m/s

14.9 Equipment cost

Cost of all the equipment was calculated by using CAPCOST software and the results are given below in the Table 14.13.

Table 14.13: Equipment cost calculated by CAPCOST

Name	Purchased equipment cost ($)	Bare module cost ($)	Total module cost ($)	Gross roots cost ($)	Capital cost ($)	Total capital cost ($)
Compressors	4449000	13100000	15460000	22060000	33090000	**400804950**
Heat Exchangers	408700	909800	1074704.18	1527000	2290500	
Heaters	3210000	91600000	108100000	111600000	167400000	
Pumps	20500	113000	117010000	124280000	186420000	
Reactors	547000	2190000	133000	166000	249000	
Turbines	2155000	7550000	2580000	2860000	4290000	
vassels	190630	1112600	4026200	4710300	7065450	

14.10 Cash flow diagram

The results in the tabular form of cash flow diagram are shown in the Table 14.14 below.

Table 14.14: Results of the cash flow diagram

Year	Investment	d_k	FCI_k-Sd_k	R	COM_d	$(R-COM_d-d_k)*(1-t)+d_k$	Cash Flow (Non-discounted)	Cash Flow (discounted)	Cumulative Cash Flow (discounted)	Cumulative Cash Flow (Non-discounted)
0	1.25		305.20				(1.25)	(1.25)	(1.25)	(1.25)
1	183.12		305.20				(183.12)	(179.53)	(180.78)	(184.37)
2	160.98		305.20				(160.98)	(154.73)	(335.51)	(345.35)
3		30.52	274.68	141.81	152.99	1.33	1.33	1.25	(334.26)	(344.02)
4		54.94	219.74	141.81	152.99	8.65	8.65	7.99	(326.26)	(335.37)
5		43.95	175.80	141.81	152.99	5.36	5.36	4.85	(321.41)	(330.01)
6		35.10	140.70	141.81	152.99	2.70	2.70	2.40	(319.01)	(327.31)
7		28.08	112.62	141.81	152.99	0.60	0.60	0.52	(318.49)	(326.71)
8		22.58	90.03	141.81	152.99	(1.05)	(1.05)	(0.90)	(319.39)	(327.76)
9		20.14	69.89	141.81	152.99	(1.78)	(1.78)	(1.49)	(320.88)	(329.55)
10		20.14	49.75	141.81	152.99	(1.78)	(1.78)	(1.46)	(322.35)	(331.33)
11		19.84	29.91	141.81	152.99	(1.88)	(1.88)	(1.51)	(323.85)	(333.21)
12		19.84	10.07	141.81	152.99	(1.88)	(1.88)	(1.48)	(325.33)	(335.08)
13		10.07	-	141.81	152.99	(4.81)	(4.81)	(3.72)	(329.05)	(339.89)
14			-	141.81	152.99	(7.83)	(7.83)	(5.93)	(334.98)	(347.72)
15			-	141.81	152.99	(7.83)	(7.83)	(5.82)	(340.80)	(355.55)
16			-	141.81	152.99	(7.83)	(7.83)	(5.70)	(346.50)	(363.37)
17			-	141.81	152.99	(7.83)	(7.83)	(5.59)	(352.09)	(371.20)
18			-	141.81	152.99	(7.83)	(7.83)	(5.48)	(357.57)	(379.03)
19			-	141.81	152.99	(7.83)	(7.83)	(5.37)	(362.94)	(386.85)
20			-	141.81	152.99	(7.83)	(7.83)	(5.27)	(368.21)	(394.68)
21			-	141.81	152.99	(7.83)	(7.83)	(5.16)	(373.37)	(402.51)
22			-	141.81	152.99	13.54	53.69	34.73	(338.65)	(348.82)

The project has total life of 22 years including 2 years of construction time and 20 years of project time As, it can be noted from the figure that the first two years was the construction period of project, so all the money was invested during this time period.

The profit started from the third year and reach its maximum value after 10 years. From this point other costs like maintenance cost, inflation etc started to influence on the project value hence the decline in the profit value was observed till the project life of 22 years. CFD was constructed between project life and project value as shown in the Figure 14.4.

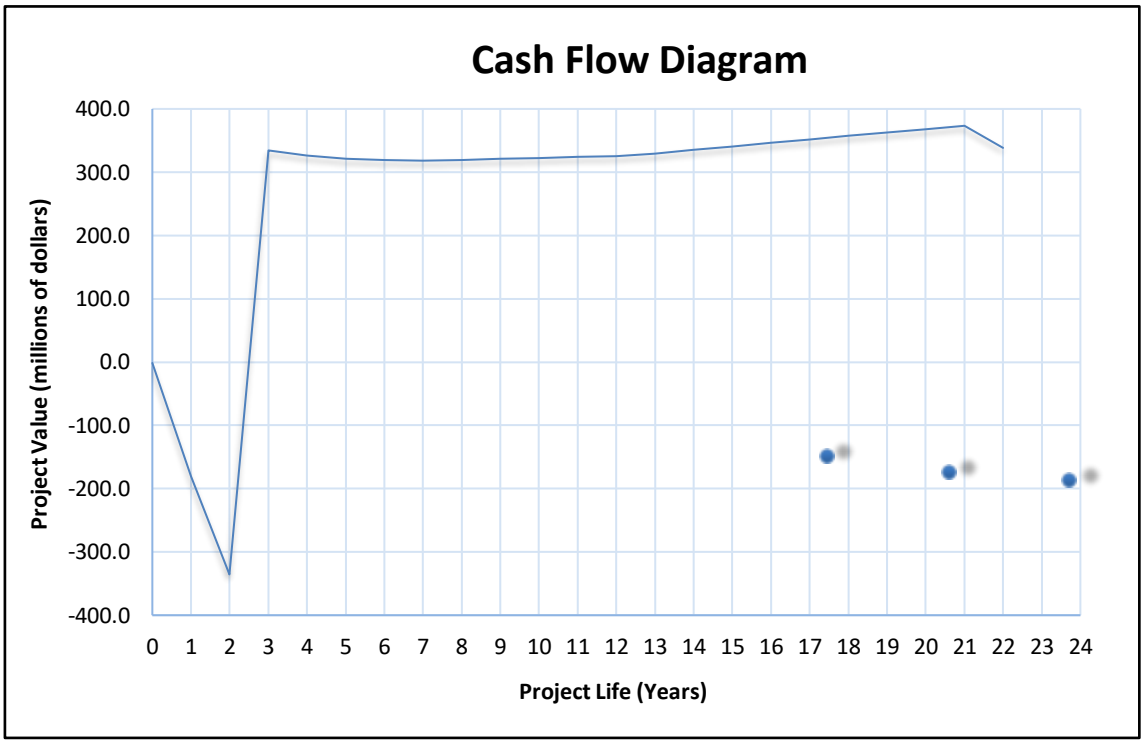

Figure 14.4: Project life v/s project value

14.11 Monte Carlo simulation

The analysis and results of the Monte Carlo simulation was done based on the parameters set in the previous chapter and are shown below in graphical forms.

14.11.1 Net Present Value Data

Net Present Value (NPV) most commonly used to estimate the profitability of a project. when project starts working initially, there are different costs associated e.g., raw material cost and labour cost.

As can be seen that in the graph the project remains in negative value till the end of five years then it starts earning money till the end life of the project. The graphical results of cumulative numbers of data point against net present value are shown in the Figure 14.5 below.

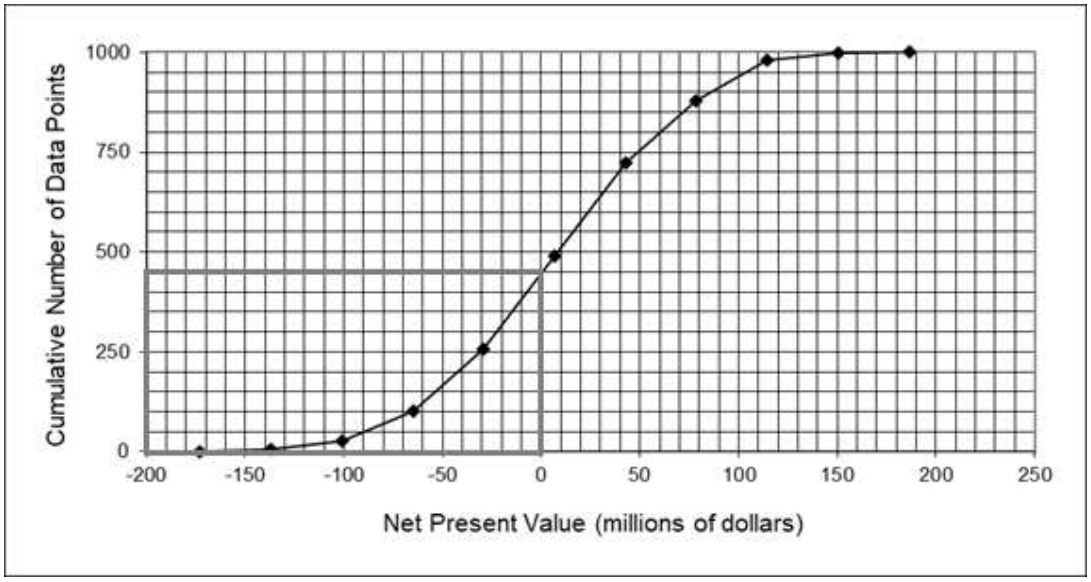

Figure 14.5: Cumulative number of data points v/s net present value

14.11.2 Rate of Return-on-Investment Data

Figure 14.6 shows the relation between rate of return on investment and cumulative number of data points. It is clear from the figure that the rate of return on investment started after second year. At third year the rate of return balanced the investment amount and started on increasing at the rate of 10% of approximate two years. Similarly, it is noted that after ten years the rate of return on investment achieved is 50%.

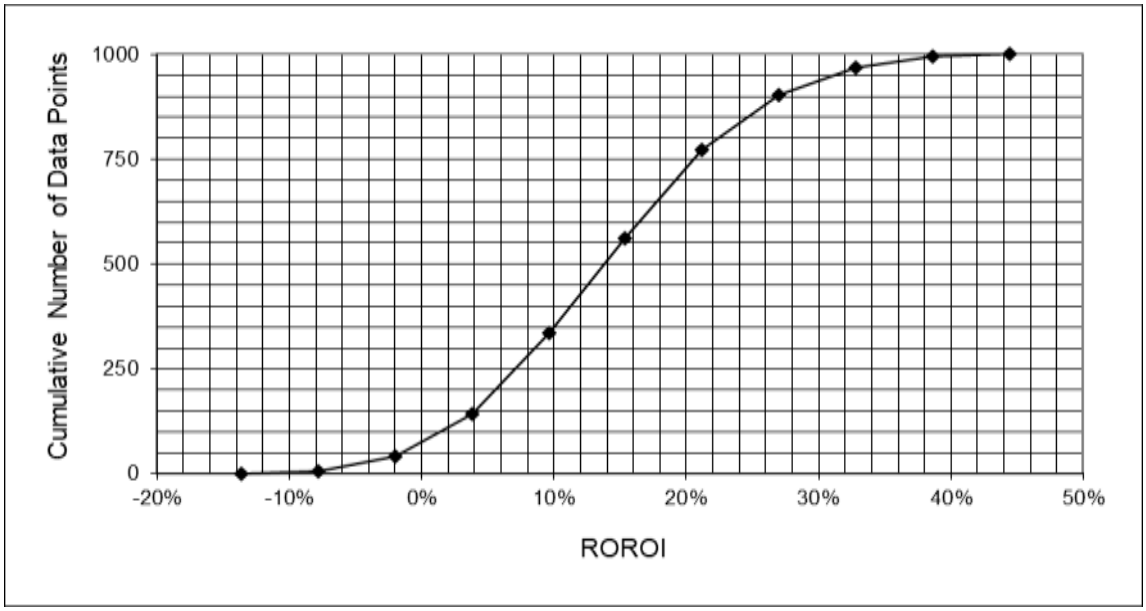

Figure 14.6: Cumulative number of data points v/s ROROI

14.11.3 Payback Period Data

The cumulative number of data points against the payback period is shown in Figure 14.7. From the figure it is observed that the pay back of the project is started after 2 years and keep on increasing with the time and reached its maximum value at the end of ten years.

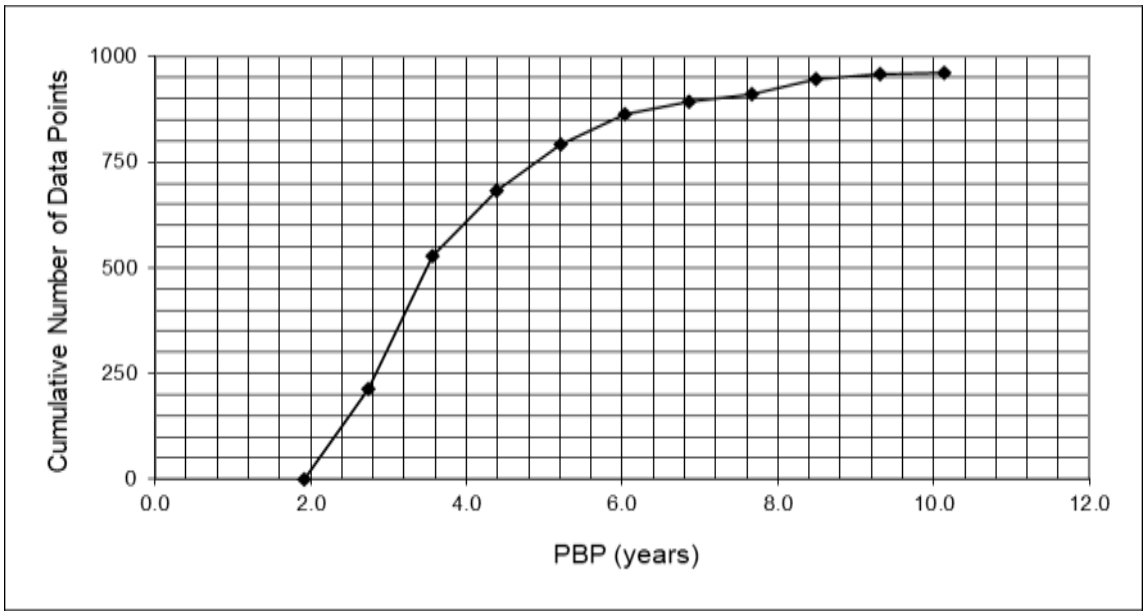

Figure 14.7: Cumulative number of data points v/s PBP

15. CONCLUSION AND RECOMMENDATIONS

15.1 CONCLUSION

The thesis work has focused on the industrial process for the production of electricity and bioplastic from biogas, as an alternative to the use of fossil fuels that are less available and have a greater environmental impact.

Four different plant configurations have been studied and developed for the production of electricity. Through the use of the "Aspen HYSYS" software, the related "process simulations" were carried out for best chosen plant configuration, in order to verify the reliability of process reproduction on an industrial scale, both for compliance with the specified design specifications and in terms of the sizing of the intended equipment.

Process flow diagrams (PFD's) have been created manually by hand using drawing sheets, for a more simplified and less detailed general view of the four process schemes and also with the use of the drawing program "AutoCAD", to deepen the process in more detail. Through PFD's it was possible to analyze more clearly how the various equipment is connected to each other within the plant, also highlighting the various control systems prepared for the various operating and procedural conditions.

Once the equipment involved and their operating conditions have been defined, the main equipment of the final fourth plant scheme has been sized. The equipment has in fact been selected and sized on the basis of a consolidated business experience of APS in the design of process plants, in order to evaluate and / or optimize the best technological solution among those analyzed. The calculations for this sizing have been carried out in accordance with the good standards of engineering and in some cases with the help of specific programs.

Finally, an economic analysis was performed using the "CapCost" spreadsheet for plant considering the Payback Period and net cash flow, through the evaluation of plant costs, management costs, utilities expenses and revenues from the sale of the final product.

This plant is producing 22 Megawatt of electricity generation and having total capital cost of 400 millions of dollars approximately.

15.2 RECOMMENDATIONS

In the future other biogas pre-treatment techniques can be used to achieve the best results and also to join the CO_2 stream in order to design a complete plant that will produce bioplastic also in addition to the electricity.

16. REFERENCES

1. Statistics, R.C., *International Renewable Energy Agency (IRENA)*. 2016, ed.
2. IEA, I.J.W.E.O., *World Energy Outlook 2019–Analysis-IEA.* 2019.
3. Vitillo, J.G., B. Smit, and L. Gagliardi, *Introduction: Carbon capture and separation*. 2017, ACS Publications.
4. IEA, I.E.A., *Technology Roadmap: Carbon capture and storage 2013*. 2013, OECD/IEA Paris.
5. NOAA National Centers for Environmental Information, S.o.t.C., *Global Climate Report for September 2018.* November 4, 2018.
6. Dimitrov, R.S.J.G.E.P., *The Paris agreement on climate change: Behind closed doors.* 2016. **16**(3): p. 1-11.
7. Hoegh-Guldberg, O., et al., *Impacts of 1.5 ºC global warming on natural and human systems.* 2018.
8. Wang, S., et al., *Lignocellulosic biomass pyrolysis mechanism: a state-of-the-art review.* 2017. **62**: p. 33-86.
9. Houghton, J. and J. Firor, *Global warming: the complete briefing*. Vol. 2. 1995: Cambridge University Press Cambridge.
10. Bicalho, T., I. Sauer, and D.J.J.o.C.P. Patiño-Echeverri, *Quality of data for estimating GHG emissions in biofuel regulations is unknown: A review of default values related to sugarcane and corn ethanol.* 2019. **239**: p. 117903.
11. Rathnayake, M., et al., *Process simulation based life cycle assessment for bioethanol production from cassava, cane molasses, and rice straw.* 2018. **190**: p. 24-35.
12. Moazeni, F., Y.-C. Chen, and G.J.J.o.C.P. Zhang, *Enzymatic transesterification for biodiesel production from used cooking oil, a review.* 2019. **216**: p. 117-128.
13. The National Academies of Sciences, E., and Medicine, *Carbon Dioxide Removal Technologies & Climate Change.* Oct. 24, 2018.
14. Harrison, D.P., *Sorption-enhanced hydrogen production: a review.* Industrial & engineering chemistry research, 2008. **47**(17): p. 6486-6501.
15. Samadiafshar, A. and A.J.E.M.f.S.D. Ghorbani, *Clean energy management.* 2018: p. 85-97.

16. Raven, R.P.J.M. and K.H. Gregersen, *Biogas plants in Denmark: successes and setbacks.* Renewable and Sustainable Energy Reviews, 2007. **11**(1): p. 116-132.

17. Bond, T. and M.R. Templeton, *History and future of domestic biogas plants in the developing world.* Energy for Sustainable Development, 2011. **15**(4): p. 347-354.

18. Walla, C. and W. Schneeberger, *The optimal size for biogas plants.* Biomass and Bioenergy, 2008. **32**(6): p. 551-557.

19. Lukehurst, C.T., P. Frost, and T.J.I.b. Al Seadi, *Utilisation of digestate from biogas plants as biofertiliser.* 2010. **2010**: p. 1-36.

20. Luo, T., et al., *Reducing biogas emissions from village-scale plant with optimal floating-drum biogas storage tank and operation parameters.* 2017. **208**: p. 312-318.

21. Kaur, H. and S.J.I.J.o.R.E.R. Kumar, *Designing of small scale fixed dome biogas digester for paddy straw.* 2017. **7**(1): p. 422-431.

22. Kanwar, S. and R.J.B.T. Guleri, *Performance evaluation of a family-size, rubber-balloon biogas plant under hilly conditions.* 1994. **50**(2): p. 119-121.

23. Ozekmekci, M., G. Salkic, and M.F.J.F.P.T. Fellah, *Use of zeolites for the removal of H2S: A mini-review.* 2015. **139**: p. 49-60.

24. Creamer, A.E. and B. Gao, *Carbon-Based Adsorbents for Postcombustion CO2 Capture: A Critical Review.* Environmental Science & Technology, 2016. **50**(14): p. 7276-7289.

25. Demirbas, A.J.E.E.S.T., *Biomass resources for energy and chemical industry.* 2000. **5**(1): p. 21-45.

26. Alatalo, S.-M., *Hydrothermal carbonization in the synthesis of sustainable porous carbon materials.* 2016.

27. Qambrani, N.A., et al., *Biochar properties and eco-friendly applications for climate change mitigation, waste management, and wastewater treatment: A review.* 2017. **79**: p. 255-273.

28. Brown, R.C., *Thermochemical processing of biomass: conversion into fuels, chemicals and power*. 2019: John Wiley & Sons.

29. Liu, C., et al., *Catalytic fast pyrolysis of lignocellulosic biomass.* 2014. **43**(22): p. 7594-7623.

30. Anwar, M., et al., *CO2 capture and storage: a way forward for sustainable environment.* 2018. **226**: p. 131-144.

31. Nie, L., et al., *Recent developments and consideration issues in solid adsorbents for CO2 capture from flue gas.* 2018. **26**(11): p. 2303-2317.

32. Olajire, A.A., *CO2 capture and separation technologies for end-of-pipe applications–a review.* Energy, 2010. **35**(6): p. 2610-2628.

33. Quintella, C.M., et al., *CO2 capture technologies: An overview with technology assessment based on patents and articles.* Energy Procedia, 2011. **4**: p. 2050-2057.

34. Zhao, Z., et al., *Adsorption of carbon dioxide on alkali-modified zeolite 13X adsorbents.* International Journal of Greenhouse Gas Control, 2007. **1**(3): p. 355-359.

35. Liu, Y., et al., *Pentaethylenehexamine loaded SBA-16 for CO2 capture from simulated flue gas.* Powder Technology, 2017. **318**: p. 186-192.

36. Ferella, F., et al., *Separation of carbon dioxide for biogas upgrading to biomethane.* Journal of Cleaner Production, 2017. **164**: p. 1205-1218.

37. Mason, J., M. Veenstra, and J. Long, *Evaluating metal–organic frameworks for natural gas storage.* Chemical Science, 2014. **5**: p. 32.

38. Sejian, V.J.A.J.A.S., *Global climate change: role of livestock.* 2011. **3**: p. 19-25.

39. Salimi, M., et al., *Optimizing the preparation of meso-and microporous canola stalk-derived hydrothermal carbon via response surface methodology for methylene blue removal.* 2017. **31**(11): p. 12327-12338.

40. Meisen, A. and X. Shuai, *Research and development issues in CO2 capture.* Energy Conversion and Management, 1997. **38**: p. S37-S42.

41. Dawson, R., A.I. Cooper, and D.J. Adams, *Chemical functionalization strategies for carbon dioxide capture in microporous organic polymers.* Polymer International, 2013. **62**(3): p. 345-352.

42. Zhao, Q., et al., *Purification technologies for biogas generated by anaerobic digestion.* 2010. **24**.

43. Kenarsari, S.D., et al., *Review of recent advances in carbon dioxide separation and capture.* Rsc Advances, 2013. **3**(45): p. 22739-22773.

44. Gielen, D. and J. Podkański, *Prospects for CO2 capture and storage*. 2004: Simon and Schuster.

45. Philibert, C., *Technology penetration and capital stock turnover: Lessons from IEA scenario analysis.* IEA, Paris, 2007.

46. Riemer, P., *Greenhouse gas mitigation technologies, an overview of the CO2 capture, storage and future activities of the IEA Greenhouse Gas R&D programme.* Energy Conversion and Management, 1996. **37**(6-8): p. 665-670.

47. Wong, S. and R. Bioletti, *Carbon dioxide separation technologies.* Alberta Research Council, 2002.

48. Neagu, M., D.L.J.J.o.N.G.S. Cursaru, and Engineering, *Technical and economic evaluations of the triethylene glycol regeneration processes in natural gas dehydration plants.* 2017. **37**: p. 327-340.

49. Burr, B. and L. Lyddon. *A comparison of physical solvents for acid gas removal*. in *Gas Processors' Association Convention, Grapevine, TX*. 2008.

50. Metz, B., et al., *IPCC Special Report on Carbon Dioxide Capture and Storage. Prepared by working Group III of the Intergovernmental Panel on Climate Change 442*. 2005, Cambridge Univ. Press.

51. Wang, M., et al., *Post-combustion CO2 capture with chemical absorption: A state-of-the-art review.* Chemical Engineering Research and Design, 2011. **89**(9): p. 1609-1624.

52. Gupta, M., I. Coyle, and K. Thambimuthu. *CO2 capture technologies and opportunities in Canada*. in *1st Canadian CC&S Technology Roadmap Workshop*. 2003.

53. Tuinier, M., et al., *Cryogenic CO2 capture using dynamically operated packed beds.* Chemical Engineering Science, 2010. **65**(1): p. 114-119.

54. Mondal, M.K., H.K. Balsora, and P. Varshney, *Progress and trends in CO2 capture/separation technologies: A review.* Energy, 2012. **46**(1): p. 431-441.

55. Favre, E., *Carbon dioxide recovery from post-combustion processes: can gas permeation membranes compete with absorption?* Journal of Membrane Science, 2007. **294**(1-2): p. 50-59.

56. Haefeli, S., M. Bosi, and C. Philibert, *Carbon dioxide capture and storage issues–Accounting and baselines under the United Nations Framework Convention on Climate Change (UNFCCC).* Paris, France: International Energy Agency. See http://www. iea. org/papers/2004/css. pdf, 2004.

57. Khan, I.U., et al., *Biogas as a renewable energy fuel–A review of biogas upgrading, utilisation and storage.* Energy conversion and management, 2017. **150**: p. 277-294.

58. Figueroa, J.D., et al., *Advances in CO2 capture technology—the US Department of Energy's Carbon Sequestration Program.* 2008. **2**(1): p. 9-20.

59. Gibbins, J. and H. Chalmers, *Carbon capture and storage.* Energy policy, 2008. **36**(12): p. 4317-4322.

60. Figueroa, J.D., et al., *Advances in CO2 capture technology—the US Department of Energy's Carbon Sequestration Program.* International journal of greenhouse gas control, 2008. **2**(1): p. 9-20.

61. Er, M.K., *Carbon Capturing and Storage Technology& current CCS initiatives in India (Emerging Technology in the field of Environmental*

Engineering). International Journal of Advanced Research in Computer Science, 2017. **8**(4).

62. Yang, H., et al., *Progress in carbon dioxide separation and capture: A review.* Journal of environmental sciences, 2008. **20**(1): p. 14-27.

63. Shifeng, L., et al., *Clathrate hydrate capture of CO2 from simulated flue gas with cyclopentane/water emulsion.* Chinese Journal of Chemical Engineering, 2010. **18**(2): p. 202-206.

64. Abu-Khader, M.M., *Recent progress in CO2 capture/sequestration: a review.* Energy Sources, Part A, 2006. **28**(14): p. 1261-1279.

65. Hossain, M.M. and H.I. de Lasa, *Chemical-looping combustion (CLC) for inherent CO2 separations—a review.* Chemical Engineering Science, 2008. **63**(18): p. 4433-4451.

66. Jahirul, M.I., et al., *Biofuels production through biomass pyrolysis—a technological review.* 2012. **5**(12): p. 4952-5001.

67. Sevilla, M., et al., *Hydrothermal carbonization of biomass as a route for the sequestration of CO2: Chemical and structural properties of the carbonized products.* 2011. **35**(7): p. 3152-3159.

68. Deng, J., M. Li, and Y.J.G.c. Wang, *Biomass-derived carbon: synthesis and applications in energy storage and conversion.* 2016. **18**(18): p. 4824-4854.

69. Gallifuoco, A., et al., *Hydrothermal carbonization of Biomass: New experimental procedures for improving the industrial Processes.* 2017. **244**: p. 160-165.

70. Fang, J., et al., *Minireview of potential applications of hydrochar derived from hydrothermal carbonization of biomass.* 2018. **57**: p. 15-21.

71. Jain, A., R. Balasubramanian, and M.J.C.E.J. Srinivasan, *Hydrothermal conversion of biomass waste to activated carbon with high porosity: A review.* 2016. **283**: p. 789-805.

72. Hill, H.C.J.P.D.K., *Fixing teacher professional development.* 2009. **90**(7): p. 470-476.

73. Román, S., et al., *Hydrothermal carbonization: Modeling, final properties design and applications: A review.* 2018. **11**(1): p. 216.

74. Román Suero, S., et al., *Hydrothermal carbonization: modeling, final properties design and applications: a review.* 2018.

75. Volpe, M., J.L. Goldfarb, and L.J.B.t. Fiori, *Hydrothermal carbonization of Opuntia ficus-indica cladodes: Role of process parameters on hydrochar properties.* 2018. **247**: p. 310-318.

76. Jiang, N., et al., *Sl-lncRNA15492 interacts with Sl-miR482a and affects Solanum lycopersicum immunity against Phytophthora infestans.* 2020. **103**(4): p. 1561-1574.

77. Jain, A., et al., *Tuning hydrochar properties for enhanced mesopore development in activated carbon by hydrothermal carbonization.* 2015. **203**: p. 178-185.

78. Mohan, D., et al., *Pyrolysis of wood/biomass for bio-oil: a critical review.* 2006. **20**(3): p. 848-889.

79. Larsson, N., et al., *Continuous flow hollow fiber liquid-phase microextraction and monitoring of NSAID pharmaceuticals in a sewage treatment plant effluent.* 2009. **1**(1): p. 59-67.

80. Wu, Z., et al., *Product distribution during co-pyrolysis of bituminous coal and lignocellulosic biomass major components in a drop-tube furnace.* 2015. **29**(7): p. 4168-4180.

81. Thomsen, M.H., et al., *Identification and characterization of fermentation inhibitors formed during hydrothermal treatment and following SSF of wheat straw.* 2009. **83**(3): p. 447-455.

82. Elbaba, I.F., C. Wu, and P.T.J.I.j.o.h.e. Williams, *Hydrogen production from the pyrolysis–gasification of waste tyres with a nickel/cerium catalyst.* 2011. **36**(11): p. 6628-6637.

83. Kambo, H.S., A.J.R. Dutta, and S.E. Reviews, *A comparative review of biochar and hydrochar in terms of production, physico-chemical properties and applications.* 2015. **45**: p. 359-378.

84. Arenillas, A., et al., *Organic and Carbon Gels: From Laboratory Synthesis to Applications*. 2019: Springer.

85. Falco, C., et al., *Tailoring the porosity of chemically activated hydrothermal carbons: Influence of the precursor and hydrothermal carbonization temperature.* 2013. **62**: p. 346-355.

86. Gallifuoco, A., L. Taglieri, and A.A.J.R.E. Papa, *Hydrothermal carbonization of waste biomass to fuel: A novel technique for analyzing experimental data.* 2020. **149**: p. 1254-1260.

87. Gallucci, K., et al., *Non-Energy Valorization of Residual Biomasses via HTC: CO2 Capture onto Activated Hydrochars.* 2020. **10**(5): p. 1879.

88. Kabakcı, S.B. and S.S.J.W.M. Baran, *Hydrothermal carbonization of various lignocellulosics: Fuel characteristics of hydrochars and surface characteristics of activated hydrochars.* 2019. **100**: p. 259-268.

89. Sevilla, M., G.A. Ferrero, and A.B.J.C. Fuertes, *Beyond KOH activation for the synthesis of superactivated carbons from hydrochar.* 2017. **114**: p. 50-58.

90. Sevilla, M., A.B.J.E. Fuertes, and E. Science, *Sustainable porous carbons with a superior performance for CO 2 capture.* 2011. **4**(5): p. 1765-1771.

91. Brunauer, S. and P.H.J.J.o.t.A.C.S. Emmett, *The use of low temperature van der Waals adsorption isotherms in determining the surface areas of various adsorbents.* 1937. **59**(12): p. 2682-2689.

92. Aloisi, I., G. Taglieri, and P.U.J.R.R.d.S.R. Foscolo, *Caratterizzazione strutturale e morfologica di sorbenti dell'anidride carbonica.* 2013.

93. Barrett, E.P., L.G. Joyner, and P.P. Halenda, *The Determination of Pore Volume and Area Distributions in Porous Substances. I. Computations from Nitrogen Isotherms.* Journal of the American Chemical Society, 1951. **73**(1): p. 373-380.

94. Fiore, I., K. Gallucci, and P.U. Foscolo, *CARATTERIZZAZIONE STRUTTURALE E MORFOLOGICA DI CATALIZZATORI E SORBENTI DA UTILIZZARE NELLA PIATTAFORMA PILOTA ZECOMIX DELLA CASACCIA.* 2014.

95. Thompson, M.J.G.E., Environment, Analysis, *Analytical methodology in the Applied Geochemistry Research Group (1950–1988) at the Imperial College of Science and Technology, London.* 2010. **10**(3): p. 251-259.

96. Postek, M.T., et al., *Scanning electron microscopy. A student's handbook. Ladd Research Industries.* 1980.

97. *RTI Laboratories*. Available from: https://rtilab.com/techniques/sem-eds-analysis/.

98. Ergun, S.J.C.E.P., *Fluid flow through packed columns.* 1952. **48**: p. 89-94.

99. Gallifuoco, A., et al., *Hydrothermal conversions of waste biomass: Assessment of kinetic models using liquid-phase electrical conductivity measurements.* 2018. **77**: p. 586-592.

100. Di Felice, L., P.U. Foscolo, and L.J.I.J.o.C.R.E. Gibilaro, *CO2 capture by calcined dolomite in a fluidized bed: experimental data and numerical simulations.* 2011. **9**(1).

101. Ferella, F., et al., *Separation of carbon dioxide for biogas upgrading to biomethane.* 2017. **164**: p. 1205-1218.

102. Kacem, M., M. Pellerano, and A.J.F.P.T. Delebarre, *Pressure swing adsorption for CO2/N2 and CO2/CH4 separation: Comparison between activated carbons and zeolites performances.* 2015. **138**: p. 271-283.

103. Woolley, O.J.R.E.L. and P. Review, *Reforming Gas Sector Governance to Promote Biomethane Injection.* 2013: p. 175-188.

104. Thommes, M., et al., *Physisorption of gases, with special reference to the evaluation of surface area and pore size distribution (IUPAC Technical Report).* 2015. **87**(9-10): p. 1051-1069.

105. Fu, P., et al., *Study on the gas evolution and char structural change during pyrolysis of cotton stalk.* 2012. **97**: p. 130-136.

106. Moon, H.Y., et al., *Relationship between average pore diameter and chloride diffusivity in various concretes.* 2006. **20**(9): p. 725-732.

107. Pevida, C., T. Drage, and C.J.C. Snape, *Silica-templated melamine–formaldehyde resin derived adsorbents for CO2 capture.* 2008. **46**(11): p. 1464-1474.

108. Siriwardane, R.V., et al., *Adsorption of CO2 on molecular sieves and activated carbon.* 2001. **15**(2): p. 279-284.

109. Rackley, S.A., *Carbon capture and storage*. 2017: Butterworth-Heinemann.

110. Przepiórski, J., M. Skrodzewicz, and A.J.A.S.S. Morawski, *High temperature ammonia treatment of activated carbon for enhancement of CO2 adsorption.* 2004. **225**(1-4): p. 235-242.

111. Chandrasekar, G., W.-J. Son, and W.-S.J.J.o.p.m. Ahn, *Synthesis of mesoporous materials SBA-15 and CMK-3 from fly ash and their application for CO 2 adsorption.* 2009. **16**(5): p. 545-551.

112. Pevida, C., et al., *Surface modification of activated carbons for CO2 capture.* 2008. **254**(22): p. 7165-7172.

113. Guan, Y., et al., *Chronic intermittent hypobaric hypoxia decreases β-adrenoceptor activity in right ventricular papillary muscle.* 2010. **298**(4): p. H1267-H1272.

114. Wahby, A., et al., *High-surface-area carbon molecular sieves for selective CO2 adsorption.* 2010. **3**(8): p. 974-981.

115. Shi, J., et al., *Enzymatic conversion of carbon dioxide.* 2015. **44**(17): p. 5981-6000.

116. Plasch, K., et al., *Pressurized CO 2 as a carboxylating agent for the biocatalytic ortho-carboxylation of resorcinol.* 2018. **20**(8): p. 1754-1759.

117. Wuensch, C., et al., *Regioselective ortho-carboxylation of phenols catalyzed by benzoic acid decarboxylases: a biocatalytic equivalent to the Kolbe–Schmitt reaction.* 2014. **4**(19): p. 9673-9679.

118. Payer, S.E., et al., *Regioselective para-Carboxylation of Catechols with a Prenylated Flavin Dependent Decarboxylase.* 2017. **56**(44): p. 13893-13897.

119. Ren, J., et al., *An unprecedented effective enzymatic carboxylation of phenols.* 2016. **6**(2): p. 564-567.

120. Buxbaum, E., *Enzymes are biocatalysts*, in *Fundamentals of Protein Structure and Function*. 2015, Springer. p. 97-110.

121. Hough, D.W. and M.J.J.C.o.i.c.b. Danson, *Extremozymes.* 1999. **3**(1): p. 39-46.

122. Prieur, D.J.T.i.B., *Microbiology of deep-sea hydrothermal vents.* 1997. **15**(7): p. 242-244.

123. Butters, M., et al., *Critical assessment of pharmaceutical processes a rationale for changing the synthetic route.* 2006. **106**(7): p. 3002-3027.

124. Feyerabend, P.J.N., NY: Verse, *Against Method, revised edition.* 1988.

125. Faber, K. and K. Faber, *Biotransformations in organic chemistry*. Vol. 4. 1992: Springer.

126. White, J.S. and D.C. White, *Source book of enzymes*. 1997: CRC Press.

127. Theil, F.J.T., *Enhancement of selectivity and reactivity of lipases by additives.* 2000. **19**(56): p. 2905-2919.

128. Ó'Fágáin, C.J.E. and m. technology, *Enzyme stabilization—recent experimental progress.* 2003. **33**(2-3): p. 137-149.

129. Mejri, M., et al., *Effect of polyhydroxylic additives on the catalytic activity of thermolysin.* 1998. **23**(6): p. 392-396.

130. Faber, K., *Special Techniques*, in *Biotransformations in organic chemistry*. 2018, Springer. p. 315-405.

131. Yamamoto, Y. and H.J.B.o.t.C.S.o.J. Kise, *Concentration-and structure-dependent effects of amides on protease activity in organic solvents.* 1994. **67**(5): p. 1367-1370.

132. Wohlgemuth, R.J.C.o.i.b., *Biocatalysis—key to sustainable industrial chemistry.* 2010. **21**(6): p. 713-724.

133. Wu, S., et al., *Biocatalysis: Enzymatic synthesis for industrial applications.* 2021. **60**(1): p. 88-119.

134. Hilterhaus, L., et al., *Applied biocatalysis: from fundamental science to industrial applications*. 2016: John Wiley & Sons.

135. Gurung, N., et al., *A broader view: microbial enzymes and their relevance in industries, medicine, and beyond.* 2013. **2013**.

136. Hori, H., et al., *High-performance liquid chromatography with conductimetric detection of perfluorocarboxylic acids and perfluorosulfonates.* 2004. **57**(4): p. 273-282.

137. Yachmenev, V.G., et al., *Intensification of the bio-processing of cotton textiles by combined enzyme/ultrasound treatment.* 2002. **77**(5): p. 559-567.

138. Maijala, P., et al., *Biomechanical pulping of softwood with enzymes and white-rot fungus Physisporinus rivulosus.* 2008. **43**(2): p. 169-177.

139. Winkler, C.K., J.H. Schrittwieser, and W.J.A.C.S. Kroutil, *Power of Biocatalysis for Organic Synthesis.*

140. Wuensch, C., et al., *Regioselective enzymatic carboxylation of phenols and hydroxystyrene derivatives.* 2012. **14**(8): p. 1974-1977.

141. Imani, R., S.H. Emami, and S. Faghihi, *Nano-graphene oxide carboxylation for efficient bioconjugation applications: a quantitative optimization approach.* Journal of Nanoparticle Research, 2015. **17**(2): p. 88.

142. Ballard, F.J. and R.W. Hanson, *Phosphoenolpyruvate carboxykinase and pyruvate carboxylase in developing rat liver.* Biochemical Journal, 1967. **104**(3): p. 866-871.

143. Lye. *Application of in situ product-removal techniques to biocatalytic processes*. 1999.

144. Tsang, Y.F., et al., *Production of bioplastic through food waste valorization.* 2019. **127**: p. 625-644.

145. *European Bioplastics Organization* Available from: https://www.european-bioplastics.org/.

146. *What is bioplastic*. Available from: https://www.solon.eco/what-is-bioplastic.

147. Johnson, K., et al. *Hydrothermal Mineral-Assisted Organic Transformations of Carboxylic Acids*. in *AGU Fall Meeting Abstracts*. 2014.

148. Granell, J. and M.J.D.T. Martinez, *Kinetico-mechanistic studies of cyclometalating C–H bond activation reactions on Pd (II) and Rh (II) centres: the importance of non-innocent acidic solvents in the process.* 2012. **41**(37): p. 11243-11258.

149. Stauffer, M.T.J.C. and V.o.A.M.A.S.o.C. Approaches, *Introductory Chapter: The Many Faces of Calibration and Validation in Analytical Methodology in the Present Day.* 2018: p. 1.

150. Cuatrecasas, P., M. Wilchek, and C.B.J.P.o.t.N.A.o.S.o.t.U.S.o.A. Anfinsen, *Selective enzyme purification by affinity chromatography.* 1968. **61**(2): p. 636.

151. Porath, J.J.J.o.p.c., *From gel filtration to adsorptive size exclusion.* 1997. **16**(5): p. 463-468.

152. Aleku, G.A., et al., *Enzymatic C–H activation of aromatic compounds through CO 2 fixation.* 2020. **16**(11): p. 1255-1260.

153. Cherubini, F., et al., *Energy-and greenhouse gas-based LCA of biofuel and bioenergy systems: Key issues, ranges and recommendations.* 2009. **53**(8): p. 434-447.

154. Collotta, M., et al., *Evaluating microalgae-to-energy-systems: different approaches to life cycle assessment (LCA) studies.* 2016. **10**(6): p. 883-895.

155. Zhang, G., et al., *Design and analysis of a biogas production system utilizing residual energy for a hybrid CSP and biogas power plant.* 2016. **109**: p. 423-431.

156. Edenhofer, O., *Climate change 2014: mitigation of climate change*. Vol. 3. 2015: Cambridge University Press.

157. Kusch-Brandt, S., *Urban Renewable Energy on the Upswing: A Spotlight on Renewable Energy in Cities in REN21's "Renewables 2019 Global Status Report"*. 2019, Multidisciplinary Digital Publishing Institute.

158. Ellabban, O., et al., *Renewable energy resources: Current status, future prospects and their enabling technology.* 2014. **39**: p. 748-764.

159. Pachauri, R.K., et al., *Climate change 2014: synthesis report. Contribution of Working Groups I, II and III to the fifth assessment report of the Intergovernmental Panel on Climate Change*. 2014: Ipcc.

160. Edenhofer, O., *Technical Summary In: Climate Change 2014: Mitigation of Climate Change. Contribution of Working Group III to the Fifth Assessment Report of the Intergovernmental Panel on Climate Change. Technical Report.* 2014.

161. Secretariat, R.J.R.P.R., *Renewables 2012 global status report.* 2012.

162. Vögeli, Y., *Anaerobic digestion of biowaste in developing countries: Practical information and case studies*. 2014: Eawag-Sandec.

163. Kapoor, R. and V.J.P.d.E.F.V.p. Vijay, *5.2 Evaluation of existing low cost gas bottling systems for vehicles use adaption in developing economies.* 2013.

164. Jingming, L.J.C.B.S.B.G.R.f.w.a.d., *The future of biogas in China.* 2014.

165. van Foreest, F., *Perspectives for biogas in Europe*. 2012: Oxford Institute for Energy Studies.

166. Zbicinski, I., *Product design and life cycle assessment*. Vol. 3. 2006: Baltic University Press.

167. Jensen, A.A., *Life cycle assessment (LCA): a guide to approaches, experiences and information sources*. 1998: European Communities.

168. Ishikawa, S., et al. *Evaluation of a biogas plant from life cycle assessment (LCA)*. in *International Congress Series*. 2006. Elsevier.

169. Huttunen, S., K. Manninen, and P.J.J.o.c.p. Leskinen, *Combining biogas LCA reviews with stakeholder interviews to analyse life cycle impacts at a practical level.* 2014. **80**: p. 5-16.

170. Zhou, S., et al., *Low temperature liquid separation technology of CO2 from biogas based on aspen HYSYS.* 2011. **42**(8): p. 111-116.

171. Leonzio, G.J.J.o.C.P., *Upgrading of biogas to bio-methane with chemical absorption process: simulation and environmental impact.* 2016. **131**: p. 364-375.

172. James, J.C., *Process modeling, simulation and control for chemical engineers*. 1989: McGraw-Hill.

173. Dialynas, E., N.J.E.J.o.D. Koskolos, and H. Safety in Automation, *Comparison of contingency enumeration and Monte-Carlo simulation approaches applied to the reliability evaluation of composite power systems.* 1995. **5**: p. 25-48.

174. *SimaPro. LCA software for fact-based sustainability*. Available from: https://simapro.com/.

175. Al-Malah, K.I., *Aspen plus*. 2016: Wiley Online Library.

176. ASPENTECH, A.G.S.B.J.A.T., Burlington, *Running a process model.* 2010.

177. Volk, M., *Pump characteristics and applications*. 2013: CRC Press.

178. Bloch, H.P., *A practical guide to compressor technology*. 2006: John Wiley & Sons.

179. *CHECALC*. Available from: https://checalc.com/index.html.

180. Turton, R., et al., *Analysis, synthesis and design of chemical processes*. 2008: Pearson Education.

Acknowledgement

Performing this PhD has been a tremendous experience for me, and it has changed my life and thinking, and this goal was impossible without the help and support of many peoples.

First, I would like to thank my first tutor, co-supervisor, and a kind personality Prof. Dr. Katia Gallucci who's continuous support, motivation and immense knowledge have given me eager and power to excel in research writing and without her guidance and support, this PhD would not have been achievable. Many thanks to my PhD coordinator Prof. Dr. Giuseppe Ferri who trusted me and offered this opportunity in the beautiful city of L'Aquila and supported me in all the ways.

Likewise, I would like to thank all the colleagues, staff, and the members of the department of Industrial engineering for their help and support during all these years. Furthermore, I thankfully acknowledge the funding received towards my PhD from the University of L'Aquila (PhD fellowship from MIUR) that allowed me to finish my research work.

I would also like to special thanks to my two other co-supervisors one from University of Graz, Austria (Dr. Christopher Winkler) and second from the company APS S.p.A. Rome, Italy (Sbarigia Clemente) because without their assistance, encouragement and support this milestone was not achievable.

Finally, I would like to thank to my sweat mother and beautiful wife who's support and love always to encourage and push me that "yes you can do it" and here comes that day which I have seen in my dreams.

UNIVERSITY OF L'AQUILA
Department of Industrial engineering and Information & Economics

The PhD scholarship was co-financed with resources from the 2014-2020 National Operational Program (CCI 2014IT16M2OP005), European Social Fund, Action I.1 "Innovative Doctorates with industrial characterization"